

A.C. Impedance of Single Muscle Fibres

By

Robert Eisenberg

A thesis presented for the degree of

Doctor of Philosophy

in the university of London

Department of Biophysics

University College London

1965

ABSTRACT

The impedance of single crab muscle fibres was determined with microelectrodes over the frequency range 1 c/s to 10 kc/s. Care was taken to analyze, reduce and correct for capacitative artifact. The impedance of the fibre was analyzed using linear cable theory, the accuracy of which is discussed. The equivalent circuit of the fibre distributed admittance is found in most cases to have two capacitances, each in series with resistance, and a resistive shunt. In just two fibres only one capacitance shunted by a resistance was found. In several fibres there was evidence of a third very large capacitance.

The values of the elements of the equivalent circuit depend on which of several equivalent circuits is chosen. The circuit considered most reasonable in the light of the anatomical evidence consists of two parallel branches: a resistance R_e in series with a capacitance C_e ; and a resistance R_b in series with a parallel combination of the resistance R_m and the capacitance C_m . The average circuit values for this model are $R_e = 21 \text{ ohm}\cdot\text{cm}^2$; $C_e = 47 \mu\text{F}/\text{cm}^2$; $R_b = 10.2 \text{ ohm}\cdot\text{cm}^2$; $R_m = 173 \text{ ohm}\cdot\text{cm}^2$; $C_m = 9.0 \mu\text{F}/\text{cm}^2$.

The relation of the equivalent circuit to the fine structure of crab muscle is discussed. R_m and C_m are attributed to the

sarcolemma; C_e , to the sarcotubular system; and R_b and R_e , to the amorphous material found around crab fibres. Estimates of actual surface area of the sarcolemma and sarcotubular system show that the average circuit values are consistent with the dielectric properties of predominantly lipid membranes.

TABLE OF CONTENTS

Abstract

Acknowledgements

Chapter 1: Introduction

Chapter 2: Theory

Linear Circuit Analysis

Cable Theory

Simple Fibre Model

Simple Distributed Resistance Model

Two Time Constant Model

Two Time Constant, Distributed Resistance Model

Other Two Time Constant, Distributed Resistance Models

Curve Fitting Methods

Appendices:

Derivation of the Equivalence Relations

Curve Fitting Computer Program

Chapter 3: Methods

Material and Apparatus

Stray Capacitances

Procedure	84
Corrections for Stray Capacitances	86
Appendices	
Derivation of the Correction Equations	92
The Cathode Follower	101
Error Analysis of the Corrections	109
Alternative Methods of Parameter Measurement	113
Chapter 4: Results	
Description	118
Second Group of Fibres	123
Third Group of Fibres	126
Errors Arising from the Neglect of Three Dimensional Spread of Current	126
Equivalent Circuits of the Muscle Fibre	130
Distributed Admittance	
Evaluation of Circuit Parameters	131
Transient Response of Muscle Fibre	138
Appendix:	
The Three Dimensional Flow of Current	142

Chapter 5: Discussion

Relation of Present Observations to Previous Findings	150
Relation of Electrical Parameters to Muscle Structure	150
 References	165

ACKNOWLEDGEMENTS

I am very grateful to P. Fatt and G. Falk for their help and encouragement. I am also indebted to the other members of the Biophysics Department and to L. Peachey and A.F. Huxley for many stimulating discussions.

I wish to thank J.L. Parkinson, L.J. Ward, K. Copeland, E. Ullrich and A.M. Paintin for technical assistance.

This work was done while I was a Graduate Fellow of the National Science Foundation. I am grateful to the Foundation for their support.

Chapter 1

INTRODUCTION

The low frequency capacitance of muscle fibres as measured with intracellular electrodes is quite large, ranging from $8 \mu\text{F}/\text{cm}^2$ in frog (Fatt & Katz, 1951) to $40 \mu\text{F}/\text{cm}^2$ in crab (Fatt & Katz, 1953a; Atwood, 1963). It is difficult to account for these large values of capacitance assuming reasonable dielectric properties of a predominantly lipid sarcolemma. Recently, the large value of capacitance in frog muscle has been explained by attributing the greater part of it to the sarcotubular system (Falk & Fatt, 1964), the structure of which is reviewed in Porter, 1961, and Franzini-Armstrong, 1964. It seemed of interest to see if the much larger capacitance of crab muscle could also be attributed in greater part to the sarcotubular system (first investigated by Veratti, 1902, with the light microscope; more recently by Peachey & Huxley, 1964, with the electron microscope).

The separation of the total capacitance of a muscle fibre into two parts, one attributed to the surface membrane, the other to the sarcotubular system, depends on the presence of a resistance in series with one part, or on the existence of

different RC products if both capacitances are in series with resistance. If either of these conditions is fulfilled, the passive electrical properties of the fibre will reveal the existence of two capacitances.

The passive properties of a linear system can most satisfactorily be studied by measuring the impedance of the system to sinusoidal currents of different frequencies; that is, by measuring the relative magnitude and phase of the current and voltage over a range of frequencies. The difficulties of separating different time constants make measurements of the transient response of a linear system less satisfactory. A detailed analysis of the relative merits of transient and frequency response methods in the determination of the number and size of the time constants of a linear system leads Lanczos (1957, p. 279) to conclude that the difficulty with transient response methods "lies not with the manner of evaluation (of the time constants from the experimental data) but with the extraordinary sensitivity of the exponents (that is time constants) and amplitudes to very small changes of the data, which no amount of statistics could remedy. The only remedy would be an increase of accuracy to limits which are far beyond the possibilities of our present measuring devices". (Comments in brackets added). In view of this analysis the measurement of frequency response seemed the best way to determine the equivalent circuit of crab muscle.

Measurements of impedance were made over a wide frequency range. The qualitative features of the data showed that the equivalent circuit of most crab fibres contained two capacitances, each in series with resistance. Values of the circuit elements were obtained from the best fit of such an equivalent circuit to the experimental data. Finally, the different forms of the equivalent circuit and the values of the circuit elements are discussed in relation to the fibre structure.

Chapter 2.

THEORY.

Linear Circuit Analysis.

The system under consideration is treated as linear and passive: linear since the values of the circuit parameters are independent of potential and current; passive since the only internal voltage source is constant and can be subtracted from all observed potentials. The theory of systems which fulfill these requirements is based on the representation of currents and voltages by complex numbers. The theory is valid for excitations of arbitrary form but the derivation of the system properties for the general case depends on the use of Laplace transforms (Kuo, 1962). Our derivation is restricted to sinusoidal excitations although the results are in fact valid for any excitation if the purely imaginary frequency variable jw (where $j = \sqrt{-1}$) is replaced by the complex frequency variable $s = \sigma + jw$ and the complex currents and voltages are interpreted as the Laplace transforms of the physical currents and voltages.

The response of any linear passive system to a sinusoidal excitation is sinusoidal with the same frequency

as the excitation after transients have died away. Any current or voltage in the system can then be written as

$$\begin{aligned} V(t) &= V_m \cos(\omega t + \phi) = \text{Re}\{V_m e^{j\phi} e^{j\omega t}\} \\ i(t) &= \text{Re}\{I_m e^{j\phi'} e^{j\omega t}\} \end{aligned} \quad (1)$$

where t is time, ϕ and ϕ' are the phase differences of voltage and current from some reference, and $\text{Re}\{\}$ denotes the real part of the complex quantity in the brackets. If we split off the time dependence (which is the same everywhere in the system) by defining a complex voltage V and complex current I as

$$\begin{aligned} V &= V_m e^{j\phi} \\ I &= I_m e^{j\phi'} \end{aligned} \quad (2)$$

then the physical voltage and currents are given by

$$\begin{aligned} V(t) &= \text{Re}\{V e^{j\omega t}\} \\ i(t) &= \text{Re}\{I e^{j\omega t}\} \end{aligned} \quad (3)$$

The physical currents and voltages are hardly ever needed in circuit analysis since the ratios of various complex currents and voltages contain all the information usually of interest (i.e. the relative phase and magnitude of the physical quantities). The ratio of complex voltage to complex current is a frequency dependent complex quantity called impedance Z , whose real part is the effective (equivalent) resistance R , and whose imaginary part is reactance X

$$Z = \frac{V}{I} = \frac{V_m}{I_m} e^{j(\phi - \phi')} = R + jX \quad (4)$$

Ratios of voltage to voltage and current to current as well as their reciprocal quantities can also be defined. The reciprocal of impedance is another complex quantity called admittance Y , with real part conductance g and imaginary part susceptance b

$$Y = \frac{1}{Z} = g + jb \quad (5)$$

It is important to note that the effective resistance is not the reciprocal of the conductance. The relations between the real and imaginary parts of the admittance and impedance are given by

$$Y = \frac{1}{Z} = g + jb = \frac{1}{R + jX} \quad (6)$$

$$g = \frac{R}{R^2 + X^2}; \quad b = \frac{-X}{R^2 + X^2}$$

The impedance of each of the common circuit elements can be defined by writing its current-voltage relation in complex form. The impedance of a resistor of r ohms is then real, independent of frequency and equal to r ; the impedance of a capacitor C is purely imaginary (i.e. purely reactive), frequency dependent and equals

$$X_C = \frac{1}{j\omega C} = \frac{-j}{\omega C}$$

It can be shown that the complex currents, voltages, and impedances all obey Kirchoff's and Ohm's laws. The analysis of the response of a network to an arbitrary excitation is then carried out as for a d.c. circuit except complex quantities are used. (The discussion above is presented in detail in a number of electrical engineering textbooks: e.g. Tuttle, 1958; Le Page & Seeley, 1952; or Guillemin, 1953).

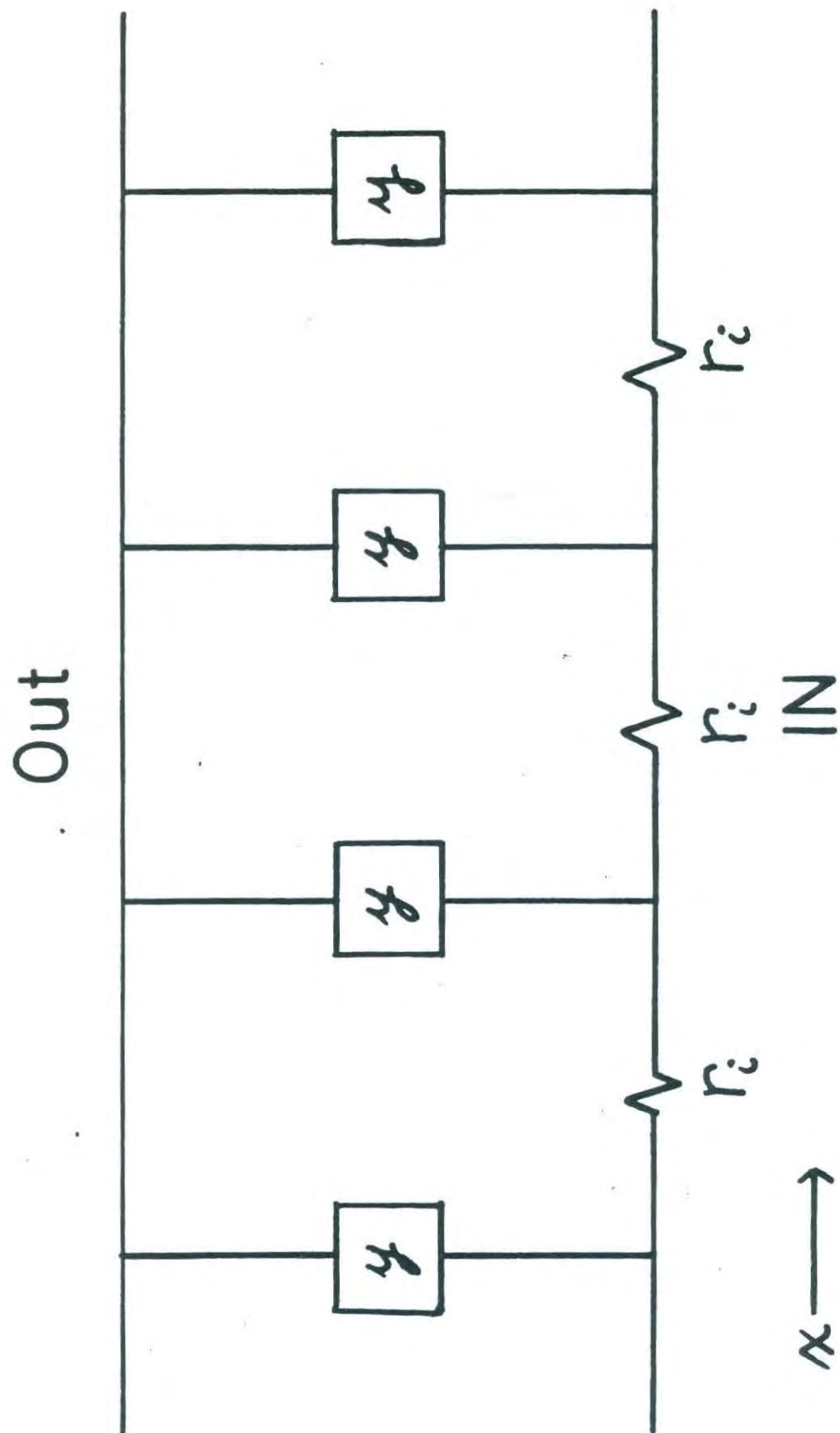
Cable Theory

It is necessary to use cable theory since current applied to the muscle fibre passes along the internal resistivity of the fibre before it crosses the fibre membrane; in other words, the current applied produces a potential drop across the internal resistance of the fibre as well as the membrane.

Figure 2.1

The Muscle Fibre Treated as a Linear Cable

r_i , the internal resistivity, and y , the complex distributed admittance, refer to the properties of a very small length of the muscle fibre; they are incremental quantities.



The membrane admittance is said to be distributed along the internal resistance. The fibre may be represented as a linear (one dimensional) cable if as a first approximation the potential at any distance along the fibre axis is assumed to be the same throughout the fibre interior. (The validity of this assumption is examined in Chapter 4: Results). It is also useful to assume that there are no potential drops in the external medium. This assumption can be tested and is found to be adequate as long as the source of current is not too focal. Figure 2.1 shows the circuit of the linear cable including both assumptions. x is the distance along the fibre axis. r_i is the internal resistivity per unit length. y is the complex admittance between inside and outside per unit length (called the distributed admittance).

The steady state response of this model to sinusoidal excitation is known (LePage & Seeley, 1952). For current I applied at $x = 0$ and potential $V(x)$ measured at x (chosen positive), and assuming the fibre to be long enough so that there is neither current flow nor potential change at the ends, the transfer impedance $Z(x)$ is

$$Z(x) = R + jX = \frac{V(x)}{I} = Z_0 e^{-\gamma x} \quad (7)$$

where

$$Z_0 = \frac{1}{2} \sqrt{\frac{r_i}{y}} ; \quad \gamma = \sqrt{r_i y} \quad (8)$$

The parameter γ is discussed in the Appendix to Chapter 4:
 Results. In these experiments potential was usually measured close to the point where current was applied. For that case (7) becomes

$$Z(x=0) = Z_0 = R + jX \quad (9)$$

An expression relating the effective lumped resistance and reactance (R and X) with the distributed conductance and susceptance (g and b) can be derived by substituting $y = g + jb$ into (8) and taking real and imaginary parts

$$R = \frac{1}{2} \left(\frac{r_i}{2g} \right)^{1/2} \frac{\left\{ \left[\left(\frac{b}{g} \right)^2 + 1 \right]^{1/2} + 1 \right\}^{1/2}}{\left[\left(\frac{b}{g} \right)^2 + 1 \right]^{1/2}} \quad (10)$$

$$-X = \frac{1}{2} \left(\frac{r_i}{2g} \right)^{1/2} \frac{\left\{ \left[\left(\frac{b}{g} \right)^2 + 1 \right]^{1/2} - 1 \right\}^{1/2}}{\left[\left(\frac{b}{g} \right)^2 + 1 \right]^{1/2}}$$

It is important to realize that equation (10) contains two physically distinct sets of variables: R and X , which refer to the total impedance seen by a source of current at $x = 0$ (the ratio of potential at $x = 0$ to the current applied there) and g and b , which refer to the admittance of an

element of fibre membrane (the ratio of the potential across that element of membrane to the current through it).

The physical difference between these two sets of parameters can be seen if one compares the effect of a resistance R_s in series with the entire current flowing through the cable with the effect of a resistance r_b in series with each element of the cable (see Figure 2.2). The effect of placing a resistance in series with all the current would be simply to add the positive real constant R_s to the impedance Z . At any frequency the only effect would be to increase the effective resistance by R_s . If a plot were made of X vs. R the curve would be displaced by R_s but its shape would not be changed. On the other hand, the addition of a distributed resistance r_b in series with the admittance $y' = g' + jb'$ produces a change which is frequency dependent (since in general both g' and b' are frequency dependent). The admittance $y = g + jb$ of an element of membrane consisting of resistance r_b in series with y' is

$$y = \frac{g'(1+r_bg') + b'^2r_b}{(1+r_bg')^2 + b'^2r_b^2} \quad (11)$$

$$b = \frac{b'}{(1+r_bg')^2 + b'^2r_b^2}$$

Figure 2.2

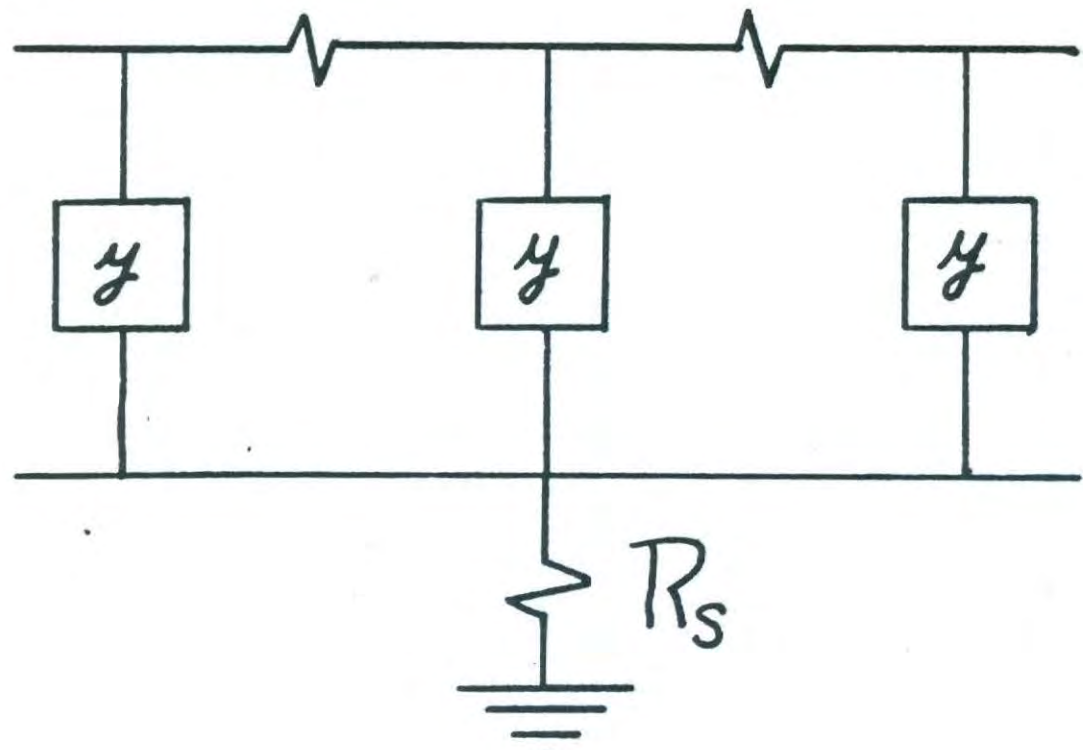
Two Kinds of Series Resistance

A: the entire fibre impedance in series with the
resistance R_s .

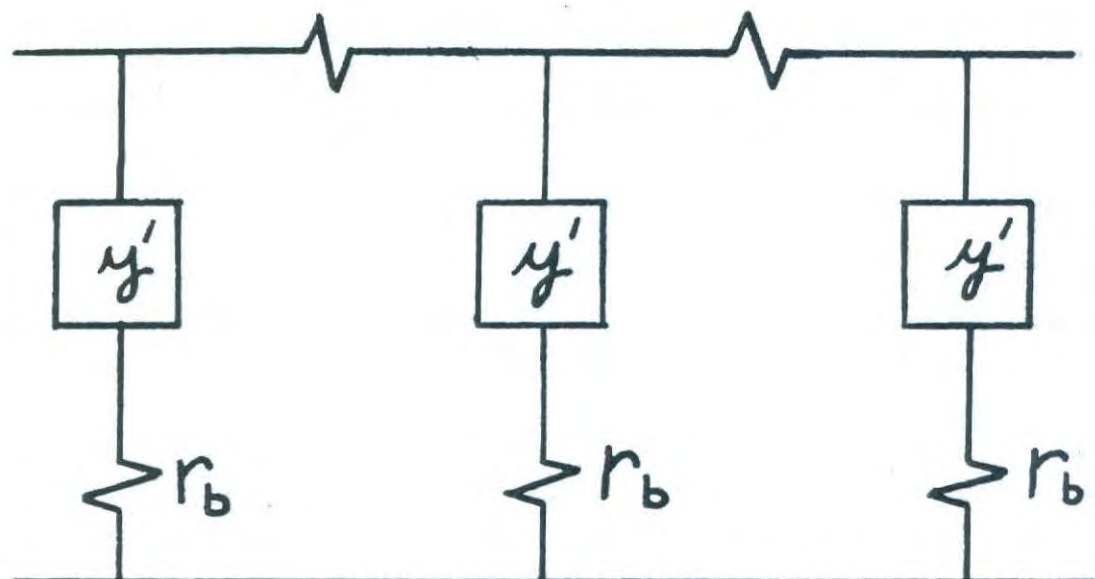
B: the distributed admittance y' in series with the
distributed resistance r_b .

All quantities except R_s refer to a very small length of
fibre.

A



B



The addition of a distributed resistance has two effects on a plot of X vs. R : first, there is a change in the shape of the curve; secondly, (if the model for y contains no inductances) at very high frequencies the capacitances in y have negligible impedance and the entire potential drop across the fibre ^{equivalent} membrane is developed across r_b . Thus, at very high frequencies a plot of X vs. R must bend down to give a pure resistance.

The only measurement made here with $x \neq 0$ are those of the d.c. space constant λ . λ is found by setting $b = 0$ (the reactance of any linear passive circuit is zero at zero frequency) in (8):

$$\lambda = \frac{1}{g_{\omega=0}} = \frac{1}{\sqrt{r_i g_{\omega=0}}} \quad (12)$$

Note that $1/g$ is identical with the total d.c. resistance of the distributed admittance y ; it is not necessarily identical with r_m , the resistance of the plasma membrane. Measurements with finite electrode separation require the use of a more complicated formula (equation 3, p. 72 in Falk & Fatt, 1964). Such measurements are not presented here.

The basic method of this investigation can now be seen. Impedance measurements were made over a wide range of frequencies and a network for y chosen which fit the observed data. In order

to choose a network for y different plots of the impedance data can be used. Phase and magnitude, or resistance and reactance can be plotted against log frequency (sometimes called the Bode plot: Bode, 1945) or reactance can be plotted against resistance (called the Cole-Cole plot: Cole and Cole, 1941). The latter plot is particularly useful in revealing the qualitative features of the impedance function because mathematically it is the plot ('mapping') used to show the behaviour of a complex function (here Z) of a real variable (w) (see Churchill, 1960). Although the explicit dependence of R and X on frequency is not given in this plot, ^{little} ~~no~~ information is lost since any impedance function is specified (within a scale factor) if a relation between two of its variables is given (see Bode, 1945, and Tuttle, 1958, for proofs and discussion for lumped circuits; see Macdonald and Brachman, 1956, for a general discussion of the physical significance of these relations and a proof that they hold for distributed linear passive systems). In practice, the scale factor is set by labelling some point of the impedance locus with the corresponding frequency.

The other plot used, that of phase vs. log frequency, has two advantages: it is sensitive at relatively low frequencies to changes in values of circuit parameters and it shows random error most clearly (since experimentally a direct measurement is made

of phase, not R or X). The plots of resistance, magnitude of impedance, or reactance against log frequency were found to be less useful since they were relatively insensitive to model or parameter changes.

Simple Fibre Model.

In a simple model of the fibre y is taken to be a capacitance in parallel with the membrane resistance r_m (Fig. 2.3). The expression for the real and imaginary parts of the admittance are then

$$g = \frac{1}{r_m} \quad (13)$$

$$b = \omega C_m$$

The d.c. space constant is

$$\lambda = \sqrt{\frac{r_m}{r_i}} \quad (14)$$

and the input resistance

$$R_{in} = \frac{1}{2} \sqrt{r_m r_i} \quad (15)$$

Figure 2.3 shows the shape of the impedance locus for this model (~~Cole & Baker, 1941~~). It should be noted that the shape of

Figure 2.3

The Impedance Locus of the Simple Fibre Model

The impedance locus of the circuit in the upper right hand corner is shown. The circuit elements are identified for use in the text. The scales are given in terms of R_{in} , the d.c. resistance. The solid 45° line represents the line approached at high frequencies by the impedance plots of all circuits without a distributed series resistance.

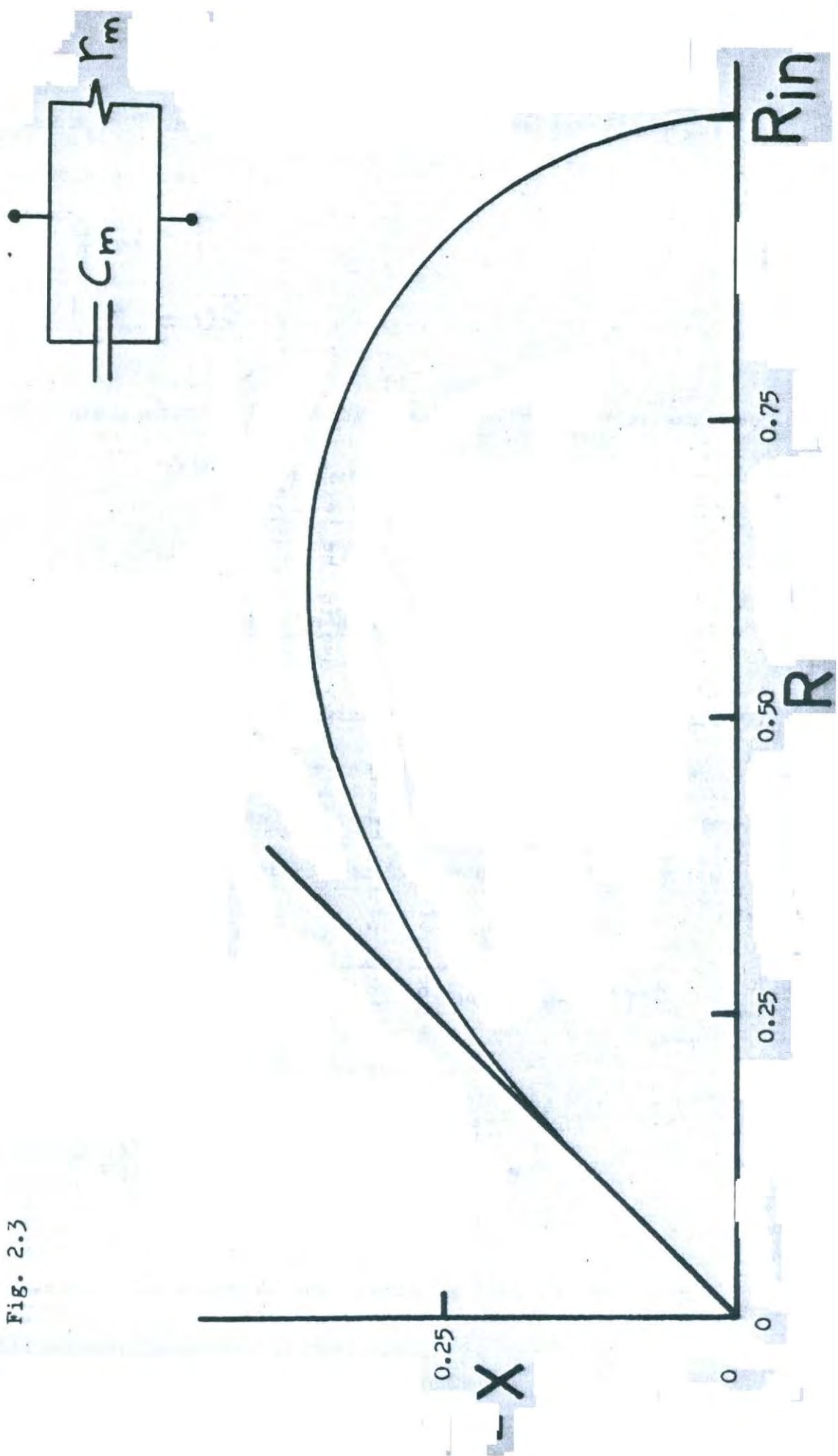


Fig. 2.3

this curve is independent of the actual values of the parameters c_m , r_m , and r_i . This can be seen by writing the equations (13) in dimensionless form.

$$qr_m = 1$$

$$br_m = \nu$$

where the scale factor r_m is set by the input resistance, and

$$\nu = \omega r_m c_m$$

Simple Distributed Resistance Model.

Another model is that in which the circuit element of the simple model is in series with a resistance (Fig. 2.4). This distributed resistance makes the impedance at infinite frequency purely resistive. The admittance of this model is given by

$$Yr_m = \frac{(1+r) + \nu^2 r}{(1+r)^2 + \nu^2 r^2} + \frac{j\nu}{(1+r)^2 + \nu^2 r^2} \quad (16)$$

where the dimensionless variables

$$r = \frac{r_b}{r_m}; \quad \nu = \omega r_m c_m$$

have been used. The shape of this locus is seen to depend on

Figure 2.4

The Impedance Loci of the One Time Constant, Distributed Resistance Model

The impedance loci of the circuit in the upper right hand corner are shown.

Circuit elements are defined for use in text. The 45° line represents the limiting high frequency locus of the circuit for $r_b = 0$; i.e. in the absence of distributed resistance. The large numbers under the abscissa give the value of R_∞/R_{in} for each curve, where R_∞ , the infinite frequency resistance, equals $0.5(r_b r_i)^{1/2}$. The small numbers on both axes give the scales in terms of R_{in} .

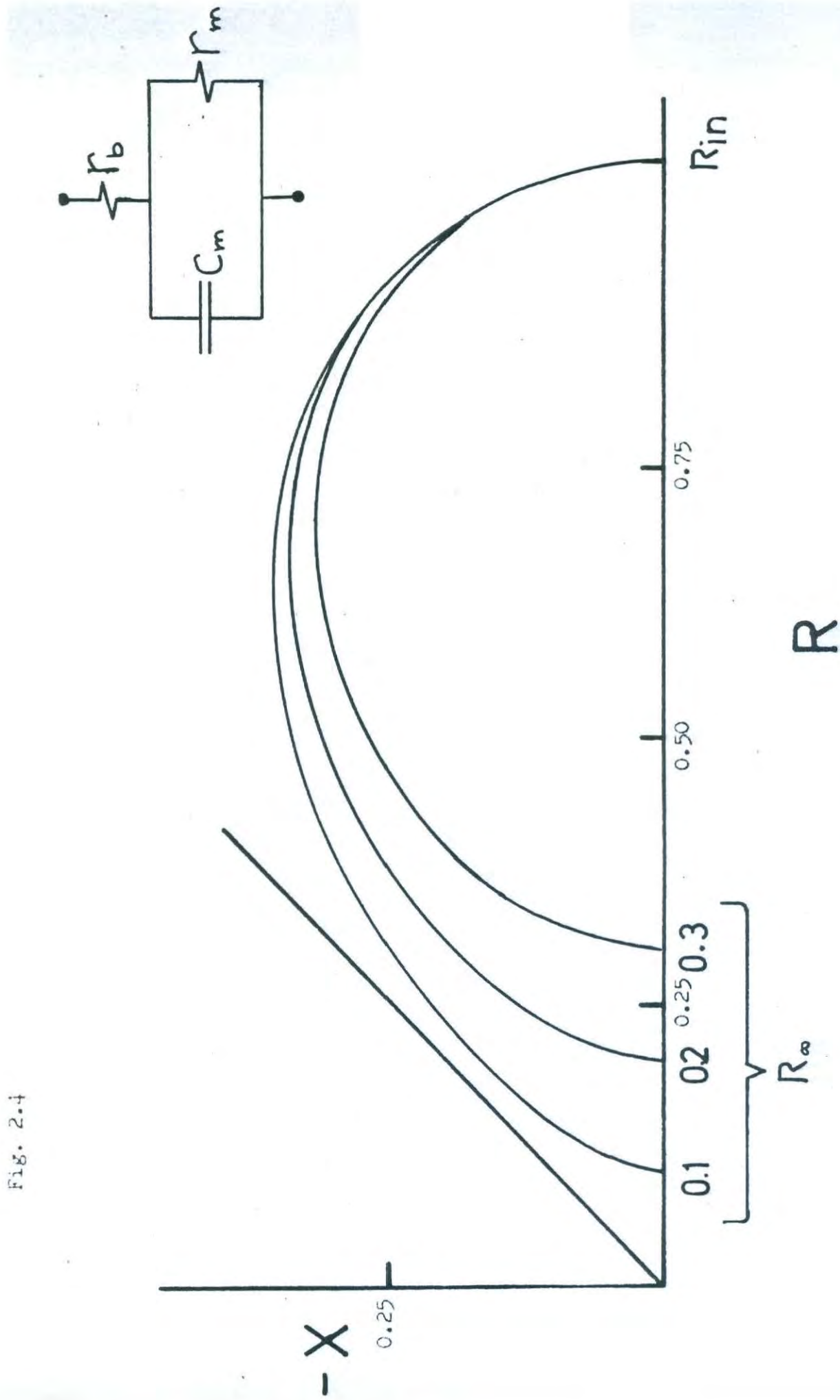


Fig. 2.4

only one parameter $r = r_b/r_m$, the scale factor r_m being set by the input resistance

$$R_{in} = \frac{1}{2} [(r_m + r_b) r_i]^{1/2} \quad (17)$$

The space constant for this model is given by

$$\lambda = \left[\frac{r_m + r_b}{r_i} \right]^{1/2} \quad (18)$$

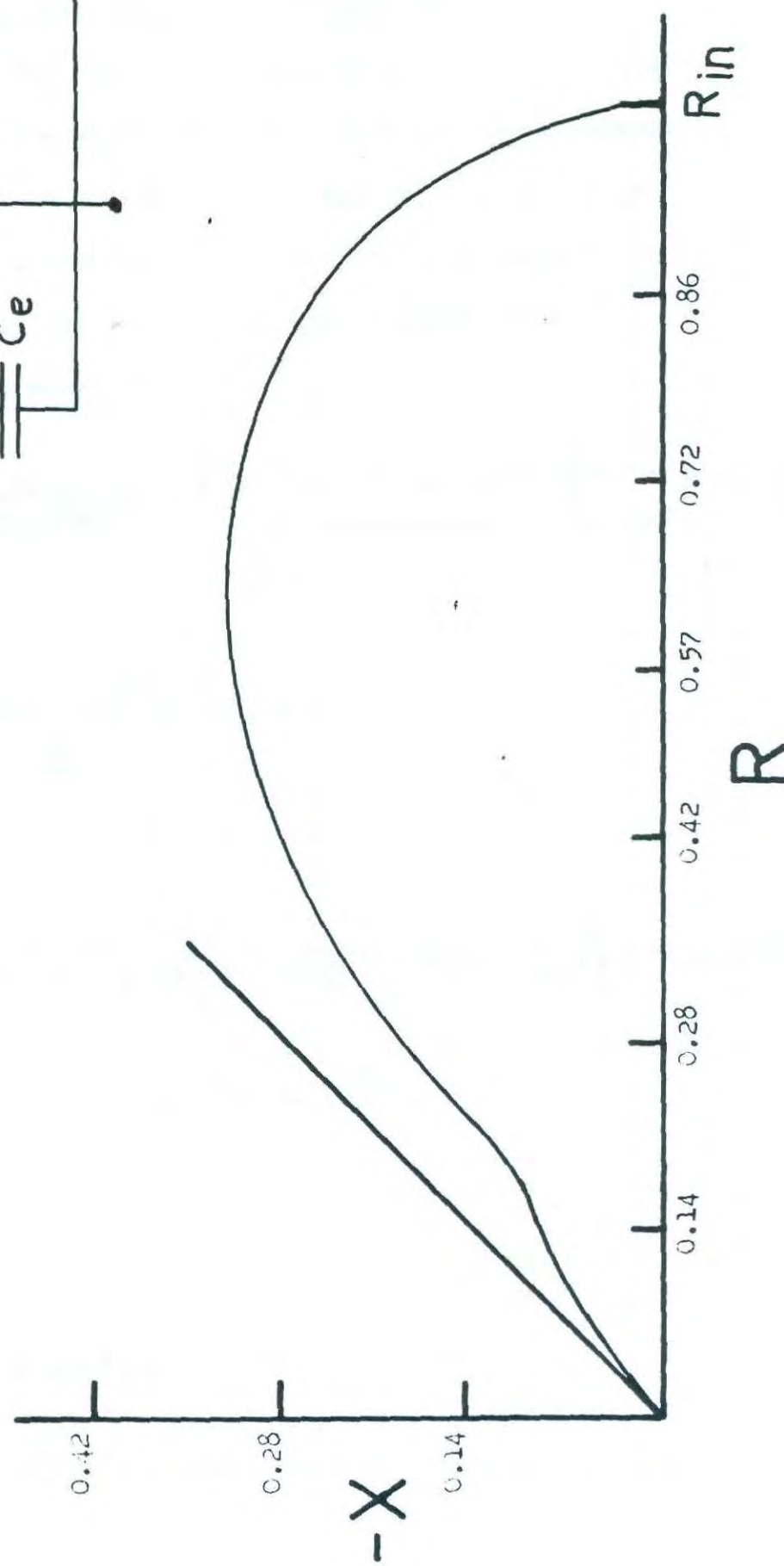
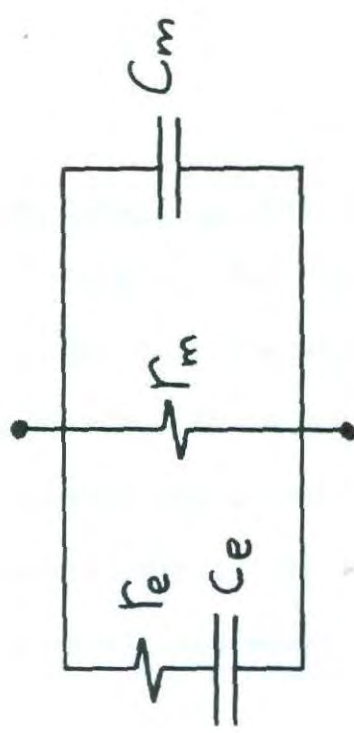
Two Time Constant Model.

Another model of the fibre is shown in Fig. 2.5. In addition to the two parallel paths formed by r_m and c_m as in the simple models, there is a third path through the resistance r_e and capacitance c_e . The inside-outside admittance of this model is given by

$$y r_m = 1 + \frac{\nu^2 r}{1 + \nu^2} + j\nu \left\{ r c + \frac{r}{1 + \nu^2} \right\} \quad (19)$$

using the dimensionless variables

$$\nu = \omega C_e r_e; \quad r = \frac{r_m}{r_e}; \quad C = \frac{c_m}{C_e}$$



Two Time Constant, Distributed Resistance Model.

The circuit for this model is shown in Fig. 2.6. This model is the only one which adequately fits all the impedance loci observed. It is somewhat more complicated than the two time constant model, but this complication is required by the experimental data. The real and imaginary parts of the admittance of this model are

$$gr_m = \frac{\nu^4 r^2 c^2 \frac{r_b}{r_m} + \nu^2 \left\{ \frac{r_b}{r_m} [(1+r)^2 + r^2 c(c+2)] + r+1 \right\} + \frac{r_b}{r_m} + b r_m}{D}$$

$$br_m = \frac{\nu^3 r c + \nu r (1+c)}{D} \quad (20)$$

with

$$D = \nu^4 \left(\frac{r_b}{r_m} \right)^2 r^2 c^2 + \nu^2 \left\{ 1 + 2 \frac{r_b}{r_m} (1+r) + \left(\frac{r_b}{r_m} \right)^2 [r^2 (1+c)^2 + 2r + \left(\frac{r_b}{r_m} + 1 \right)^2] \right\}$$

where the dimensionless variables

Figure 2.6

An Impedance Locus for the Two Time Constant, Distributed Resistance Model

An impedance locus of the circuit shown in the upper right hand corner is shown.

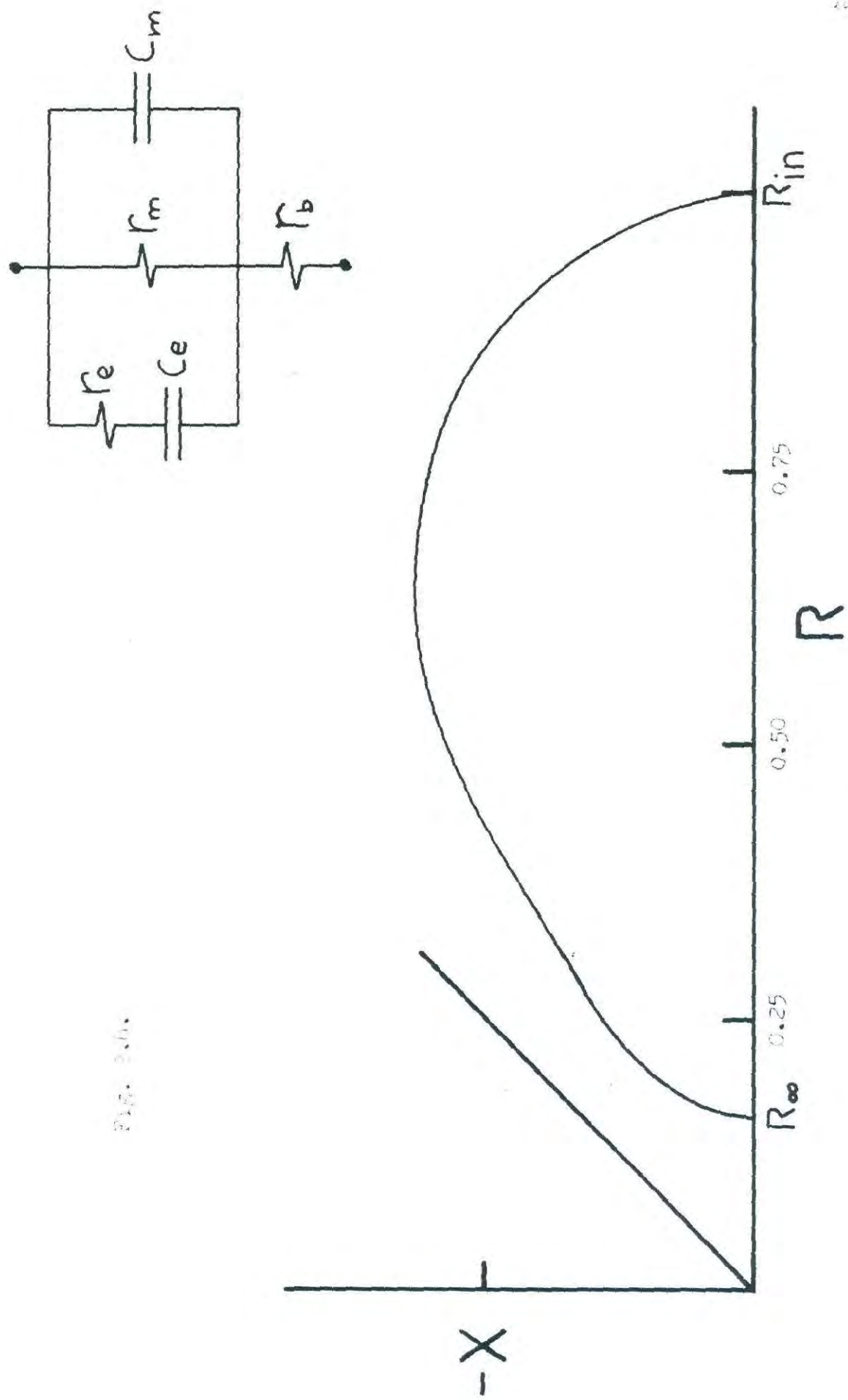
The locus was calculated for the circuit values $C_m/C_e = 1.5$; $R_m/R_e = 2.7$;

$R_b/R_m = 2.4 \times 10^{-2}$; $c_e/r_i = 7.2 \times 10^{-13}$ F/ohm. The impedance locus would

approach the 45° line through the origin if the distributed series resistance

r_b were not present. Scales given in terms of R_{in} . R_∞ , the infinite

frequency resistance equals $0.5 (r_b r_i)^{1/2}$.



$$V = \omega C_e R_e; \quad r = \frac{r_m}{R_e}; \quad C = \frac{C_m}{C_e}$$

are used.

It is instructive to examine the behaviour of this model at high frequencies. The high frequency limiting properties of the distributed admittance are

$$\dot{g} \rightarrow \frac{1}{r_b}; \quad b = \frac{1}{\omega C_m r_b^2} \rightarrow 0; \quad \frac{b}{\dot{g}} = \frac{1}{\omega C_m r_b} \rightarrow 0$$

(neglected terms differ by factors of ω^2).

The corresponding limited behaviour of the lumped impedance is

$$R = \frac{1}{2} (r_o r_i)^{1/2} = R_\infty$$

$$-X = \frac{1}{4\omega C_m} \left(\frac{r_i}{r_b} \right)^{1/2}$$

In other words the resistance remains constant at high frequencies while the reactance decreases in inverse proportion to the frequency. The impedance locus in the X/R plot should then approach the real axis at an angle of 90° . This behaviour is in marked contrast to that of the models without distributed

resistance, where a similar analysis of high frequency behaviour shows that the impedance locus at high frequencies coincides with a 45° line drawn through the origin (Falk & Fatt, 1964). Furthermore, in the model with distributed resistance it is clear that the angle between the real axis and a line drawn from the origin to a point on the impedance locus (the phase angle) must pass through a maximum and then decrease to zero. This can be seen analytically since at high frequency

$$\phi = \arctan \frac{1}{2r_b \omega c_m} \rightarrow 0$$

Other Two Time Constant, Distributed Resistance Models.

It is a basic property of impedance functions that the synthesis problem (the problem of finding a network with a given impedance function) does not have a unique solution. There are many circuits with an impedance function identical with that of the above model. These circuits may be classified into those with the minimum number of circuit elements and those with more than the minimum number of circuit elements.

Only one other equivalent circuit with the minimum number of circuit elements is used here (see Fig. 2.7 for the circuit and the identification of variables). The admittance of this model is

Figures 2.7, 2.8, 2.9

Three Different ~~Nonminimum Resistance~~ Circuits

The equations for these circuits are given in the text. The symbols in the figure identify the circuit elements.

Fig. 2.7

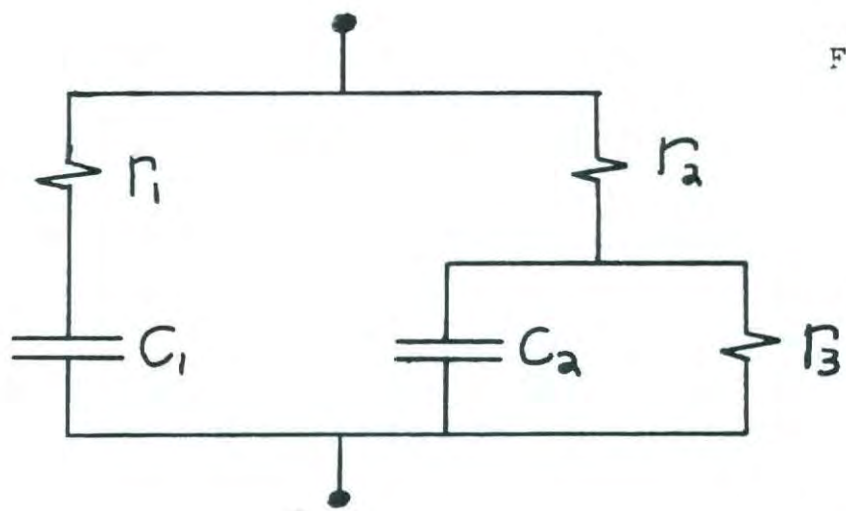


Fig. 2.8

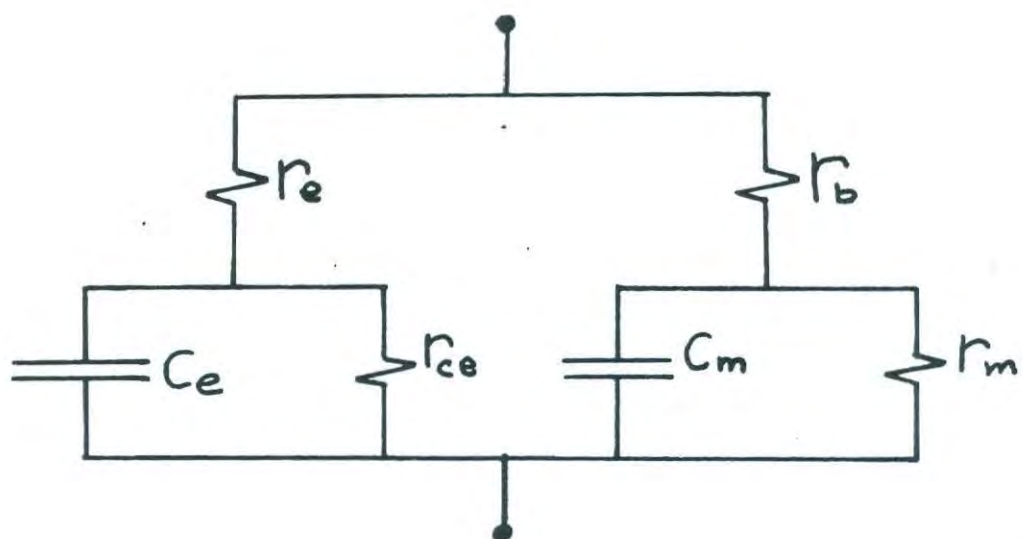
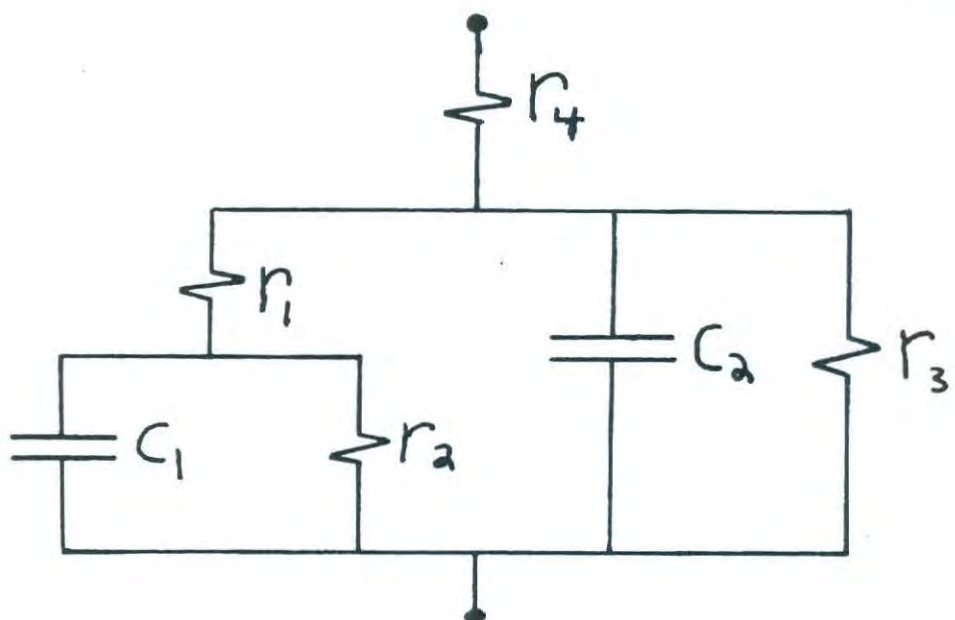


Fig. 2.9



$$\gamma r_3 = \frac{v^2 r}{1 + v^2} + \frac{v^2 r^2 c^2 \frac{r_2}{r_3} + \frac{r_2}{r_3} + 1}{\left[1 + \frac{r_2}{r_3}\right]^2 + v^2 r^2 c^2 \left(\frac{r_2}{r_3}\right)^2} \quad (21)$$

$$+ jv \left\{ \frac{rc}{\left[1 + \frac{r_2}{r_3}\right]^2 + v^2 r^2 c^2 \left(\frac{r_2}{r_3}\right)^2} + \frac{r}{1 + v^2} \right\}$$

where

$$v = \omega C_1 R_1; \quad C = C_2/C_1; \quad r = r_3/r_1$$

It is useful to give the circuit parameters of the model shown in Fig. 2.7 in terms of the circuit parameters of the model shown in Fig. 2.6. The solution to this problem is not unique since the d.c. path across the circuit may be made to shunt either the larger or smaller capacitance. The mathematical reason for this ambiguity is discussed in Appendix 1 to this chapter where the equivalence relations are derived.

This ambiguity does not occur in circuits where the infinite frequency resistance is all located in one circuit element. The values of the circuit elements in a model like that shown in Fig. 2.6 are thus well determined.

The equivalence relations are

$$r_1 = \frac{-H_1(H_2 - H_1)r_b}{(H_1 - d_1)(H_1 - d_2)}$$

$$C_1 = \frac{(H_1 - d_1)(H_1 - d_2)}{r_b H_1^2 (H_2 - H_1)}$$

$$r_2 = \frac{r_b H_1 (H_2 - H_1)}{H_1 H_2 - H_1 (d_1 + d_2) + d_1 d_2} \quad (22)$$

$$r_3 = \frac{r_b H_1^2 (H_2 - d_1)(H_2 - d_2)}{d_1 d_2 [H_1 H_2 - H_1 (d_1 + d_2) + d_1 d_2]}$$

$$C_2 = \frac{-[H_1 H_2 - H_1 (d_1 + d_2) + d_1 d_2]^2}{r_b H_1^2 (H_2 - H_1)(H_2 - d_1)(H_2 - d_2)}$$

where

$$q_{1,2} = \frac{-B \pm \sqrt{B^2 - 4A}}{2A}$$

$$B = r_e C_e + r_m C_m + r_m C_e$$

$$A = r_m r_e C_m C_e$$

$$H_{1,2} = \frac{-D \pm \sqrt{D^2 - 4EF}}{2F}$$

$$D = r_m r_e C_e + r_b [r_e C_e + r_m C_m + r_m C_e] \quad (23)$$

$$E = r_b + r_m$$

$$F = r_b r_m r_e C_m C_e$$

The other set of equivalence relations (for the shunt on the other capacitance) can be found simply by interchanging H_2 and H_1 in (22).

The two circuits with more than the minimum number of circuit elements which are of interest are shown in Fig. 2.8 and Fig. 2.9. In each case one of the resistive shunts on the capacitance is redundant. The equations relating the circuit values of the model shown in Fig. 2.8 with those of the model in Fig. 2.7 are

$$r_e = \frac{1}{K + (1-\alpha)J}$$

$$c_e = \frac{-[K + (1-\alpha)J]^2}{KD_1}$$

$$r_b = \frac{1}{\alpha J + L} \quad (24)$$

$$r_m = \frac{L}{\alpha J(\alpha J + L)}$$

$$c_m = \frac{-(\alpha J + L)^2}{LD_2}$$

With

$$K = \frac{H(D_1 - N_1)(D_1 - N_2)}{D_1(D_1 - D_2)}$$

$$J = \frac{H N_1 N_2}{D_1 D_2}$$

$$L = \frac{H(D_2 - N_1)(D_2 - N_2)}{D_2(D_2 - D_1)}$$

$$N_{1,2} = \frac{-B \pm \sqrt{B^2 - 4A}}{2A}$$

$$D_{1,2} = \frac{-D \pm \sqrt{D^2 - 4FG}}{2G}$$

$$H = A/G ; \quad A = c_1 c_2 r_3 (r_1 + r_2)$$

$$G = c_1 c_2 r_1 r_2 r_3$$

$$B = r_1 c_1 + r_3 c_2 + c_1 (r_2 + r_3)$$

$$D = r_1 c_1 (r_2 + r_3) + r_2 r_3 c_2$$

$$F = r_2 + r_3$$

Finally, the value of r_{ce} (which must be known independently) can be used to determine the parameter 'a' (used in equations

(24))

$$1 - a = \frac{\sqrt{K r_{ce} (K r_{ce} + 4)}}{2 r_{ce} J} - \frac{K}{2J}$$

These equations are ambiguous in that the symmetry of the circuit shown in Fig. 2.8 makes the two parallel branches indistinguishable.

The circuit values of the model shown in Fig. 2.9 can easily be derived from those shown in Fig. 2.6 since both r_b and c_m are unchanged by the presence of r_2 . That is,

$$r_4 = r_b$$

$$c_2 = c_m$$

Physically, this is reasonable since the high frequency behaviour of either circuit is unaffected by the other circuit elements.

The equations giving the other values are

$$\begin{aligned} r_3 &= [\beta/r_m]^{-1} \\ r_1 &= \frac{r_e r_m}{r_m + r_e(1-\beta)} \\ c_1 &= \frac{c_e [r_m + r_e(1-\beta)]^2}{r_m^2} \end{aligned} \tag{25}$$

where β is given (in terms of the independently known parameter r_2) by

$$1 - \beta = \frac{-r_m r_2 + r_m \sqrt{r_2^2 + 4 r_2 r_e}}{2 r_2 r_e}$$

Curve Fitting Methods.

An attempt was made to fit the observed impedance loci using the methods of Falk & Fatt (1964). Each of the approximations used there presented difficulties here. The low frequency plot was unreliable because of the presence of a very low frequency dispersion. The high frequency plot was applicable at only the very highest frequencies and thus was quite inaccurate. The mid-frequency approximation to the shape of the curve was not applicable because of the particular parameter values of crab fibres. Finally, the strong interaction of the various parameters prevented the refinement of inaccurate values by successive approximation. It was thus necessary to develop another curve fitting technique.

The principle of the technique developed was to choose circuit parameters so that the deviation of the theoretical curve from the observed points was minimized. The deviation was defined as the sum of the squared deviations from each experimental point. The most satisfactory fits were found if the theoretical curve was fitted simultaneously to the phase characteristic and the X/R plot. (The reason for this is that the phase characteristic is particularly sensitive to small parameter changes.) The function minimized was

$$\sum_{i=1}^K \left\{ a_i^2 [R_{\text{cal}}^{(i)} - R_{\text{obs}}^{(i)}]^2 + b_i^2 [-X_{\text{cal}}^{(i)} - (-X_{\text{obs}}^{(i)})]^2 + c_i^2 [P_{\text{cal}}^{(i)} - P_{\text{obs}}^{(i)}]^2 \right\} \quad (26)$$

$i = 1, 2, 3, \dots$

where

K is the number of experimental observations (the number of frequencies at which impedance measurements were taken).

i represents the i^{th} observation, made at frequency f_i .

$R_{\text{obs}}^{(i)}$, $-X_{\text{obs}}^{(i)}$, and $P_{\text{obs}}^{(i)}$ are the resistance and reactance (in kohms) and phase (in degrees) measured at frequency f_i , respectively.

$R_{\text{cal}}^{(i)}$, $-X_{\text{cal}}^{(i)}$, and $P_{\text{cal}}^{(i)}$ are the resistance, reactance, and phase (same units as above) calculated at frequency f_i , respectively.

a_i , b_i , c_i are the weights assigned to the resistance, reactance, and phase measurements made at frequency f_i , respectively.

(Absolute rather than relative deviation is minimized since the random error was felt to be relatively independent of frequency)

An electronic digital computer (The London University Atlas) was used to compute and minimize the function defined above.

Library Routine 970, written by D.C. Cooper and D.J. McConalogue using the method of Rosenbrock (1961) and McConalogue and Strickland (1963), found the minimum reasonably quickly, provided none of the parameters were too near zero. The program was checked by using different step lengths, initial values, and accuracies of minimization. The major difficulty with this method is that it cannot distinguish between systematic and random errors. The choice of the weights could compensate for this difficulty to some extent. Because relatively small changes in circuit parameter values (say 15 per cent) produced large changes in the fit of the curve, it is felt that the parameter values are well determined by the impedance measurements, to an accuracy of about fifteen per cent.

A version of this program, written in Extended Mercury Autocode (EMA) is presented in Appendix 2 of this chapter.

APPENDIX 1 TO CHAPTER 2.

Derivation of the Equivalent Relations.

The conventional method of finding the relations between circuit values in potentially equivalent circuits involves the simultaneous solution of several equations, usually those describing the infinite frequency and zero frequency behaviour of the circuit, and those describing the time constants of response to a step function of applied current or voltage (Starr, 1938). Since these equations are usually quadratic, the mathematical difficulties in finding the simultaneous solution are formidable. Another method of developing equivalence relations is given here.

If the impedance function is regarded as known, the problem of finding the equivalence relations reduces to the problem of synthesizing a network of given configuration from a known impedance function. This is a problem similar to those handled in the theory of network synthesis and so the methods developed in Tuttle (1958) ~~and Guillemin (1957)~~ can be used. The basic approach is to synthesize part of the network from the given impedance function and then remove that part of the circuit. The remaining circuit is synthesized one part at a time, each time removing the part just synthesized. This process of synthesis and removal is continued until the entire network is synthesized. By

using different standard ('canonic') forms for realizing (synthesizing) each part of the circuit, almost any configuration can be built up. For example, one way of synthesizing the circuit in Fig. 2.7 (not the method used below) is by first using the parallel branch canonic form and then treating the remainder as a ladder standard form. In some cases the possibility of using different methods of synthesis leads to ambiguity in the final equivalence relations. These cases will be discussed as they arise.

The first equivalence relations derived are those between the networks shown in Fig. 2.6 and Fig. 2.7. The admittance of the circuit shown in Fig. 2.6 is known. The problem is then to synthesize a network of form given in Fig. 2.7 from the admittance function given in (20).

It is convenient to write the admittance in terms of the complex frequency variable s

$$Y_{R_b} = \frac{s^2 + s \frac{r_{eC_e} + r_m C_m + r_m C_e}{r_m r_e C_m C_e} + \frac{1}{r_m r_e C_m C_e}}{s^2 + s \frac{r_m r_e C_e + r_b(r_{eC_e} + r_m C_m + r_m C_e)}{r_b r_m r_e C_m C_e} + \frac{r_b + r_m}{r_m r_e C_m C_e}}$$

Factoring numerator and denominator gives

$$\frac{Y}{r_b} = \frac{(s - q_1)(s - q_2)}{(s - H_1)(s - H_2)} \quad (27)$$

where the symbols on the right hand side of the second equation are defined in (23) of the text.

This admittance is now divided by s and expanded into partial fractions.

$$\begin{aligned} \frac{Y}{s} &= \frac{q_1 q_2}{H_1 H_2 r_b} \frac{1}{s} + \frac{(H_1 - q_1)(H_1 - q_2)}{r_b H_1 (H_1 - H_2)} \frac{1}{s - H_1} \\ &\quad + \frac{(H_2 - q_1)(H_2 - q_2)}{r_b H_2 (H_2 - H_1)} \frac{1}{s - H_2} \end{aligned} \quad (28)$$

Either the second or the third term can be synthesized as the branch containing r_1 , c_1 (Fig. 2.7). Only one of these two ambiguous cases will be developed here. It is clear that the other can be derived simply by interchanging H_1 and H_2 in all the following equations. The form of the admittance of the branch containing r_1 and c_1 in series is

$$\frac{1}{r_1 + \frac{1}{SC_1}} = \frac{SC_1}{1 + SC_1 r_1} \quad (29)$$

The equivalence relations can be found simply by examining the behaviour of (29) and the second term of (28) at the extremes of frequency.

The admittance remaining when this branch has been synthesized and removed is called Y' and can be written as

$$Y' = \frac{q_1 q_2}{H_1 H_2 r_b} + \frac{(H_2 - q_1)(H_2 - q_2)}{r_b H_2 (H_2 - H_1)} - \frac{s}{s - H_1} \quad (30)$$

$$= \frac{s - \frac{q_1 q_2 (H_2 - H_1)}{H_1 H_2 - H_1 (q_1 + q_2) + q_1 q_2}}{s \left\{ \frac{r_b H_1 (H_2 - H_1)}{H_1 H_2 - H_1 (q_1 + q_2) + q_1 q_2} \right\} - \frac{r_b H_1 H_2 (H_2 - H_1)}{H_1 H_2 - H_1 (q_1 + q_2) + q_1 q_2}}$$

But this has the same form as the admittance of the second branch (consisting of r_2 , r_3 , and c_2) in Fig. 2.7. The admittance of this second branch is

$$Y' = \frac{1 + SC_2r_3}{r_2 + r_3 + SC_2r_3r_2} = \frac{s + \frac{1}{r_2C_2}}{sr_2 + \frac{r_2 + r_3}{C_2r_3}} \quad (31)$$

Again, examination of the behaviour of these expressions at the extremes of frequency enables the equivalence relations to be derived.

The equivalence relations between circuits with redundant parameters are also required. It is straightforward, using the above techniques, to go from the parameter values of a redundant circuit to those of a non-redundant circuit. However, we need the relations the other way round: going from the parameter values of a non-redundant circuit to those of a redundant circuit, the redundant parameter assumed known from other information. The difficulty here is that some, perhaps all the parameter values of the circuit being synthesized depend on the value of the redundant parameter. The synthesis of the circuit shown in Fig. 2.8 from the impedance of the circuit shown in Fig. 2.7 is a case in point since all the parameter values depend on the value of the redundant element r_{ce} .

If the admittance function (21) is written in terms of the complex variable s , divided by s , expanded into partial

fractions, and multiplied by s , the result is

$$y = J + \frac{KS}{s - D_1} + \frac{LS}{s - D_2} \quad (32)$$

where the symbols J , K , D_1 , D_2 are as defined in (24). Since the circuit we wish to synthesize has two d.c. paths, it is necessary to split the corresponding term (the first term in (32)) into two parts.

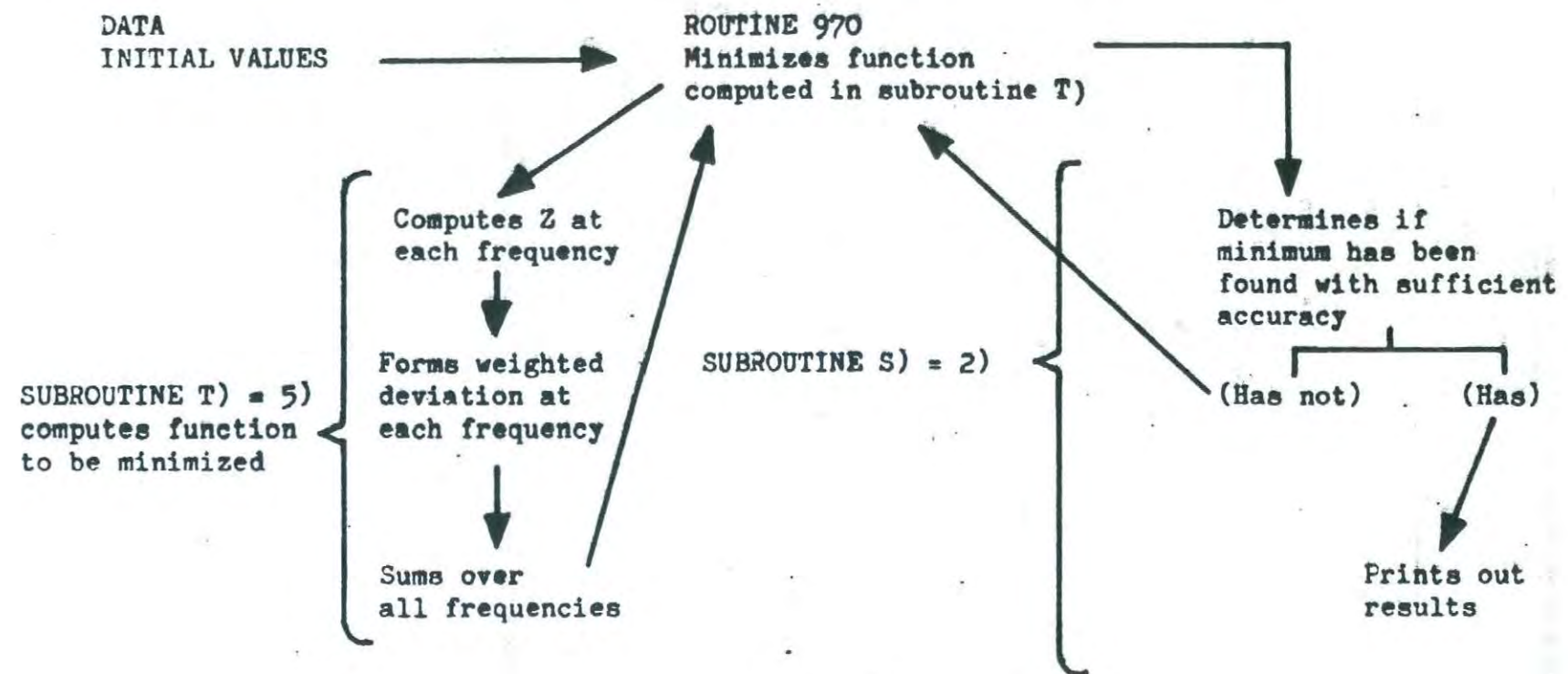
$$y = (1-a)J + \frac{KS}{s - D_1} + aJ + \frac{LS}{s - D_2} \quad (33)$$

$$0 \leq a \leq 1$$

The procedure is then to synthesize the desired circuit, one branch being equivalent to the first two terms of (33), the other to the last two terms of (33). The expressions for all the parameters will contain the parameter 'a' but 'a' can be found by solving for 'a' in the expression for r_{ce} .

A similar procedure enables the equivalence relations (25) to be derived.

FIGURE 2.10: FLOW CHART OF COMPUTER PROGRAM FOR CURVE FITTING



APPENDIX 2 TO CHAPTER 2.

Curve Fitting Computer Program.

The following is an annotated version of one of the computer programs used to fit the impedance measurements. The program is written in a user oriented computer language Extended Mercury Autocode (Brooker, Richards, Berg, and Kerr, 1961). A flow diagram illustrating the basic method of computation is shown in Fig. 2.10. This program fits the impedance data with the model shown in Fig. 2.6.

PROGRAM	COMMENTS
JOB LSM ₃₂ EAR, RS EISENBERG RUN 5 SEPT 30 COMPUTING 15000 INSTRUCTIONS OUTPUT o LINE PRINTER 2000 LINES STORE 25 BLOCKS COMPILER EMA	Job description which names the program, allocates total computing time, output space, and memory space.
AUXILIARY(0,100) DUMPS o	Sets number of auxiliary variables required
MAIN>600	Sets number of subscripted variables required
ROUTINE 970	

Instead of the text of Routine 970 which would appear here in the program, we present the specifications of the Routine.

The minimum value of the function is left in F' and the corresponding values of the independent variables in $Y_0, Y_1 \dots Y(N - 1)$.

$I, J, Q, R, S, T, N, U', V', F', G', H', E'$ are used by the routine. I, J, Q may be used for working space by either subroutine. G', H', E' may be used as working space by subroutine S).

Subroutine T) computes the function of the variables Y_0, \dots to be minimized

Subroutine S) determines when the minimum is known with sufficient accuracy. It then prints out the desired data and, by setting $R = 0$ instructs the routine to return to the appropriate place in Chapter O.

The program works most efficiently if all the Y 's are of the same order of magnitude. For that reason one of our variables c_e/r_i is written as the product $X' Y_2$. Y_2 can then be chosen to be of the same magnitude as the other Y 's.

CHAPTER 0

A>50
B>50
C>50
D>50
E>50

Directives allocating space for subscripted variables

V>35

H>35
U>35

G>50
Y>10
E>10
V>50
X>50

F=0.02
N=3
Un=0
Vm=50

Setting variables required by Routine 970

S)=2)
T)=5)

Setting labels required by Routine 970

READ(Kn)
In=r(1)Kn

Cycle enabling K batches of data to be processed in one run

F=0.02

NEWLINE
1065, 0, 0, 5.1
NEWLINE
CAPTION
RUN ON DATA NO.
PRINT(In) 1,0
*
READ(en)

Identifies each batch of data in output

Sets accuracy with which minimum is computed

N=4

A is R_{in} (kohms)

READ(A)
READ(Y3)

Y_3 is the initial guess for R_{∞} (kohms)

A=1000A

Converts to ohms

READ(Y0)
READ(Y1)
READ(Y2)

Y_0 is the initial guess for C_m/C_e

Y_1 is the initial guess for R_m/R_e
 Y_2 times X' is the initial guess for C_e/R_f

READ (Xn)
READ (P)
READ (M)

P is the number of observed impedances

M is the number of sets of reactance weightings

L=0

JUMP 17

>>COMPUTES R, -X AND MINIMIZES DEVIATIONS FROM OBSERVED DATA

S) F=0

Subroutine for computing function to be minimized: the deviation from the theoretical curve

U=r1000Y3
C=XDIVIDE(UU,AA-UU)
U=xSQRT(AA-UU)

Computes theoretical curve for given set of Y's

K=r(1)P
V=4XnY2WKUU/Yr

>>COMPUTES DENOMINATOR OF LUMPED EQUATIONS

D=CCVVVVVYoYrYrYr+VVCCYrYrYrYo+2VVCCYrYrYrYo+VVCCYrYr+2VVC*Yr
D=2VVCCYr+2VVC+VVCC+VV+CC+2C+D+r

>>COMPUTES RM XG

XG=VVVVVCYoYrYrYr+VVCYrYrYrYo+2VVCYrYrYrYo+VVCYrYr+2VVCYr+VVYr
G=VVC+VV+C+*XG+r

Computes the distributed conductance

G=G/D

*>>COMPUTES RM XB

B=VVVYrYr+VYr+VYrYo
B=B/D

Computes the distributed susceptance

E=GG
Y=xSQRT(r+BB/G)

Computes lumped parameters

W=xSQRT(2G+2BB/G)
E=xSQRT(Y+r)

G=UE/W
X=xSQRT(Y-r)

X=UX/W

Converts to kohms

GKX=G/r1000
XK=X/r1000

>>COMPUTES THE WEIGHTED DEVIATIONS SQUARED

HK=XARCTAN(GK,XK)
UK=XARCTAN(AK,BK)

HK=1.80HK/E
UK=1.80UK/E

F=F+VKHKHK-2VKHKUK+VKUKUK

H=CKAKAK-2CKAKGK+CKGKGK+DKBKBK-2DKXKBK+DKXXK

F=F+H

REPEAT

RETURN

2) L=L+1
EL=F

Determines if minimum has been found with sufficient accuracy

JUMP 3, L=1
V=EL-E(L-1)
V=XMOD(V/EL)

JUMP 3, V>E

10) R=0

Prints output

NEWLINE

CAPTION

NUMBER OF ITERATIONS IS

PRINT(L) 2,0

NEWLINE

CAPTION

MINIMUM SUM OF DIFFERENCES SQUARED**IS

*

PRINT(F) 0,6

NEWLINE

CAPTION

FOR CM/CE=

PRINT(Y) 3,3

CAPTION

,RM/RE=

PRINT(Y) 3,3

CAPTION

,CE/R=

PRINT(XNY) 0,4

CAPTION

AND R00=

PRINT(Y₃) 3,3
 NEWLINE
 1065, 0, 0, 5, 1
 NEWLINE
 NEWLINE
 NEWLINE

Explanation of what is being printed
 can be found in program itself

K=r(r)P
 Wn=0.5WK
 Wn=Wn/E

NEWLINE
 PRINT(Wn) 5,3
 CAPTION
 C/S

NEWLINE
 CAPTION
 R WEIGHTING IS
 PRINT(CK) 2,0
 NEWLINE
 CAPTION
 -X WEIGHTING IS
 PRINT(DK) 2,0

NEWLINE
 CAPTION
 R OBS.=
 PRINT(AK) 2,3
 CAPTION
 R CALC.=
 PRINT(GK) 2,3

NEWLINE
 CAPTION
 -X OBS=
 PRINT(BK) 2,3
 CAPTION
 -X CALC.=
 PRINT(XK) 2,3

NEWLINE
 NEWLINE

Z=XRADIUS(AK,BK)
 CAPTION
 /Z0BS/=
 PRINT(Z) 2,3
 Zn=XRADIUS(GK,XK)
 CAPTION
 ,/ZCALC/=

Computes magnitude of impedance

```

PRINT(ZN) 2,3
NEWLINE
CAPTION
OBS. PHASE IS
Z=XARCTAN(AK,BK)          Computes phase

PRINT(180Z/E) 3,2
CAPTION
DEGREES, CALC. PHASE IS

Z=XARCTAN(GK,XK)
PRINT(180Z/E) 3,2
CAPTION
DEGREES

GN=XSIN(KE/4)
GN=XMOD(GN)

JUMP 47, GN>0.0001
NEWLINE
1065, 0, 0, 50
47)GN=0

NEWLINE
NEWLINE
NEWLINE
NEWLINE
REPEAT
3)RETURN

17)K=1                         Reads in data
K=1(P)
READ(WK)
READ(AK*)                      Cycle reads in at each frequency:
                                 Wk, the frequency
                                 Ak, R (resistance)

READ(CK)
READ(BK)
READ(DK)                        Ck, the R' weighting
                                 Bk, X (reactance)
                                 Dk, X weighting

READ(VK)                        Vk, the phase weighting

WK=2EWK
REPEAT

O=1(M)

JUMP 57, O=1

```

X=1(1)P
READ(DK)

Reads in additional set of
X weightings, if desired

REPEAT

F=0.03

*

NEWLINE

1065, 0, 0, 5.1

S1)JUMPDOWN(R970)

Calls in Routine 970.

REPEAT

REPEAT

END

CLOSE

>

***T

End of program tape

The following explains the format of the data. In the typewritten text brackets surround the name and meaning of the number found in the corresponding position (but without brackets) on the print out of a data tape shown on the next page. Every end of a line in the print out is indicated below with the symbol NL. To illustrate: π' corresponds to the first number on the second line of the print out; A, to the second number in the second line; etc.

(K' the number of batches of data) NL

(π' the accuracy of the minimum)

(A the value of the input resistance)

(Y3 the estimate of the infinite frequency resistance)

(Y0 the estimate of C_m/C_e)

(Y1 the estimate of R_m/R_e)

(Y2 a factor of the estimate of c_e/r_i)

(X' a factor of the estimate of c_e/r_i)

(P the number of observed impedances)

(M the number of batches of reactance weightings) NL

(ω_k the frequency)

(Ak the observed resistance)

(Ck the weighting of the resistance)

(Bk the observed reactance)

(Dk the weighting of the observed reactance)

(V_k the phase weighting) NL

This last line is repeated once for each frequency at which impedance measurements were made; that is, P times.

The entire set of data is repeated (with the exception of K') for each batch of data.

Only the first batch of data is shown here:

2

0.0001	20.73	0.5	2	1	8	1,-13	24	1
--------	-------	-----	---	---	---	-------	----	---

1.000	20.79	1	1.69	1	0.5
1.168	20.09	1	2.86	1	0.25
2.154	19.70	1	3.43	1	0.25
3.162	19.23	1	4.11	1	0.25
4.642	17.89	1	5.52	1	0.25
6.814	15.67	1	6.30	1	0.25

10.00	13.46	1	6.74	1	0.25
14.68	11.02	1	7.05	1	0.25
21.54	9.02	1	6.87	1	0.25
31.62	7.13	1	5.89	1	0.25
46.42	5.97	1	5.22	1	0.25
68.14	4.24	1	3.90	1	0.25

10000	3.72	1	3.24	1	0.25
1468	3.28	1	2.68	1	0.25
2154	2.83	1	2.16	1	0.25
3162	2.53	1	1.90	1	0.25

XXXXXX					
16.42	2.10	1	1.50	1	0.25
68.14	1.91	1	1.21	1	0.25

1000	1.59	1	1.03	1	0.25
1468	1.48	1	0.84	1	0.25
2154	1.42	1	0.74	1	0.25
3162	1.31	1	0.58	1	0.25
4642	1.06	1	0.56	1	0.25
6814	1.00	1	0.41	1	0.25

Chapter 3.

METHODS.

Material and Apparatus.

The preparation used in these experiments was the flexor of the carpopodite of the first walking leg of Fortunus depurator and Carcinus maenas bathed in crab Ringer solution (Pantin, 1934; Fatt & Katz, 1953a). The flexor muscle was exposed by removing the opposite part of the shell, together with the extensor muscle and limb nerves. The shell beneath the flexor was removed to improve visibility and the muscle viewed in transmitted light. Surface fibres in the middle half of the muscle and on the wide side of the apodeme were used for these experiments.

Micropipettes with resistances of about 4 megohms (measured when dipping into crab Ringer) were inserted into fibres on the exposed surface of the muscle under microscopic observation. Microelectrodes used to apply current to the muscle fibre were filled with 2M sodium citrate (pH 6) since these passed greater currents than the microelectrodes, filled with 3M KCl, which were used to record potential. Measurements of distance were made with the eyepiece graticule of the microscope.

Figure 3.1 shows a schematic drawing of the experimental set-up. The cathode followers (shown in Fig. 3.1 as triangles

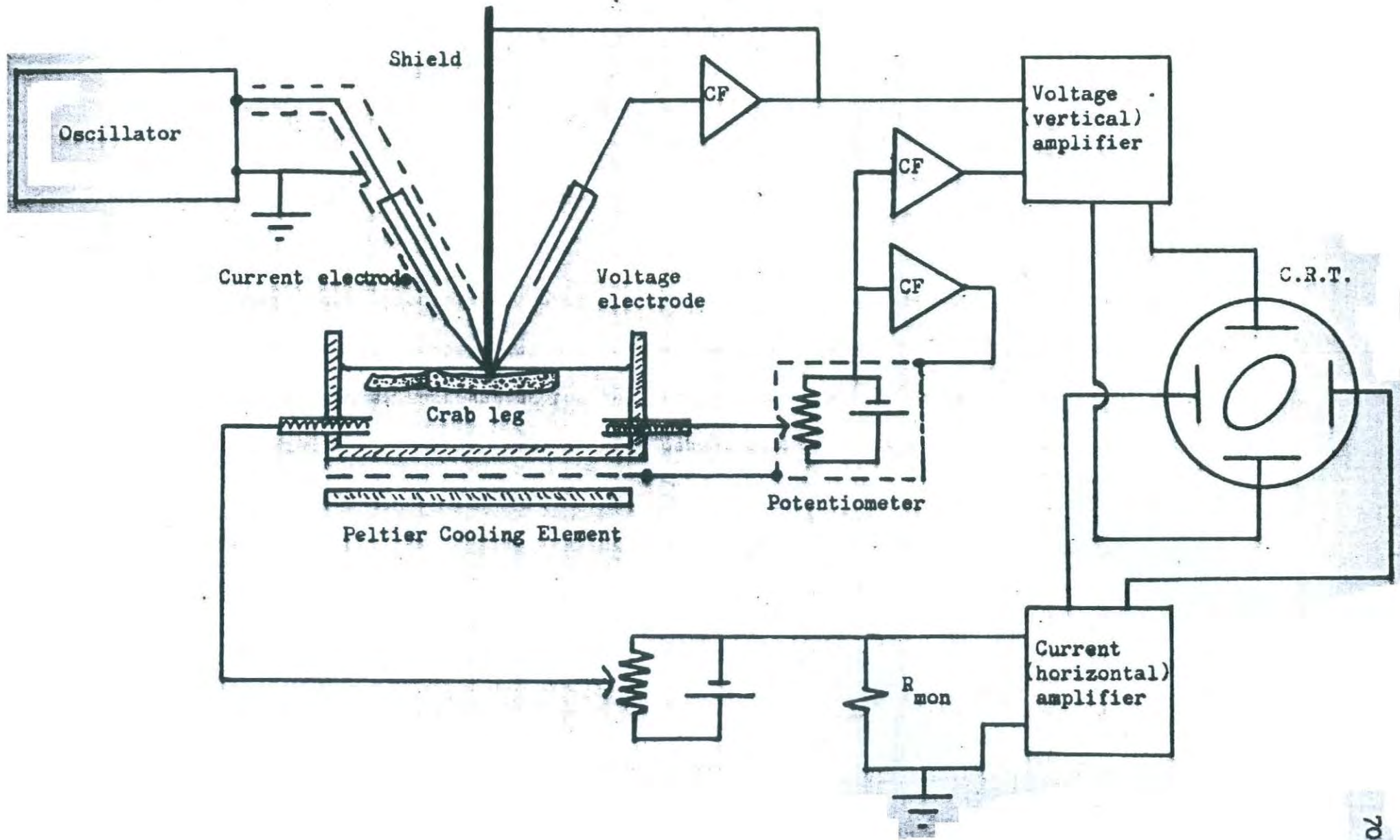
Figure 3.1

Diagram of the Set-up used for the Measurement of Impedance with Microelectrodes

The triangles surrounding the letters "CF" represent cathode followers.

In most experiments a cathode follower was used between R_{mon} and the current amplifier. Identification of symbols and further discussion found in text.

Fig. 3.1



surrounding the letters "CF") used for differential voltage measurements were arranged so that a small amount of attenuation could be applied to one or the other to improve the rejection ratio of the recording system. The potentiometer was a d.c. voltage source used to offset the resting potential of the muscle fibre and was replaced with a calibrator to measure the gain of the voltage and current recording channels. The potentiometer was enclosed in a screening box driven by a separate cathode follower in order to reduce the capacitance to earth, which would otherwise significantly shunt the current monitoring resistance at high frequency. The calibrator could not be used to offset the resting potential since its ^{effective} capacitance to earth was quite large even when enclosed in a driven box.

Because of the large temperature co-efficient of membrane resistance in crab muscle (Fatt & Katz, 1953a) temperature had to be accurately controlled. A semiconductor constant temperature device (Copeland, 1961, 1962) was used to maintain the muscles at a constant temperature ($\pm 0.1^{\circ}\text{C}$) around 5°C . This device introduced a large capacitance to earth since the cooling elements in the circuit were essentially earthed and were close to the bathing solution. This capacitance was reduced by placing an insulated shield between the cooling elements and the bath and driving it from the same cathode follower which drove the potentiometer box.

The current monitoring resistance (R_{mon} in Fig. 3.1) was a wire-wound resistor of negligible inductance of 5.1, 10.2, or 20 kohms. A small battery and voltage divider, as shown in Fig. 3.1 were used to apply a d.c. voltage between the monitor resistance and the bath electrode to prevent d.c. current from flowing through the current microelectrode. With some electrodes the net d.c. current was made inwards since this increased the stability of the electrode resistance and enabled the electrode to pass more current. This inward current produced a change in membrane potential of about 5 mV.

An oscilloscope with high gain d.c. amplifiers (in early experiments a Furzehill 0.180, later a Tektronix 502A) was used to display the instantaneous current-voltage relation as a Lissajous figure. In other words, the oscilloscope was connected for XY plotting with the current signal applied to the horizontal amplifier and the voltage signal applied to the vertical amplifier. A particular Lissajous figure, an ellipse, is described by the oscilloscope spot when the current and voltage signals are both sinusoidal with the same frequency. The characteristics of the ellipse give the phase angle between the signals and their relative magnitude. If one of the signals represents current flowing through a system and the other represents the potential across the system, the phase angle and relative magnitude represent the phase and magnitude of the complex impedance of the

system. Lissajous figures give a more accurate measurement of phase under most conditions than the measurement of delay between two signals, each displayed on a time base.

The measured parameters of the ellipse are shown in Fig. 3.2. The phase angle was computed by one of the three formulae

$$\sin \phi = \frac{D_w}{D_y} ; \quad \sin \phi = \frac{D_x}{D_z}$$

$$\sin \phi = \frac{AB}{D_y D_z}$$

where

ϕ = the phase angle

D_y is the maximum horizontal displacement

D_z is the maximum vertical displacement

D_x is the vertical displacement at half width

D_w is the horizontal displacement at half height

A is the major axis of the ellipse

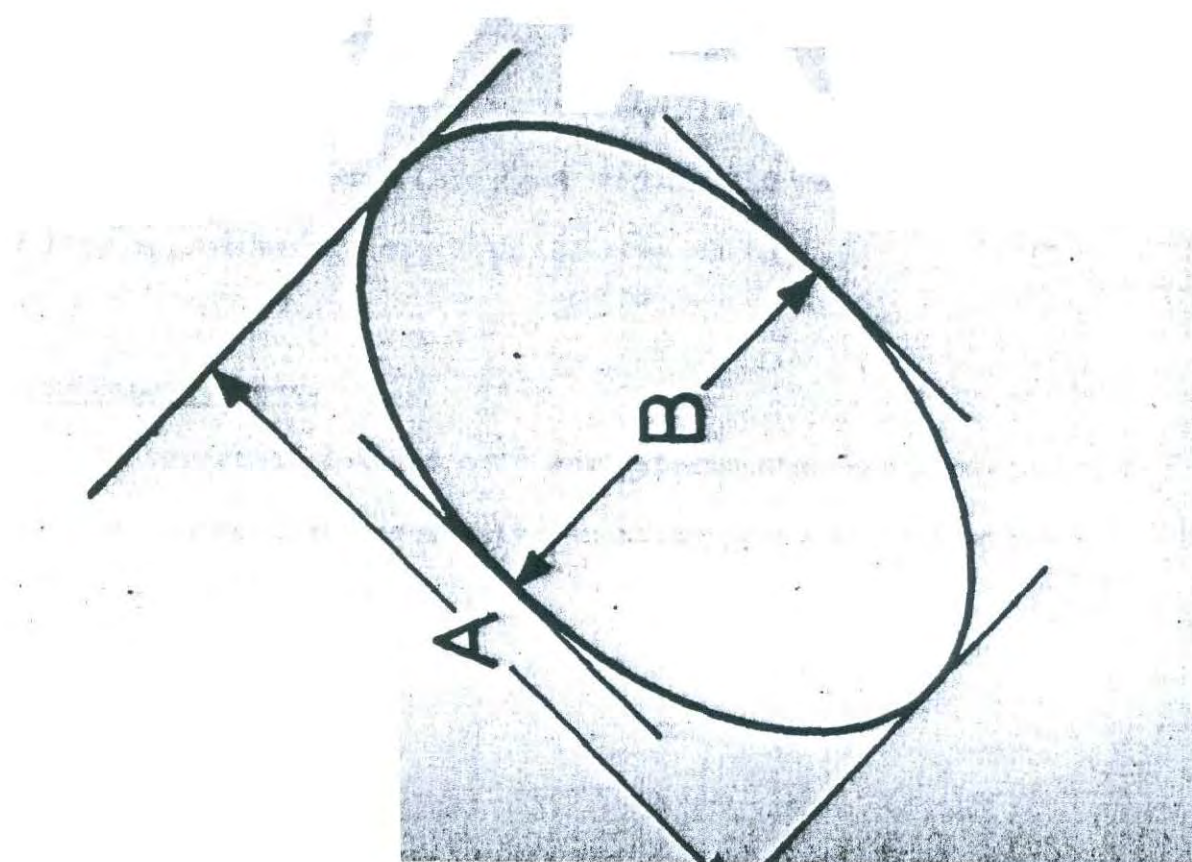
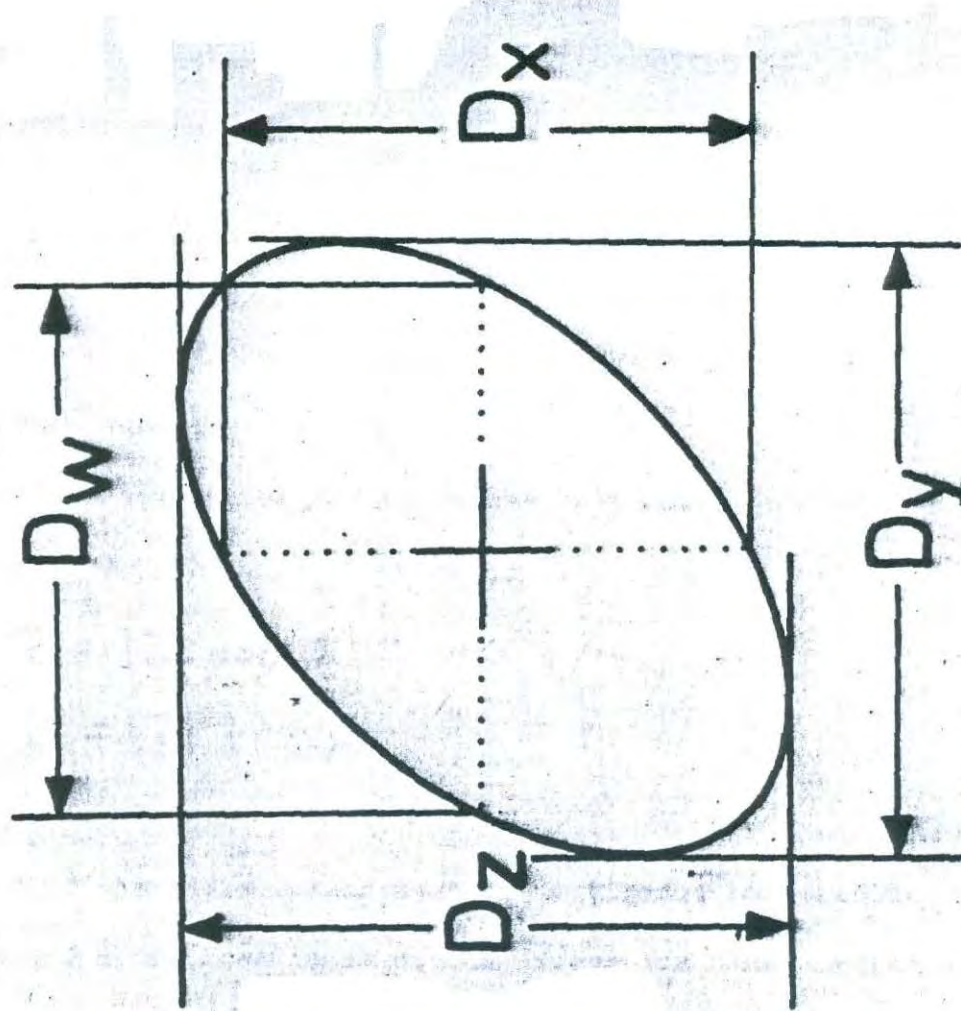
B is the minor axis of the ellipse

The average of the three values was taken when particular accuracy was desired.

Figure 3.2

A Diagram showing the Method of Measurement of Phase Angle Ellipses

Symbols defined in text. The ellipses represent the path followed by the oscilloscope spot when sinusoidal signals of the same frequency are applied to both the horizontal and vertical plates of the cathode ray tube. The phase angle and relative magnitude of the signals applied to the two sets of plates can be calculated from the characteristics (A , B , D_z , etc.) of the ellipse by the equations given in the text.



The magnitude of the impedance is

$$|Z| = k \frac{D_z}{D_y}$$

where k is the gain of the voltage channel divided by the gain of the current channel.

From these quantities the effective resistance and reactance can be calculated:

$$R = |Z| \cos \phi$$

$$X = |Z| \sin \phi$$

The accuracy of the basic measurements is estimated to be about 2° in phase and 2 per cent in magnitude except for phase angles close to 90° where the phase error is about 6° . A discussion of the measurement of phase angle ellipses and the errors involved can be found in Benson & Carter (1950) and Benson (1953). As might be expected intuitively, the overall ratio of signal to noise is largest when k is chosen so that the height of the ellipse (D_z) is approximately equal to the breadth (D_y).

Stray Capacitances.

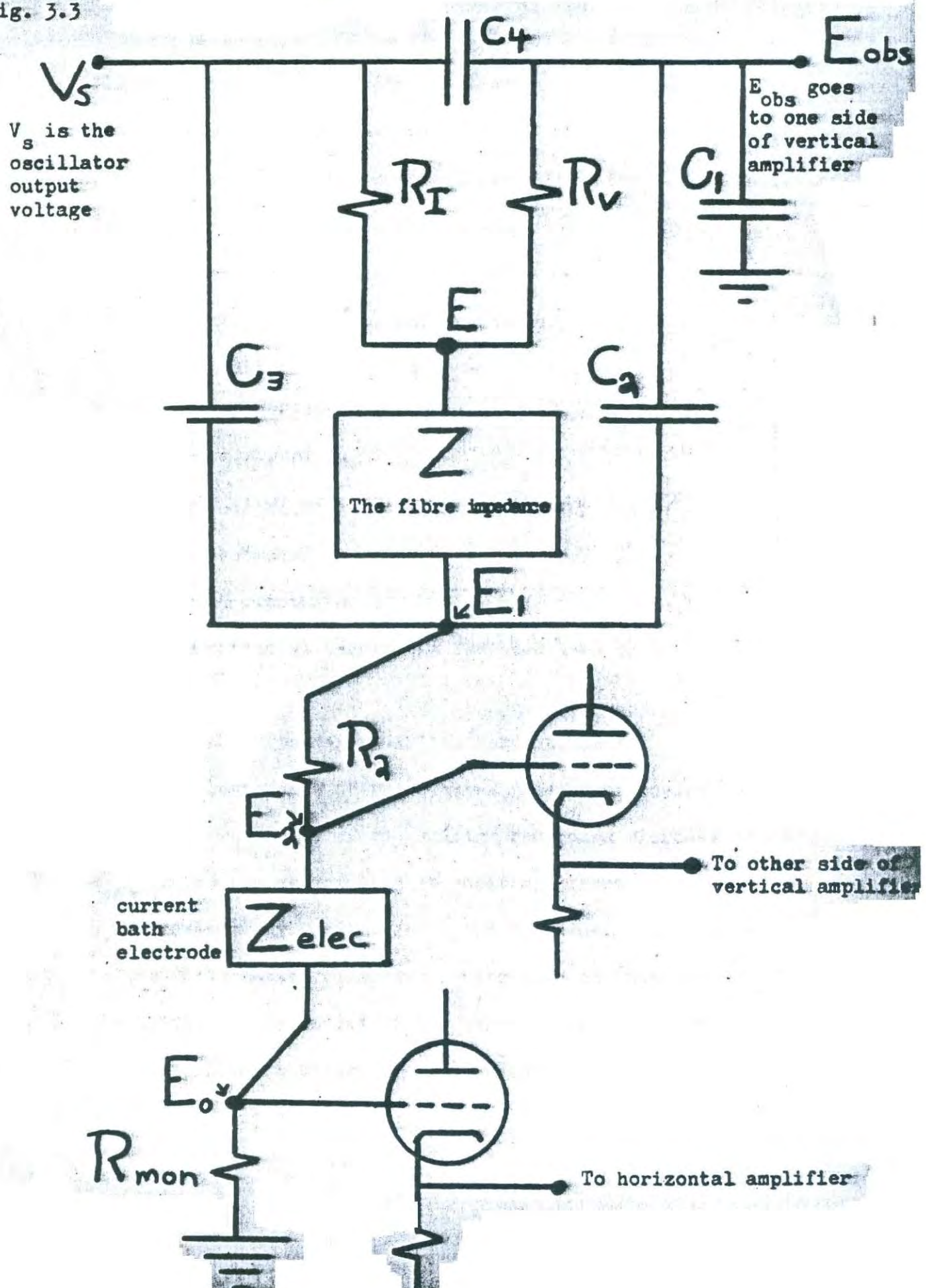
An important feature of these experiments were the measures taken to reduce the capacitative artifact produced by the stray

Figure 3.3

Stray Capacitances Effective in Producing Artifact

Symbols defined in figure and text. The cathode followers were actually pentodes. E_{obs} was connected to a cathode follower, the output of which led to one side of the vertical amplifier. In some experiments the cathode follower connected to E_0 was not used.

Fig. 3.3



capacitances around the current and voltage microelectrodes.

Figure 3.3 shows the stray capacitances in the equivalent circuit of the set-up. The symbols for the potentials, all of which are measured with respect to earth, are defined as follows:

V_s is the oscillator output voltage

E_{obs} is the voltage at the grid of the recording cathode follower

E is the actual potential inside the muscle fibre at the tip of the voltage microelectrode

E_1 is the potential just outside the fibre membrane near the tips of the microelectrodes

E_2 is the potential of the bathing solution away from the microelectrodes, the potential measured by the voltage bath electrode

E_o is the potential across the resistor used to monitor current

The symbols for the impedances in the circuit are

R_I is the resistance of the current passing microelectrode

R_V is the resistance of the voltage recording microelectrode

R_{mon} is the resistance used to monitor current

R_2 represents any resistance in the solution, any imbalance in the differential recording system used to measure potential, or any effect of the three dimensional spread of current (in the bathing solution) which acts as if it were a constant resistance

Z_{elec} is the impedance of the current passing bath electrode

The symbols for the capacitances are

C_1 is the total effective capacitance from the voltage electrode to earth

C_2 is the capacitance between the voltage electrode and the bath

C_3 is the capacitance between the current electrode and the bath

C_4 is the capacitance coupling the two microelectrodes

The analysis of the circuit shown in Figure 3.3 is given

in Appendix 1 of this chapter. Some of the results of that analysis are used in the discussion below of the stray capacitances and methods taken to reduce them.

C_1 , the input capacitance of the voltage recording valve, has two components: the residual grid to cathode capacitance not neutralized by the following action of the cathode and the direct capacitance to earth. The first component is fully analyzed in Appendix 2, where a discussion of the frequency response of the cathode follower can also be found. The residual capacitance was minimized by running the cathode follower (an ME1400) at relatively high anode currents and thus high transconductance (about 700 μ A/volt) and gain. The gain measured at the cathode was found to be 0.96 and the resulting residual capacitance was about 0.4 pF. The direct capacitance to earth was reduced by using a very fine short wire and by removing conducting objects, including the microscope, from the vicinity of the preparation.

The total input capacitance was about 0.95 pF. Attempts to shield the entire input and thus reduce the direct capacitance to earth even further were not successful since the resulting increase in grid to cathode capacitance produced severe ringing.

There are two main ways in which the input capacitance might be reduced even further; compensation and elimination. Compensation has been used by many workers (Valley & Wallman, 1948, p.83; MacNichol & Wagner, 1954; Bak, 1958). The problems involved are discussed in Amatniek (1958); Yang, Hervey, and Smith (1958); Schoenfeld (1962); ~~and Moore (1962)~~. This technique is not considered suitable for quantitative work with small signals at high frequencies for the following reasons: 1) the very large bandwidth required in the input amplifier leads to a prohibitive increase in noise 2) phase shifts in the input amplifier make a quantitative treatment of the residual input reactance difficult 3) it is difficult to find an unambiguous criterion of input capacitance neutralization since capacitance between the bath and the microelectrode is inevitably present.

Elimination of the input capacitance, or at least reduction to a much smaller value might be possible if an electrometer input stage with precise unity gain and negligible phase shift over the entire frequency range were available. Some promising circuits can be found in the electronics literature (Macdonald, 1957; Murray, 1958).

C_2 and C_3 , the capacitances between the microelectrodes and the bath, are approximately proportional to the depth of immersion of the microelectrodes and amount to about 1 pF/mm (Nastuk & Hodgkin, 1950). In these experiments there was some difficulty in lowering the fluid level because not all the muscle fibres are parallel with the fluid surface. The leg was so mounted that the angle the fibres made with the surface could be adjusted, permitting the use of a lower fluid level.

Since in fact the capacitances C_1 and C_2 are distributed along the resistance of the microelectrode, there is some question as to whether they can be treated as lumped capacitances shunting the whole of the microelectrode resistance. (See Harris, 1952, p. 234 and de Levie, 1965, for a discussion of the equations applicable to an untapered microelectrode. de Levie also presents, on p. 123, the equations for a tapered electrode). The theoretical analysis of Amatniek (1958); Krnjevic, Mitchell and Szerb (1963); and Woodbury (1952) suggests that almost all the resistance of the microelectrode is located within a few micra of the tip. This is supported experimentally. If a 5 megohm microelectrode is broken off some 10μ from the tip, its resistance falls typically to less than one megohm. Since the capacitance into the bath is approximately proportional to the depth the electrode is immersed and since the microelectrodes in these experiments were immersed in at least 500μ of solution, it is clear that essentially

all the capacitance shunts all the microelectrode resistance.

C_4 , the capacitance between the voltage and current microelectrodes, is a capacitance critical to these measurements. Appendix 1 shows that the correction term containing C_4 is $wC_4 R_V R_I$; for $R_V = R_I = 5$ megohms and $f = w/2\pi = 10^4$ c/s the correction term is $2 \times 10^{15} C_4$ (in kohms). Because C_4 appears in the corrections multiplied by the product of the electrode resistances, it must be kept below 10^{-15} F. (10^{-15} F is approximately 0.2% of the capacitance between two 3 mm diameter cylinders 4 cm long and 3 cm apart. The dimensions chosen are a rough approximation to those of the two microelectrodes). The following methods were used to keep C_4 below the required value. All leads carrying the oscillator signal were double shielded. (The oscillator output impedance was low enough so that the current through the capacitance to the shielding was unimportant). The current passing microelectrode was shielded as far down its length as possible. Finally, a thin aluminium shield insulated along its bottom edge with plastic film was placed in the Ringer solution between the current and voltage electrodes. The shield was coated with silicone grease to prevent an increase in the fluid level and was driven from the cathode of the recording cathode follower to keep C_1 small. The reduction in C_4 when the shield touched the fluid was by a factor of between five and ten.

Appendix 1 shows that the artifact also depends on the size of the parameters R_{mon} , R_V , R_I , and Z_{elec} . R_{mon} in these experiments was always less than 11 kohms at frequencies above 10 kc/s. It would perhaps be better to use an operational amplifier as an ammeter since this would make R_{mon} effectively zero. Complications are then produced by the necessity of correcting for Z_{elec} . R_V and R_I were kept as small as possible consistent with the need to prevent damage to the fibre used (around 5 megohms). Metal electrodes are not suitable for these experiments since, while having much lower resistance at high frequencies, they have an impedance which is not a simple function of frequency. This makes it difficult to correct for the remaining artifact. Z_{elec} was kept around 100 ohms by using a long (6 cm) length of coiled chlorided silver wire, separated from the bathing solution by a piece of filter paper with relatively large surface area.

Procedure.

With the shield raised two microelectrodes were inserted into a muscle fibre around 40μ apart in the direction of the fibre axis. The electrodes were placed approximately in the middle of the fibre in both length and breadth. The shield was carefully lowered into the solution. Measurements were then taken with currents of frequencies between 1 c/s and 10 kc/s in early experiments and 0.1 c/s and 10 kc/s in later ones. Six

measurements were taken per decade, the ratio of frequencies of successive measurements being $10^{1/6} \approx 1.47$. After the measurement at 10 kc/s, measurements were taken in descending order, one per decade. The monitor resistance was changed to keep the height of the ellipse D_z approximately equal to the breadth D_y . Signals of about 6 mv were used, requiring currents of typically 0.3 μ A. Most current microelectrodes showed nonlinearities when passing this much current, especially in the frequency range 100 c/s to 500 c/s. Only current electrodes without this nonlinearity were used. It was rarely possible to take records from fibres with input resistance less than 10 kohms, even though almost all the fibres in some muscles were of this low input resistance. Nonlinearities in the fibre properties themselves were hardly ever observed at the signal level used.

In some experiments the response to a step function of applied current was observed after the impedance measurements had been made. A current sufficient to give a step hyperpolarization of about 5 mV was used. After this the current electrode was withdrawn and a series of measurements taken at different frequencies. These measurements were used to calculate the value of the coupling capacitance C_4 .

In only a few fibres was it possible to reinsert the current electrode some distance away from the voltage electrode and thus measure the d.c. space constant. The difficulty was caused by the

large size of the electrodes used and the problem of inserting them properly. Measurements of the space constant in which either the removal or insertion of the current electrode caused marked change in resting potential were rejected.

Diameter of the fibres was measured by observation and in doubtful cases a map of the region was made showing the presence or absence of input resistance. Measurements of diameter were subject to considerable error on account of overlap of adjacent fibres, difficulty of measurement, and non-circular cross section of the fibre.

Corrections for Stray Capacitance.

Appendix 1 presents the derivation of the correction equations for a slightly more general case than that of Falk & Fatt (1964). Using the fact that R_2 and R_{elec} are much less than R_{mon} and that $-X_{elec}$ is negligible, the expressions reduce to those of Falk & Fatt:

$$\begin{aligned}
 R = & -R_2 + R_{obs} [1 - \omega^2 (c_1 + c_2) c_3 R_V R_I] \\
 & + (-X_{obs}) \omega [R_V (c_1 + c_2) + R_I c_3] = \omega^2 c_1 c_3 R_V R_I R_m \\
 -X = & -X_{obs} [1 - \omega^2 (c_1 + c_2) c_3 R_V R_I] \\
 & - [R_{obs} - R_2] \omega [R_V (c_1 + c_2) + R_I c_3] \\
 & + \omega R_V [c_4 R_I - c_1 R_{mon}]
 \end{aligned} \tag{1}$$

These equations have a very important property: the correction for capacitative artifact itself depends on the impedance being measured. (Equation (1) expresses the correction as a function of R_{obs} , $-X_{obs}$. Equation (10) of Appendix 1 expresses it in the physically more meaningful way as a function of R , $-X$.) Thus, any technique for correcting the observed impedance for artifact must itself measure the impedance. Electronic ^{compensation} correction is not practicable (cf. Pugsley, 1964) since the electronic measurement of impedance is difficult. It is not even possible to use ^{compensation} electronic correction networks at frequencies where the artifact is not so large (below 3 kc/s) since the largest term in the corrections at these frequencies is precisely the one which depends on the observed impedance (see equation (9') of Appendix 1). Moreover, even if it were practically possible to arrange the circuit parameters so that the various terms in the corrections cancelled at one frequency, the variation of R_{obs} and $-X_{obs}$ with frequency would ensure that the artifact would not vanish at another frequency. Finally, the expressions for R_{obs} , $-X_{obs}$ presented in Appendix 1 show that simple subtraction of the impedance observed with the current electrode outside the cell from the impedance observed with the electrode inside the cell at the same frequency will not give R , $-X$. Again this is because the correction depends on the impedance being measured.

The corrections given in equation (1) require a knowledge of the size of the various stray capacitances and R_V and R_I . The electrode resistances are measured conventionally: R_I by Ohm's law, R_V by connecting a known shunt to the grid of the recording cathode follower. The errors involved are considered small. The method of measurement of each of the capacitances and the errors in the measurements are discussed below.

C_1 , the input capacitance, is measured from the time constant of the potential change when a step function is applied to the bath, the recording microelectrode just touching the solution. The input capacitance was found to be 0.95 pF. The major error in this measurement is the assumption that the capacitance shunting the microelectrode resistance into the bath is zero when the microelectrode is just touching the bath. In fact it seems likely that a few tenths of a picofarad remain even when the microelectrode is out of the bath. The effect of this capacitance is to reduce the observed rise time, giving too low a value for C_1 (see Nastuk & Hodgkin, 1950). Theoretically, the size of C_2/C_1 could be estimated by the size of the 'instantaneous' step in potential produced by a step voltage applied to the potential divider formed by C_1 and C_2 . Such a step is not easily observed, however, because of the limited frequency response of the cathode follower itself. The error is estimated to be about 0.1 pF, probably positive.

The capacitances shunting the microelectrodes into the bath are assumed equal, i.e. $C_2 = C_3$. The source of error here is the difference in the length of microelectrode submerged in the solution since the capacitance per unit length of different microelectrodes is quite constant. This error is estimated as not more than 0.3 pF, probably positive since the recording electrode was usually at a more oblique angle than the current electrode. Another method of measuring C_1 and C_2 is discussed in Appendix 4.

C_3 is itself measured by the decrease in the impedance of the current electrode with increasing frequency. If Z_I is the magnitude of the electrode impedance at the frequency $\omega/2\pi$ and if R_I is the magnitude of the low frequency electrode impedance

$$C_3 = \frac{1}{\omega} \sqrt{\frac{1}{Z_I^2} - \frac{1}{R_I^2}}$$

The error involved is estimated to be no more than 0.1 pF in either direction.

No method seemed available to measure C_4 directly so the following indirect method was used. Immediately after a series of records were taken from a fibre, the current electrode was removed to just outside the fibre and records taken at different frequencies. If the value of the fibre reactance $-X$

is set to zero, equation (1) can be solved for C_4 in terms of R_{obs} , $-X_{\text{obs}}$ and the other circuit parameters. In other words the value of C_4 was chosen which made equation (1) correctly describe the extracellular artifact. Solving (1) for C_4 with $-X = 0$, we get

$$C_4 = \frac{1}{\omega R_V R_I} \left\{ -(-X_{\text{obs}}) [1 - \omega^2(c_1 + c_2) C_3 R_V R_I] \right. \\ \left. + \omega [R_{\text{obs}} - R_3] [R_V (c_1 + c_2) + R_I C_3] \right. \\ \left. + \omega R_{\text{mon}} R_V C_1 \right\} \quad (2)$$

Some test of the validity of the above procedure is given by calculating C_4 at different frequencies. To the extent that the treatment is valid, the calculated value of C_4 should remain constant. It remains constant within the estimated total error of about 15%.

This method of measuring C_4 is important for the success of these experiments since it minimizes the effects of errors in the measurements of the other stray capacitances. Because the expression for $\omega C_4 R_V R_I$ involves the same terms as the expression for $-X$ except with opposite sign (compare equations (1) and (2)), the error in $-X$ caused by the errors in the measurement of the stray capacitances is balanced by the equal and opposite error in $\omega C_4 R_V R_I$ caused by the errors in the values of the stray

capacitances used to calculate C_4 . The cancellation is perfect, however, only if the circuit parameters have the same value in the expressions for C_4 and $-X$. The measurements used in the expression for C_4 , however, are taken with the current electrode outside the fibre, whereas the measurements used in the expression for $-X$ are taken with the current electrode inside the fibre. Therefore, the observed impedance R_{obs} , $-X_{obs}$ and the current electrode resistance R_I are significantly different in the two expressions. The cancellation of error is then not complete. The error expressions and the extent of cancellation is treated quantitatively in Appendix 3. The final estimated maximum error is

$$dR = 700 \text{ ohms}$$

$$d(-X) = 600 \text{ ohms}$$

The error becomes small below about 4 kc/s.

The Derivation of the Correction Equations.

The derivation presented here differs slightly from that used by Falk & Fatt (1964) in that it includes the effect of a series resistance and of the impedance of the current passing bath electrode. The circuit to be analyzed is given in Fig. 3.3 where all potentials are measured with respect to earth. The analysis of this circuit without approximation has not been carried past the initial steps because the resulting expressions are quite unwieldy. It seems unlikely that any of the approximations used below would cause difficulty since they are strongly satisfied.

There are four basic equations. The definition of the observed impedance:

$$Z_{obs} = \frac{E_{obs} - E_a}{I_{obs}} = \frac{E_{obs} - I_{obs} [R_{mon} + Z_{elec}]}{I_{obs}}$$

which can be rewritten using the relation $I_{obs} = E_o / R_{mon}$:

$$Z_{obs} = \frac{E_{obs} - E_o}{E_o} R_{mon} - Z_{elec} \quad (1)$$

The definition of the actual impedance sought is the second equation.

$$Z = \frac{E - E_1}{I} = \frac{E - I_{obs}[Z_{elec} + R_2 + R_{mon}]}{I}$$

Let

$$R_3 = R_2 + Z_{elec}$$

Then,

$$Z = \frac{E - I_{obs}[R_{mon} + R_3]}{I} \quad (2)$$

We now seek an equation for Z in terms of Z_{obs} and the minimum number of most easily observed variables. The relation is developed by setting the algebraic sum of currents at the recording junction equal to zero.

$$0 = -E_{obs}(j\omega C_1) + (V_s - E_{obs}) j\omega C_4 + \frac{E - E_{obs}}{R_v} + j\omega C_2(E_o + R_3 I_{obs} - E_{obs}).$$

or

$$E = E_{obs}[1 + j\omega R_v(C_1 + C_2 + C_4)] - V_s(j\omega C_4 R_v) - E_o(j\omega C_2 R_v) \left[1 + \frac{R_3}{R_{mon}} \right]$$

Since C_4 is much smaller than C_1 or C_2 , this can be simplified to the third of our basic equations

$$\begin{aligned} E = E_{\text{obs}} & [1 + j\omega R_V(C_1 + C_2)] - V_s(j\omega C_4 R_V) \\ & - E_o(j\omega C_2 R_V) \left[1 + \frac{R_3}{R_{\text{mon}}} \right] \end{aligned} \quad (3)$$

Our fourth basic equation is developed from an expression for I_{obs}

$$\begin{aligned} I_{\text{obs}} = \frac{E_o}{R_{\text{mon}}} & = I + (V_s - E_o - I_{\text{obs}} R_3)(j\omega C_3) \\ & + (E_{\text{obs}} - E_o - I_{\text{obs}} R_3)(j\omega C_2) \end{aligned}$$

The oscillator output V_s is much larger than the observed potential E_{obs} so this may be written as our fourth basic equation

$$I = \frac{E_o}{R_{\text{mon}}} - [V_s - E_o - I_{\text{obs}} R_3] [j\omega C_3] \quad (4)$$

There is now enough information in these equations to solve for Z in terms of potentially observable quantities. The expression for Z can be derived by substituting (3) and (4) into (2) and

using the definition

$$Z_s = \frac{E_{obs}}{E_o} R_{mon} = Z_{obs} + R_{mon} + Z_{elec}$$

$$Z = \frac{Z_s [1 + j\omega R_v (C_1 + C_2)] - \frac{V_s}{E_o} (j\omega C_1 R_v R_{mon}) - (R_3 + R_{mon})(1 + j\omega C_3 R_3)}{1 + j\omega C_3 R_3 - \frac{j\omega C_2 R_{mon} (V_s - E_o)}{E_o}} \quad (5)$$

In principle (5) contains all the information needed to calculate Z in terms of Z_{obs} . Equation (5) requires, however, the measurement of the phase and magnitude of both V_s and E_o : such measurements would necessitate the taking of two complete impedance loci. If another relation involving V_s and E_o were available, both these variables could be eliminated from the expression for Z . Such a relation can be derived since almost all the current that leaves the oscillator flows through the left hand side of the circuit (Fig. 3.3) - through R_I and C_3 and then R_{mon} - with little leaking across to the right hand side through R_v or C_2 . The actual total current through R_{mon} is

$$\frac{E_o}{R_{mon}} = \frac{V_s - E}{R_I} + j\omega C_3 (V_s - E) + j\omega C_2 (E_{obs} - E) + \frac{E_{obs} - E}{R_v} \quad (6)$$

But the oscillator output is much greater than any other voltage in the system and the two capacitances (C_2 and C_3) are approximately equal, as are the two electrode resistances (R_V and R_I). Then the third and fourth terms on the right hand side of (6) can be neglected. A final simplification can be introduced because $V_s - E$ is approximately equal to $V_s - E_0$ and to $V_s - E_1$. Equation (6) simplifies using these approximations

$$\frac{V_s - E_0}{E_0} = \frac{1}{R_{\text{mon}}} \frac{1}{\frac{1}{R_I} + j\omega C_3}$$

$$\frac{E_0}{R_{\text{mon}}} = [V_s - E_0] \left[\frac{1}{R_I} + j\omega C_3 \right]$$

This equation is simply the mathematical statement that almost all the current that leaves the oscillator crosses R_{mon} . This relation can be used to eliminate V_s and E_0 from (5), thus giving the desired formula for Z .

$$(7)$$

$$Z = \frac{-\omega^2 C_3^2 R_I^2 - j\omega C_4 R_V R_I}{1 - j\omega C_3 (R_I - R_3) + j\omega^2 C_3^2 R_I^2 R_3}$$

The denominator of this expression can be simplified since the resistance of the current microelectrode R_I is much greater than R_3 . Furthermore, even at $w/2\pi = 10 \text{ kc/s}$

$$\omega c_3 R_I \doteq 6 \cdot 10^4 \cdot 2 \cdot 10^{-12} \cdot 10^7 \doteq 1$$

whereas

$$\omega^3 c_3^3 R_I^3 R_3 \doteq (6 \cdot 10^4)^3 (2 \cdot 10^{-12})^3 \cdot 10^{14} \cdot 10^3 \doteq 2 \cdot 10^{-4}$$

The denominator of (7) then reduces to

$$1 - j\omega c_3 R_I \quad (8)$$

The numerator of (7) is exactly divisible by (8). Performing the division and separating real and imaginary parts, we have the general result

$$-X = (-X_{obs}) [1 - \omega^2(c_1 + c_2)c_3 R_V R_I]$$

$$-R_{obs}\omega [R_V(c_1 + c_2) + R_I c_3]$$

$$+ \omega [c_4 R_V R_I + R_2(c_3 R_I + c_2 R_V) - R_V c_1 (R_{mem} + R_{out})]$$

$$- \omega^2 (-X_{eloc}) R_V R_I c_1 c_3$$

$$\begin{aligned}
 R = & -R_2 + R_{\text{obs}} [1 - \omega^2(c_1 + c_2) c_3 R_v R_I] \\
 & + (-X_{\text{obs}}) \omega [R_v(c_1 + c_2) + R_I c_3] + (-X_{\text{elec}}) \omega R_v c_1 \\
 & + \omega^2 R_v R_I c_3 [R_2 c_2 - c_1 (R_{\text{mon}} + R_{\text{elec}})]
 \end{aligned}$$

where

$$R_{\text{elec}} + j X_{\text{elec}} \equiv Z_{\text{elec}}$$

It can be seen from this relation that the current passing bath electrode impedance Z_{elec} is of little importance as long as it is much smaller than R_{mon} . Z_{elec} was typically 100 ohms in these experiments and showed no reactance at the frequencies where the X_{elec} term might become important. Thus, both R_{elec} and X_{elec} can be neglected.

As discussed above R_2 represents the resistance of the Ringer solution, any imbalance in the voltage recording system, and any other lumped resistance in series with both the current and voltage electrodes. Impedance measurements made with the electrodes widely separated showed a resistive component of a few hundred ohms; this is much less than R_{mon} . Using the approximation R_2 is much smaller than R_{mon} .

$$\begin{aligned}
 R &= -R_2 + R_{obs} [1 - \omega^2(c_1 + c_2)c_3 R_v R_I] \\
 &\quad + (-X_{obs})\omega [R_v(c_1 + c_2) + R_I c_3] = \omega^2 c_1 c_3 R_v R_I R_{mon} \\
 -X &= -X_{obs} [1 - \omega^2(c_1 + c_2)c_3 R_v R_I] \\
 &\quad - [R_{obs} - R_2]\omega [R_v(c_1 + c_2) + R_I c_3] \\
 &\quad + \omega R_v [c_4 R_I - c_1 R_{mon}]
 \end{aligned} \tag{9}$$

Equations (9) can be solved to give R_{obs} and $-X_{obs}$ as functions of R and $-X$.

$$\begin{aligned}
 &[R + R_2][1 - \omega^2(c_1 + c_2)c_3 R_v R_I] - (-X)\omega [R_v(c_1 + c_2) + c_3 R_I] \\
 &- \omega^2 [c_1(c_1 + c_2)R_v^3 R_{mon} - c_3 c_4 R_v R_I^2 - R_v^2 R_I c_4(c_1 + c_2)] \\
 R_{obs} &= \frac{-\omega^4 R_v^2 R_I^2 c_3^2 c_1(c_1 + c_2) R_{mon}}{1 + \omega^2[R_v^2(c_1 + c_2)^2 + c_3^2 R_I^2] + \omega^4(c_1 + c_2)^2 c_3^2 R_v^2 R_I^2} \\
 \\
 -X_{obs} &= \frac{(-X)[1 - \omega^2(c_1 + c_2)c_3 R_v R_I] + [R + R_2]\omega [R_v(c_1 + c_2) + R_I c_3]}{1 + \omega^2[R_v^2(c_1 + c_2)^2 + c_3^2 R_I^2] + \omega^4(c_1 + c_2)^2 c_3^2 R_v^2 R_I^2} \\
 &\quad + \omega^3 R_v R_I^2 c_3 [c_1 c_3 R_{mon} + c_4(c_1 + c_2) R_v] \\
 &\quad + \omega R_v [R_{mon} c_1 - R_I c_4]
 \end{aligned} \tag{10}$$

It is instructive to substitute typical numerical parameters into (9) and (10) and get a feel for the size of the corrections involved. The values of the parameters chosen for this purpose are $R_V = R_I = 5$ megohms; $C_1 = 1.0$ pF; $C_2 = C_3 = 2$ pF; $C_4 = 0.001$ pF; $R_{\text{mon}} = 10$ kohms; frequency f is in kc/s; all impedances in ohms.

$$R = -R_2 + R_{\text{obs}}(1 - 0.006f^2) + (-X_{\text{obs}})(0.15f) - 18f^3 \quad (9')$$

$$-X = -X_{\text{obs}}(1 - 0.006f^2) - 0.15f(R_{\text{obs}} - R_2) - 150f \quad (9')$$

$$R_{\text{obs}} = \frac{[R + R_2][1 - 0.006f^2] - f(0.15)(-X) + [0]f^2 - 0.1f^4}{1 + 0.014f^2 + 4 \cdot 10^{-5}f^4} \quad (10')$$

$$-X_{\text{obs}} = \frac{-X[1 - 0.006f^2] + 0.15f(R + R_2) + 150f + 1.6f^3}{1 + 0.014f^2 + 4 \cdot 10^{-5}f^4}$$

APPENDIX 2 TO CHAPTER 3:

The Cathode Follower.

Early in the course of these experiments it became clear that a cathode follower run under electrometer conditions (transconductance about $100 \mu\text{A/volt}$) was an unsatisfactory headstage device. The gain of the cathode follower under these conditions showed phase shift at higher frequencies and the response to a step function showed marked ringing. An analysis of the frequency response of a cathode follower was therefore carried out.

Donaldson (1958) has presented the equation for the gain of a cathode follower as a function of (real) frequency and Hodgkin (in Donaldson, 1958) has given the response to an applied step function. Clapp (1949) gives a definitive analysis of the high frequency behaviour of a cathode follower but his analysis is most suited to low source impedances. The treatment here is rather more general than those in Donaldson and by its identification of the cathode follower equation with that of the damped galvanometer, permits the use of the figures and discussion in Harris (1952).

Figure 3.4

The Equivalent Circuit of the Recording Cathode Follower
Symbols defined and further discussion in text. V is the
grid to cathode potential. The cathode follower was actually
a pentode.

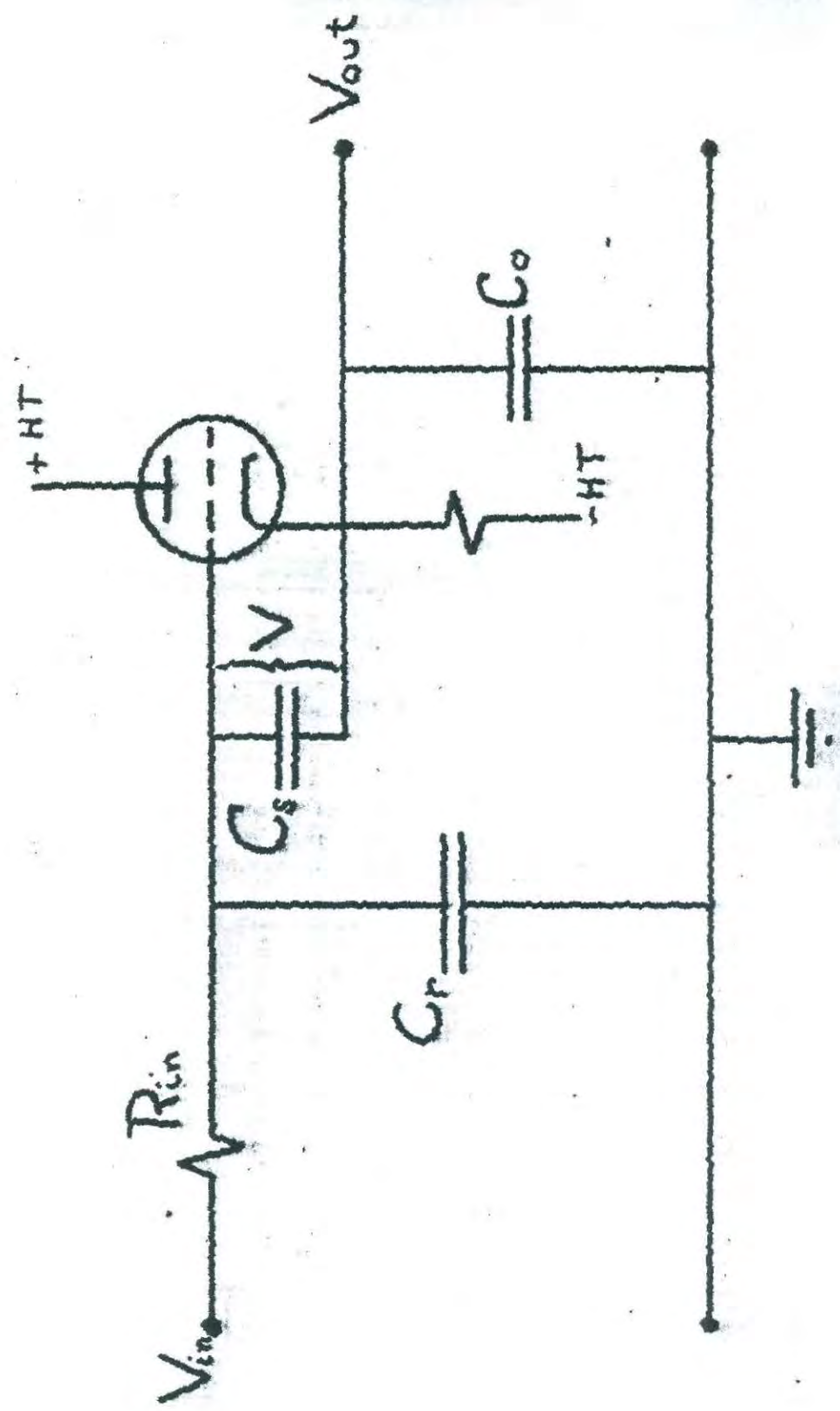


Fig. 3.4 shows the equivalent circuit of the cathode follower including source resistance. The gain can be found by the standard techniques of circuit analysis (LePage & Seeley, 1952) and is given below as a function of the complex frequency s

$$G(s) = \frac{V_{out}}{V_{in}} =$$

$$= \frac{R_K(g_m + sC_s)}{1 + g_m R_K + s[R_K C_o + R_{in}(C_s + C_r) + g_m R_{in} R_K C_r] + s^2 C_o [C_s + C_r] R_{in} R_K}$$

R_K is the cathode load resistance

g_m is the mutual conductance of the valve

C_o is the capacitative load impedance

R_{in} is the source resistance

C_r is the input capacitance

C_s is the grid to cathode capacitance

V is the grid to cathode potential

At $s = j10^5$, the highest frequency of interest here, and with

$C_s = 10 \text{ pF}$ the second term of the numerator is very small (that

is, all the current through the load is supplied by the valve)

and the gain becomes

$$G(s) = \frac{g_m R_K}{1 + g_m R_K + s[R_K C_o + R_{in}(C_s + C_r) + g_m R_{in} R_K C_r] + s^2 C_o [C_s + C_r] R_{in} R_K}$$

or using the constants

$$P = C_o [C_s + C_r] R_{in} R_k$$

$$U = I + g_m R_k$$

$$A = R_{in} R_k g_m C_r + R_{in} (C_s + C_r) + C_o R_k$$

$$m_{1,2} = \frac{-A \pm \sqrt{A^2 - 4UP}}{2P}$$

the expression for the gain becomes

$$G(s) = \frac{U-I}{P(s-m_1)(s-m_2)}$$

The response of the cathode follower to a step function of applied potential is found by taking the inverse Laplace transform of $G(s)/s$ and is found to be

$$A^2 \neq 4UP:$$

$$V_{out}(t) = \Theta_f \left[1 - \frac{m_2}{m_2 - m_1} e^{m_1 t} + \frac{m_1}{m_2 - m_1} e^{m_2 t} \right]$$

$$A^2 = 4UP \text{ (i.e. } m_1 = m_2 = m)$$

$$V_{out}(t) = \frac{U-I}{m^2 P} \left[1 - (1-mt) e^{mt} \right]$$

where

$$\Theta_f = \frac{U-1}{P(m_1 - m_2)}$$

This is exactly of the form of the response of a damped galvanometer to a step excitation. The analysis and discussion given in Harris (1952) are then applicable. In particular the damping constant γ is given by

$$\gamma = \frac{A}{2\sqrt{UP}} = \frac{g_m R_k R_{in} C_m + R_{in}(C_s + C_r) + C_o R_k}{2[C_o(C_s + C_r) R_{in} R_k (g_m R_k + 1)]^{1/2}}$$

The natural frequency ω_0 is

$$\omega_0 = \sqrt{\frac{U}{P}} = \sqrt{\frac{1 + g_m R_k}{C_o(C_s + C_r) R_{in} R_k}}$$

and the dimensionless frequency variable is

$$\eta = \frac{\omega}{\omega_0}$$

(Harris' universal curves are given in terms of these parameters. Step function response and associated functions are given in Fig.'s 2, 3, 4 pp. 56-58. Curves giving overshoot as a function of damping are given in Fig.'s 5 & 7 pp. 61 & 63 and Fig. 7, p. 629. Frequency response curves are given in Fig.'s 5, 6, 53 on pp. 627, 628, and 750.

Almost all relevant information about the properties of cathode followers can be found with the help of these curves).

The cathode follower when run as an electrometer had a transconductance of about $100 \mu\text{A/volt}$ and a damping constant under one. As predicted by Fig. 2, p. 56 of Harris, the response to a step function showed considerable ringing. This undesired behaviour was removed by increasing the anode current of the valve and thus increasing the transconductance to about $700 \mu\text{A/volt}$. The damping constant was then greater than one and the cathode follower showed no ringing.

The input impedance of the cathode follower can be computed by short circuiting R_{in} in Fig. 3.4. The total input capacitance C_1 is then the computed capacitance plus C_r . V_{in} is given by

$$V_{in} = V \left[1 + \frac{g_m R_k}{1 + j\omega C_o R_k} \right]$$

where the symbols are as before. I_{in} is

$$I_{in} = V(j\omega C_s)$$

Then Z_{in} is

$$Z_{in} = \frac{1 + g_m R_k + j\omega C_o R_k}{j\omega C_s (1 + j\omega C_o R_k)} = -\frac{1}{\omega C_s} + \frac{g_m R_k}{j\omega C_s - \omega^2 C_o C_s R_k}$$

The real term in the denominator is negligible even if carried right through the analysis. Then, to a good approximation, the input impedance is purely capacitative and is given by, as one would expect,

$$C_s[1 - \text{gain}] = \frac{C_s}{1 + g_m R_K}$$

Adding the shunt capacitance C_r , one has an expression for the total input capacitance

$$C_i = C_r + C_s[1 - \text{gain}] = \frac{C_s}{1 + g_m R} + C_r$$

(The discussion above assumes the cathode follower to be a linear device. At short times, however, the cathode of the valve cannot faithfully follow the grid potential. Thus, it becomes much easier to drive the grid into a non-linear range of its characteristic. In other words, the dynamic range of the cathode follower is severely reduced at short times (cf. Valley & Wallman, 1948). In these experiments such an effect was easily observable with pulses exceeding 200 mV. Since measurements were always made with signals much smaller than this, no error was introduced by non-linear behaviour of the cathode follower).

APPENDIX 3 TO CHAPTER 3:

Error Analysis of the Corrections.

The error in R and $-X$ is determined by the errors in the quantities from which they are calculated. The mathematical measure of the change in a function produced by an 'error' in one of its independent variables is the differential, the first term in a Taylor expansion (see Widder, 1961). We assume w , R_V , R_I , and R_{mon} to be precisely known. The errors in R and $-X$ are then found by taking the differential of the expression (9) for R and $-X$ found in Appendix 1:

$$\begin{aligned} dR = & \frac{\partial R}{\partial R_{\text{obs}}} dR_{\text{obs}} + \frac{\partial R}{\partial (-X_{\text{obs}})} d(-X_{\text{obs}}) + \frac{\partial R}{\partial c_1} dc_1 \\ & + \frac{\partial R}{\partial c_2} dc_2 + \frac{\partial R}{\partial c_3} dc_3 \end{aligned} \quad (1)$$

$$\begin{aligned} d(-X) = & \frac{\partial (-X)}{\partial R_{\text{obs}}} dR_{\text{obs}} + \frac{\partial (-X)}{\partial (-X_{\text{obs}})} d(-X_{\text{obs}}) + \frac{\partial (-X)}{\partial c_1} dc_1 \\ & + \frac{\partial (-X)}{\partial c_2} dc_2 + \frac{\partial (-X)}{\partial c_3} dc_3 + \frac{\partial (-X)}{\partial c_4} dc_4 \end{aligned}$$

The partial derivatives can be calculated from (9) if necessary.

If the numerical values used in equation (9') of Appendix 1 are used along with the error estimates $dC_1 = dC_3 = 0.1 \text{ pF}$; $dC_2 = 0.3 \text{ pF}$; $d(-X_{\text{obs}}) = 100 \text{ ohms}$; $dR_{\text{obs}} = 500 \text{ ohms}$, the total error in R at 10 kc/s is

$$dR = 700 \text{ ohms}$$

- The calculation of the error in $-X$ is more complicated since it involves the error in a quantity (C_4) which is itself computed from other quantities. In fact the error in C_4 itself is given by

$$dC_4 = \frac{\partial C_4}{\partial (-X_{\text{obs}})} d(-X_{\text{obs}}) + \frac{\partial C_4}{\partial R_{\text{obs}}} dR_{\text{obs}} + \frac{\partial C_4}{\partial C_1} dC_1 + \frac{\partial C_4}{\partial C_2} dC_2 + \frac{\partial C_4}{\partial C_3} dC_3 \quad (2)$$

where the partial derivatives can be calculated from (2) of the chapter if necessary.

The measurement of C_4 is made under different conditions than that of $-X$, in particular the sizes of R_I , R_{obs} , and $-X_{\text{obs}}$ are different. The measurements made for determining C_4 are marked with a prime below to distinguish them from the corresponding quantities used in the calculation of $-X$. When the expression for the error in C_4 (2) is substituted into the expression for the error in $-X$ (equation (1) above), the quantities which do not change

from one measurement to the other cancel exactly. This is because the expression for the error in $-X$ caused by the error in C_4 (namely, $wR_V R_I dC_4$) is exactly the negative of the expression for the rest of the error in $-X$. The remaining uncancelled error is then all caused by the change in R_{obs} , $-X_{obs}$, and R_I and is given by

$$\begin{aligned} d(-X)_{net} = & \frac{\partial(-X)}{\partial R_{obs}} dR_{obs} + \frac{\partial(-X)}{\partial(-X_{obs})} d(-X_{obs}) + \frac{\partial(-X)}{\partial C_1} dC_1 \\ & + \frac{\partial(-X)}{\partial C_2} dC_2 + \frac{\partial(-X)}{\partial C_3} dC_3 \end{aligned}$$

where

$$\frac{\partial(-X)}{\partial R_{obs}} = \omega c_3 [R'_I - R_I]$$

$$\frac{\partial(-X)}{\partial(-X_{obs})} = 1 - \omega^2 [c_1 + c_2] c_3 R_V [R'_I - R_I]$$

$$\begin{aligned} \frac{\partial(-X)}{\partial C_1} = & \frac{\partial(-X)}{\partial C_2} = -\omega^2 c_3 R_V [-X'_{obs} R'_I - (-X_{obs}) R_I] \\ & - \omega R_V [R'_{obs} - R_{obs}] \end{aligned}$$

$$\begin{aligned} \frac{\partial(-X)}{\partial C_3} = & -\omega^2 (c_1 + c_2) R_V [-X'_{obs} R'_I - (-X_{obs}) R_I] \\ & - \omega [R'_I R'_{obs} - R_I R_{obs}] \end{aligned}$$

With the same estimates of circuit values and errors this gives at 10 kc/s

$$d(-X) = 600 \text{ ohms}$$

APPENDIX 4 TO CHAPTER 3:

Alternative Methods of Parameter Measurement.

Because of the importance of the measurement of the stray capacitances another method of measuring C_1 and C_2 was developed. The technique was to apply an A.C. signal of different frequencies directly to the bath and then, by analyzing the results, derive precise values for C_1 and C_2 . The circuit analyzed is shown in Fig. 3.5. The circuit elements defined there correspond to those defined in Fig. 3.3 of the main body of the chapter. The procedure used is the same as that used in deriving the basic artifact equation. The observed transfer function T is

$$T = A + jB = \frac{E_{obs}}{E_o}$$

(E_{obs} is measured instead of $E_{obs} - E_o$ in order to keep the height of the phase angle ellipse approximately equal to its breadth, thus ensuring more accurate measurements). Another equation can be derived by setting the sum of the currents at the recording junction equal to zero, neglecting the bath electrode impedance

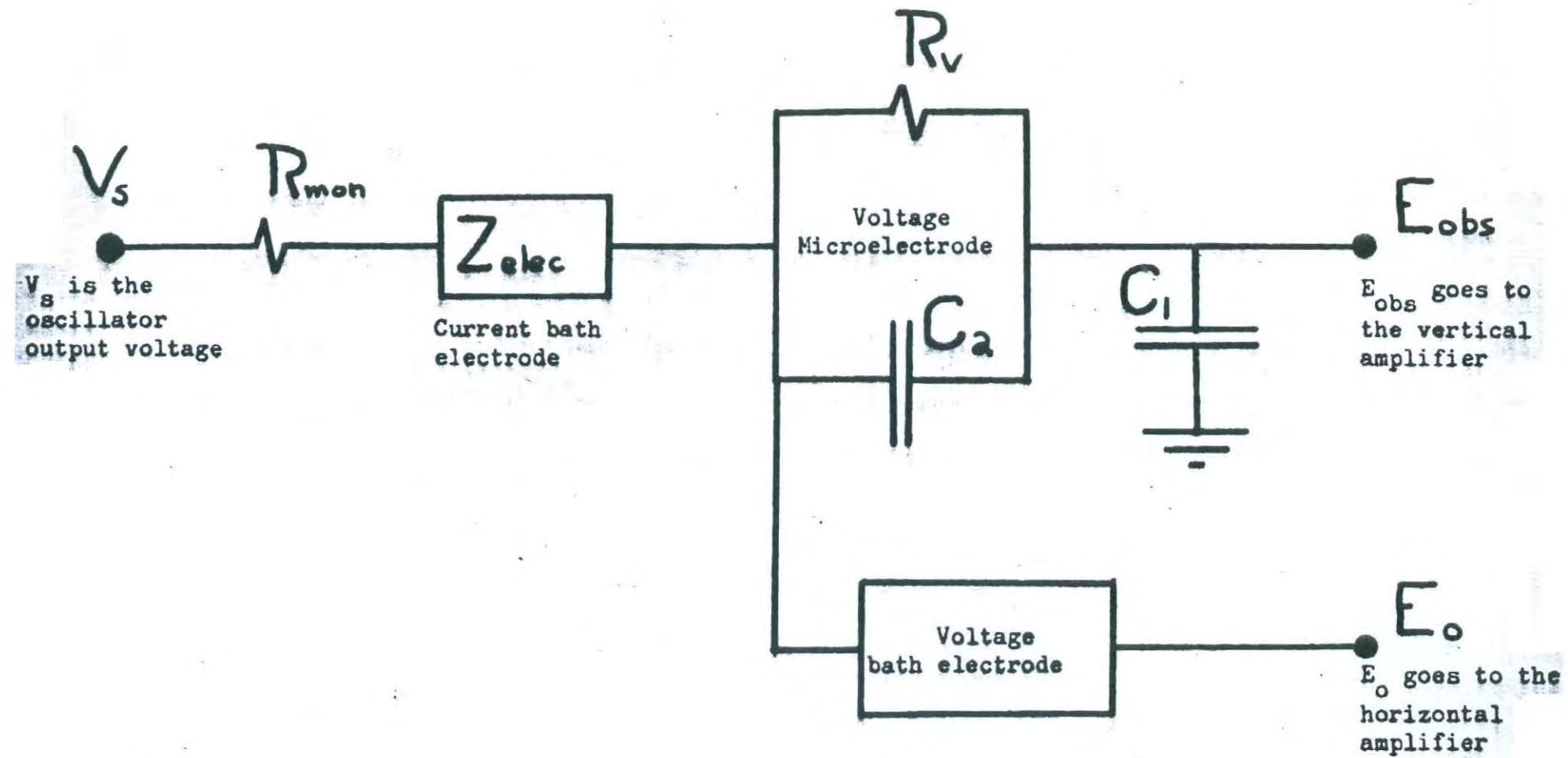
$$0 = \frac{E_{obs} - E_o}{R_v} + j\omega E_{obs}(c_1 + c_2) - j\omega E_o c_2$$

Figure 3.5

An Alternative Set-up for Measuring Some Stray Capacitances

E_{obs} was always, and E_o usually connected to a cathode follower
before being led to the amplifier. Further discussion in text.

Fig. 3.5



These equations may be solved simultaneously to give expressions for A and B in terms of C_1 and C_2 ; or they may be solved to give C_1 and C_2 in terms of A and B:

$$A = \frac{1 + \omega^2 C_2 (C_1 + C_2) R_v^2}{1 + \omega^2 R_v^2 (C_1 + C_2)^2}$$

$$-B = \frac{\omega C_1 R_v}{1 + \omega^2 R_v^2 (C_1 + C_2)^2}$$

$$C_2 = \frac{1}{\omega R_v} \left[B + \frac{A(A-1)}{B} \right]$$

$$C_1 = \frac{1}{\omega R_v} \left[\frac{-(A-1)^2}{B} - B \right]$$

An error analysis like those in Appendix 3 gives the result

$$dC_1 = \frac{1}{\omega R_v} \left[\frac{2(1-A)}{B} \right] dA + \frac{1}{\omega R_v} \left[\frac{(A-1)^2}{B^2} - 1 \right] dB$$

$$dC_2 = \frac{1}{\omega R_v} \left[1 + \frac{A(1-A)}{B^2} \right] dB + \frac{1}{\omega R_v} \left[\frac{2A-1}{B} \right] dA$$

With the same circuit values as used in Appendix 3, these become
at 10 kc/s

$$A = 0.85$$

$$B = -0.165$$

$$\begin{aligned} dC_1 &= 6.7 \cdot 10^{-12} dA + 4.5 \cdot 10^{-13} (-dB) \\ dC_2 &= 1.3 \cdot 10^{-11} dA + 1.7 \cdot 10^{-11} dB \end{aligned} \quad \left. \right\} \text{farads}$$

$$(\text{calculated for } C_1 = 1 \cdot 10^{-12} F; C_2 = 2 \cdot 10^{-12} F)$$

In other words a two per cent error in the measurement of A and B produces a maximum error of about 10 per cent in the calculated values of C_1 and C_2 . Measurements made by this method showed the expected scatter in the calculated values of C_1 and C_2 and so the simpler techniques described in the text were used.

Chapter 4.

RESULTS

Description.

The impedance loci showed considerable variation and will be discussed in three groups.

The first group of fibres (fibres 1 - 7 in Table 1) had impedance loci like those shown in Figs. 4.1 and 4.2. The hollow circles are the raw experimental data. The filled circles represent the impedance of the fibre itself, determined from the raw data by applying the corrections for capacitative artifact discussed in Chapter 3. The frequency at which the impedance measurements were made is shown near some of the points. The frequency of the other points can easily be found since measurements were taken at constant intervals of log frequency, each frequency being 1.47 times the previous one. The solid 45° line through the origin is shown since any model of the distributed admittance which includes a capacitance directly across its terminals will approach this line at high frequencies.

The measurements at either extreme of frequency are subject to error. At high frequencies the observed (i.e. uncorrected) phase tends to be close to 90° . As discussed in

Figures 4.1 & 4.2

input
Plots of Impedance of Single Crab Muscle Fibres

- A: A plot of phase angle against log frequency. The filled circles represent observations corrected for capacitative artifact. The solid line is the 'best' fit of the two time constant, distributed resistance model. The dotted line is the theoretical curve fitted by eye for the one time constant, distributed resistance model.
- B: Impedance locus, a plot of reactance against resistance. The hollow circles represent observations uncorrected for stray capacitance; the filled circles, observations corrected for stray capacitance. The solid line is the theoretical curve of the two time constant, distributed resistance model. The dotted line is the theoretical curve for the one time constant, distributed resistance model. The numbers near some points represent the frequency at which those measurements were made.

Fig. 4.1 is the plot of the impedance of fibre 1, Table 1; Fig. 4.2 is the plot of fibre 4, Table 1.

Fig. 4.1

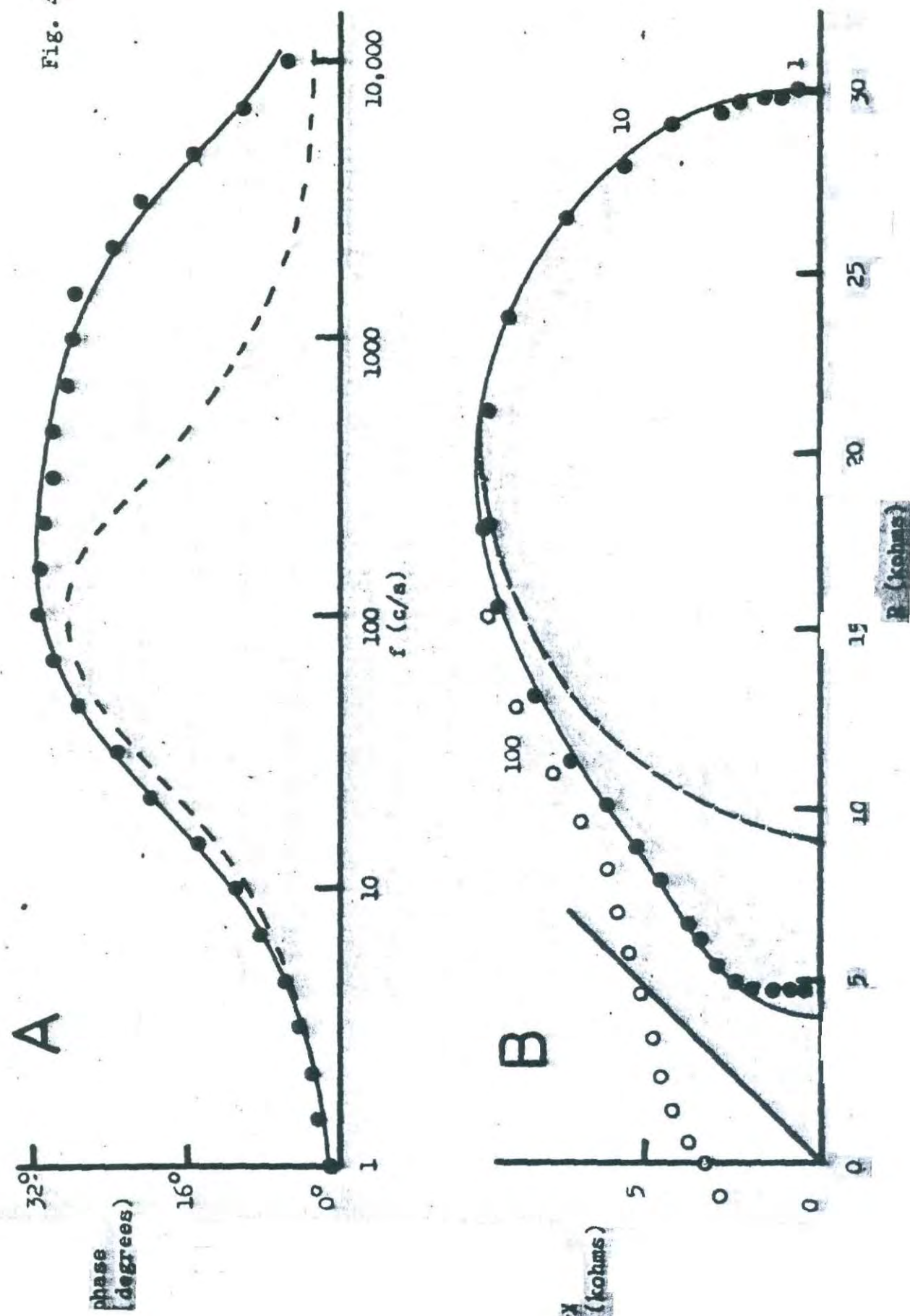
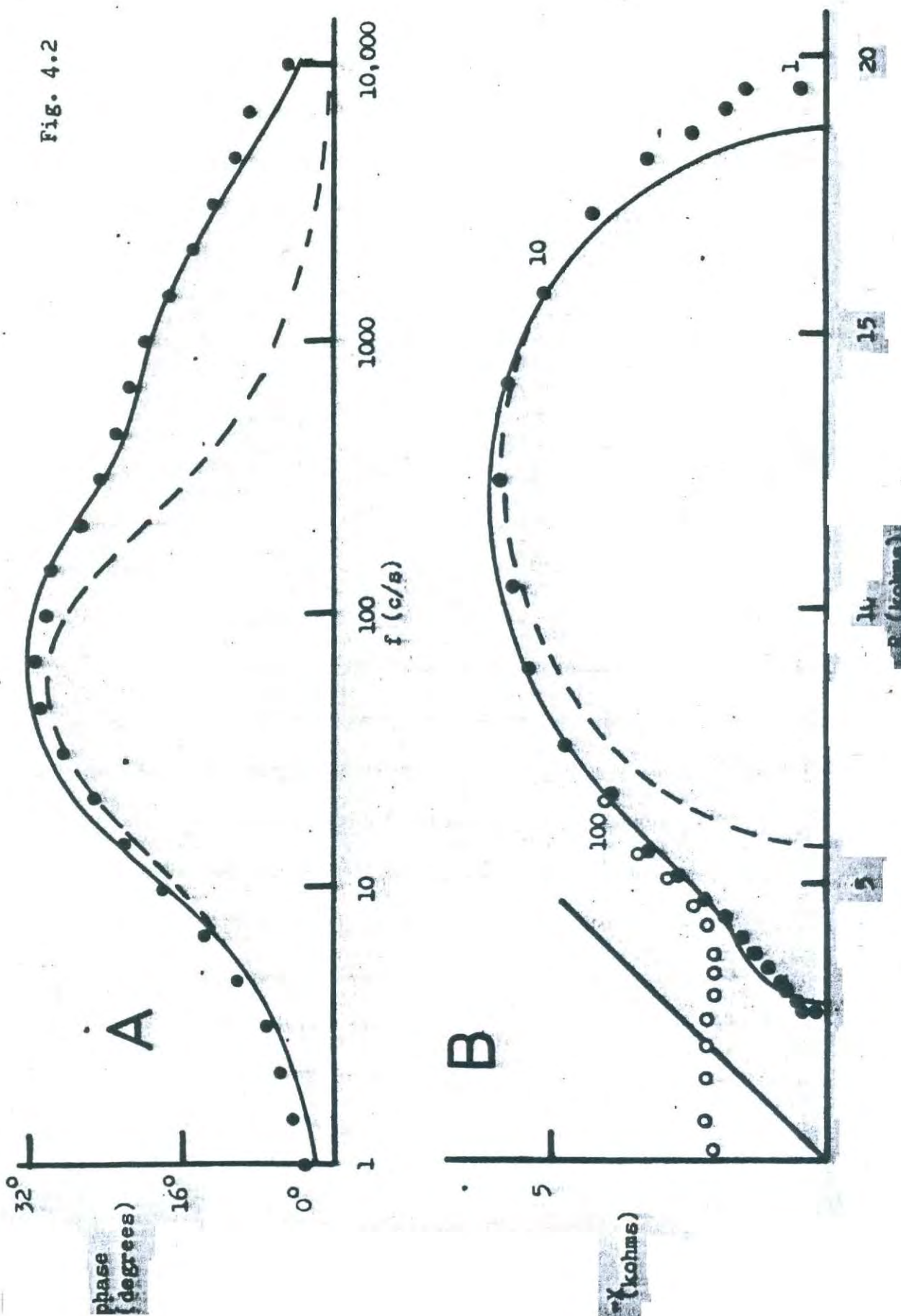


Fig. 4.2



Chapter 3, errors in phase measurement by Lissajous figures increase rapidly at phase angles near 90° . Another source of error at high frequencies is caused by systematic error in the corrections for capacitative artifact. This error amounts to less than 1 kohm in both resistance and reactance even at the highest frequencies (see Appendix 3, Chapter 3). Low frequency measurements are subject to a different source of error. As shown in a later section of this chapter some crab fibres show an unequivocal low frequency dispersion; that is, there are two maxima in the impedance locus, one occurring at very low frequencies, below say 10 c/s. The presence of this low frequency dispersion is masked in most fibres, but its effect may be seen in the deviation of reactance and phase from the theoretical curves at low frequencies: in almost all cases the observed points lie above the theoretical curve. The presence of these difficulties at either extreme of frequency ruled out the use of the low and high frequency plots given in Falk & Fatt (1964).

The solid line in each impedance plot represents the theoretical curve for the distributed resistance, two time constant model (Fig. 2.6). The curve was fitted with a digital computer as described in Chapter 2. The dotted line is the theoretical curve, fitted by eye, for the distributed resistance, one time constant model (Fig. 2.4). Reference to Figures 2.3 and 2.5 shows that the models without distributed resistance fail

to fit the observed locus: they approach the 45° line through the origin at high frequency and thus neither intersect the real axis at a finite value nor show a downward bend at high frequencies.

Fig. 4.1 and 4.2 also include plots of phase angle against log frequency. Only the points corrected for capacitative artifact are shown. The solid line represents the theoretical curve for the two time constant, distributed resistance model; the dotted line, the curve for the one time constant distributed resistance model. The phase plot shows a trend downwards at frequencies above 400 c/s in one case, 100 c/s in the other. On the other hand, models of fibre admittance without distributed resistance have phase plots which never decrease with frequency (assuming an admittance made up of only resistors and capacitors). ~~and neglecting effect of
3D spread of current.~~

Second Group of Fibres.

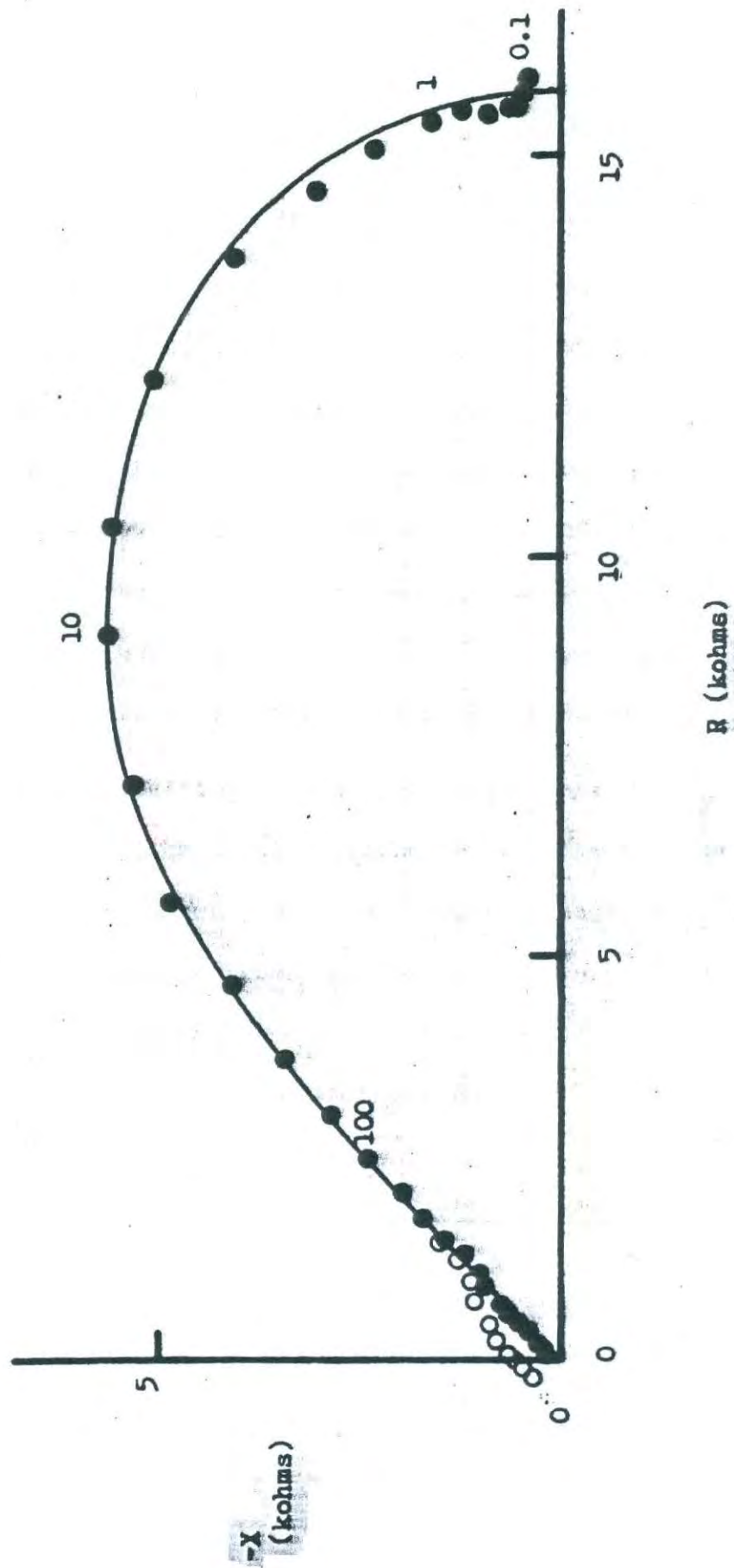
Fig. 4.3 shows the impedance locus of one of the two fibres of the second group. This locus is qualitatively different from those shown in Fig. 4.1 and 4.2: the locus is seen to approach the 45° line through the origin at frequencies above 100 c/s, and the magnitude of the impedance becomes very small above 1 kc/s. The solid line represents the theoretical curve for a simple cable

Figure 4.3

The Impedance Locus of a 'Simple Cable' Fibre

The hollow circles are points uncorrected for capacitative artifact; the filled circles are points corrected for capacitative artifact. The solid line is the theoretical curve for the simple cable model. The fibre whose impedance plot is given here is fibre 2, group 2, Table 1. The numbers near some points represent the frequency at which the measurement was taken.

Fig. 4.3



(see Fig. 2.3). The fit achieved with more complicated models of the fibre admittance is no better than that of the simple model.

Third Group of Fibres.

These fibres all had low input resistances and so records taken at higher frequencies were swamped by the capacitative artifact and are not shown here. At low frequencies, however, a second dispersion in the impedance locus could clearly be seen.

Fig. 4.4 shows the low frequency impedance locus of one of the three fibres which unequivocally showed this behaviour.

There was no indication that these fibres were abnormal. Their resting potentials were satisfactory (over 60 mV) and they showed no sign of dissection damage even after being kept in the cold for many hours. The input resistances seem low because impedance measurements over the whole frequency range were only possible on fibres with particularly high input resistances. Thus, the fibres in groups one and two had much higher input resistances than most of the fibres examined.

Errors Arising from the Neglect of Three Dimensional Spread of Current.

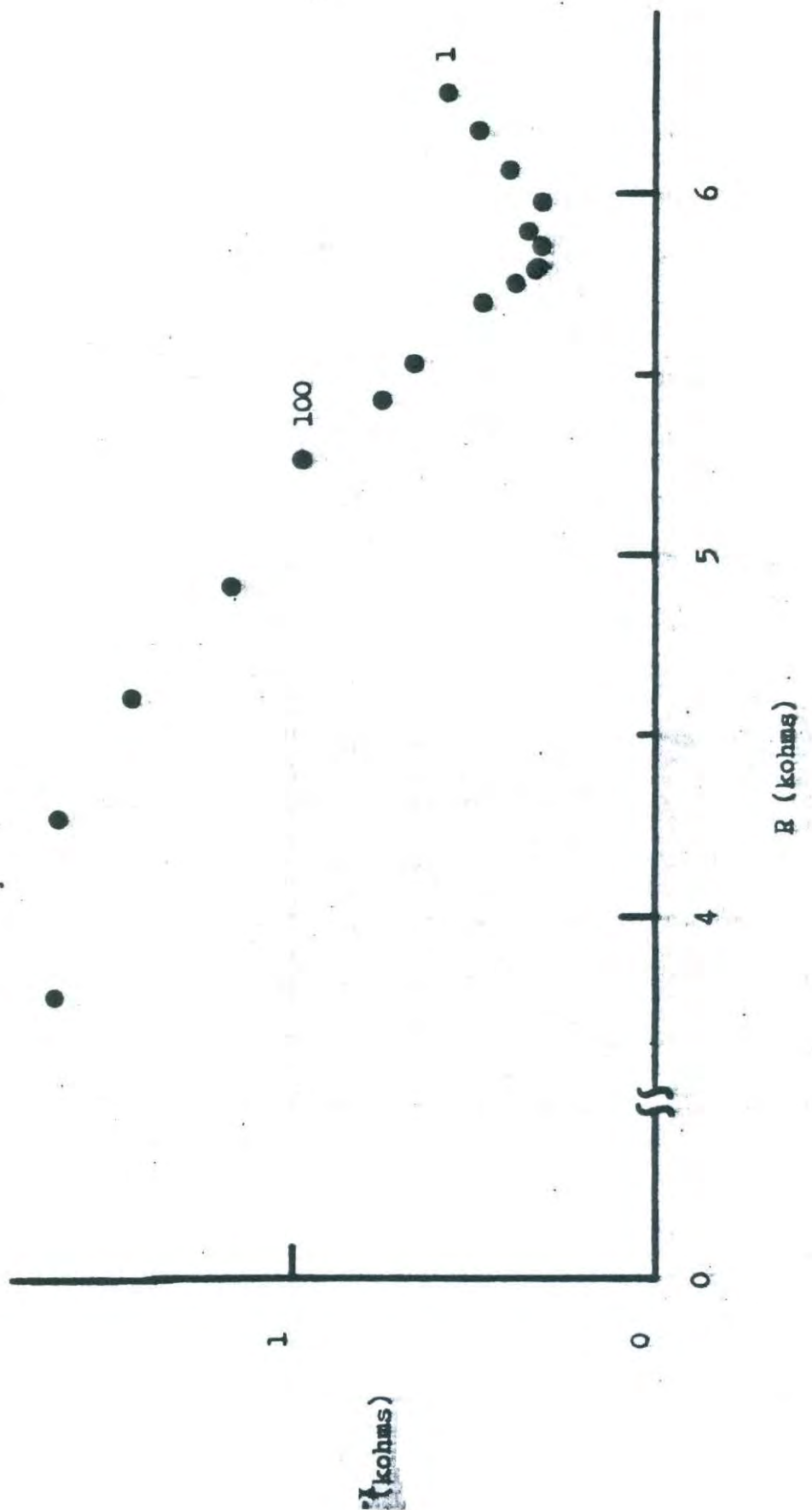
A potentially serious source of error is the distortion of the impedance locus caused by the assumption of purely one

Figure 4.4

Impedance Plot of Low Frequency Measurements on a Fibre of Group 3.

Note the discontinuity in the abscissa. The frequency at which some
of the measurements were made is shown near the appropriate points.

FIG. 4.4



dimensional flow of current. The solution to the problem of three dimensional flow of current around a cylinder with a high impedance coating, the current being applied from a point source just under the coating, can be found from the solution to a similar problem in Carslaw & Jaeger (1959) (Falk & Fatt, 1964). (See Appendix 1 of this chapter for a discussion of the solution). The solution shows that the three dimensional spread of current produces an additional resistance caused by the convergence of current near a point source. There is also a small effect on the reactance at the highest frequencies. For electrode spacing of the order of half a fibre radius (about 40μ) the main effect of the three dimensional spread of current is to produce an almost constant shift to the right of the impedance locus of about 1 kohm. The effect on the reactance is to produce an upward displacement of the impedance locus at high frequencies of about 0.5 kohms. Neither of these figures is big enough to change the interpretation of our results qualitatively, although they do lead to some error in the estimate of the size of the distributed resistance. Indeed, the effect on the reactance is in the wrong direction to explain the downward bend in the impedance locus at high frequencies. If our electrodes had been much closer together, however, the effects would be appreciable. If the electrodes were 16μ apart, for instance, the displacement in resistance would be about 6 kohms. For this reason, the electrodes were kept about 40μ apart in these experiments.

Another piece of evidence suggesting that the high-frequency resistance is not caused by three dimensional spread of current is the large size of the infinite frequency resistance ($R_{\infty} = 13.8$ kohms) in one fibre (fibre 3, in the tables). The electrodes would have had to be less than 10μ apart (instead of the observed 40μ) to explain this displacement. It is unlikely that the electrode separation was over-estimated by this amount. Indeed, because of the dimpling of the fibre membrane caused by the insertion of relatively large microelectrodes, the electrode separation was probably under-estimated.

[the possible presence of clefts between the electrodes]

In two fibres, however, (numbers 6 and 7 in the tables) the high-frequency resistance was small enough so that the possibility that it was caused by three dimensional effects could not be ruled out.

Equivalent Circuits of the Muscle Fibre Distributed Admittance.

It is clear from the small size of the three dimensional corrections and from the shape of the impedance loci of the fibres of the first group that any equivalent circuit chosen must include a resistance in series with all the capacitance (a distributed resistance). Furthermore, since the fit achieved with the model containing two capacitances is much better than the fit of the model containing only one, the circuit must

contain at least two independent capacitances. The presence of still more independent capacitances cannot be ruled out but the accuracy of our measurements is not sufficient to warrant their inclusion: the fit achieved using three capacitances is hardly better than that achieved with two. There are, however, many equivalent circuits which have two capacitances, both in series with resistance, and a resistive shunt. The choice among these must be made on the basis of anatomical data about the structure of the muscle fibre. Further discussion of the choice of equivalent circuits is left until Chapter 5.

The second group of fibres had impedance loci with no sign of either a distributed resistance or two time constants. They could be fit by the simple cable model as shown in Fig. 4.3.

No equivalent circuit could be found for the third group of fibres since impedance measurements over a wide frequency range were not available. It is clear, however, that the equivalent circuit must contain a large capacitance to explain the low-frequency dispersion. There is no evidence here as to whether two additional capacitances are necessary to explain the high-frequency behaviour of these fibres.

Evaluation of Circuit Parameters.

The circuit parameters determined by the computer fit of the theoretical curve of the two time constant, distributed

CIRCUIT VALUES REFERRED TO OUTER SURFACE AREA.

TABLE 2

Expt. & Genus	λ (μ)	$C_e + C_m$ ($\mu F/cm^2$)	C_e ($\mu F/cm^2$)	C_m ($\mu F/cm^2$)	R_b ($ohm \cdot cm^2$)	R_m ($ohm \cdot cm^2$)	R_e ($ohm \cdot cm^2$)
3 <u>Portunus</u>	743	36	24	12	21	128	52
5 <u>Carcinus</u>	750	108	91	17	5.1	129	14
6 <u>Carcinus</u>	851	150	122	28	---	146	6.1
7 <u>Carcinus</u>	935	75	50	25	0.16	113	13.2

CIRCUIT VALUES OF TWO TIME CONSTANT, DISTRIBUTED RESISTANCE MODEL.

TABLE 1

Expt. & Genus	R_{in} (kohms)	R_∞ (kohms)	c_m/c_e	r_m/r_e	r_b/r_m (x 10^{-2})	$\frac{c_m + c_e}{r_i}$ (μ F/megohm)	2a or $\begin{cases} 2a_1 \\ 2a_2 \end{cases}$ (μ)
Group 1:							
1 <u>Portunus</u>	30.1	3.91	1.23	4.50	1.73	1.77	(365)
2 <u>Portunus</u>	23.7	2.84	0.67	13.5	1.48	4.34	(192)
3 <u>Portunus</u>	36.6	13.8	0.49	2.44	16.5	1.00	87*
4 <u>Carcinus</u>	18.5	2.76	0.74	10.6	2.28	8.60	(198)
5 <u>Carcinus</u>	28.0	5.50	0.19	8.96	3.95	4.62	$\begin{cases} 122 \\ 81^* \end{cases}$
6 <u>Carcinus</u>	23.4	---	0.23	23.9	---	9.96	116*
7 <u>Carcinus</u>	11.7	0.44	0.52	8.56	1.38	16.5	172
Group 2:							
1. <u>Carcinus</u>	20.7	---	---	---	---	16.1	(167)
2 <u>Carcinus</u>	15.5	---	---	---	---	33.6	(182)

* calculated; not a measured diameter

() enclose measured diameters which could not be checked for agreement with internal resistivity of $R_i = 58$ ohm-cm

resistance model were r_b/r_m , r_m/r_e , c_m/c_e , and c_e/r_i . (Symbols and model are defined in Chapter 2 and shown in Fig. 2.6). The values obtained are shown in Table 1. R_{in} and R_∞ are the resistance observed at zero and infinite frequency, respectively. The second group of fibres in Table 1 are those which the simple cable model (Fig. 3, Chapter 2) described adequately.

Parameters for a unit length of fibre can be found if one additional quantity, the d.c. space constant

$$\lambda = \sqrt{\frac{r_m + r_b}{r_e}}$$

is known. In four of the seven fibres of group one the space constant was successfully determined. In the other fibres loss of resting potential and resistance upon removal of the micro-electrode made an accurate determination impossible. The failure to determine more values of the space constant was not considered serious since the main object of the investigation was to determine the equivalent circuit of single crab muscle fibres, and having done that, the parameters r_b/r_m , r_m/r_e , and c_m/c_e .

Knowledge of a further parameter (the fibre radius 'a' or the internal resistivity R_i) allows the parameters to be referred to the surface area of a cylinder of given shape and

size. The surface area so assumed certainly does not correspond to the actual surface area of crab muscle fibres because of the deep clefts formed by gross infolding of the surface membrane (Peachey & Huxley, 1964). Since the amount of this infolding is likely to be quite variable, considerable scatter in the size of parameters referred to the equivalent cylindrical surface area is to be expected. Significance should be attached only to the order of magnitude of these surface parameters.

Because the measurement of 'diameter' is subject to considerable error even if a mapping procedure is used (see Procedure, Chapter 3: Methods) and because the surface parameters depend on the cube of the diameter (see (2) below), another procedure, depending on an assumed value for R_i , (Fatt & Katz, 1951; Falk & Fatt, 1964) was used here. If a value for the internal resistivity R_i were known, a value for the fibre radius 'a' could be calculated (assuming the fibre to be a circular cylinder).

$$a = \sqrt{\frac{\lambda R_i}{2\pi R_{in}}} \quad (1)$$

The value $R_i = 58 \text{ ohm-cm}$ was taken from Atwood (1963). If the calculated radius was in reasonable agreement with the observed diameter, the fibre was assumed to be a circular cylinder and the surface parameters calculated from

$$R_b = \frac{8\pi^2 a^3 R_{in}^3}{R_i}$$

$$C_e = \frac{R_i}{2\pi^2 a^2} \cdot \frac{c_e}{r_i}$$

$$R_m = \frac{R_b}{\frac{r_i}{r_m}}$$

$$C_m = \frac{c_m}{c_e} \cdot C_e \quad (2)$$

$$R_e = \frac{R_b}{\frac{r_b}{r_m} \cdot \frac{r_m}{r_e}}$$

If the calculated value for the fibre radius 'a' was not in reasonable agreement with the observed diameter, the cylinder was assumed to be elliptical. One axis a_1 was taken to be the observed 'diameter', the other a_2 was calculated from the formula

$$a_2 = \frac{\lambda R_i}{2\pi a_1} \cdot \frac{1}{R_{in}}$$

The two values are indicated in Table 1 in brackets, the asterisk marking the computed value. The surface parameters were then calculated by

$$C_e = \frac{R_i}{\pi a_1 a_2 \Gamma} \cdot \frac{c_e}{r_i}$$

$$R_b = \frac{2 R_{in}^3 \lambda \Gamma}{R_i}$$

$[R_m, R_e, C_m]$
calculated
as in (a).

where Γ is the circumference of the ellipse and is given by

$$\Gamma = 4a E(m)$$

$$m = 1 - \left(\frac{a_2}{a_1}\right)^2$$

where $E(m)$ is a complete elliptic integral of the second kind expressed as a function of the parameter m (Abramowitz & Stegun, 1964). In two cases (marked with an asterik in Table 1) no reliable measurements of fibre diameter were made. In these cases the fibre was assumed to be a circular cylinder and the radius and surface parameters were calculated from (1) and (2) above. The surface parameters calculated by the above procedure are listed in Table 2.

It is valuable to include in the average of the surface parameters the three fibres for which λ and thus the other surface parameters were not determined. The procedure for doing this, developed by Falk & Fatt (1964), depends on the assumption that C_m and R_m are independent of the fibre radius. Equations (2) then imply that c_m/r_i varies as a^3 and R_{in} varies as $a^{-3/2}$ so $(c_m/r_i)^{1/3}$ and $R_{in}^{-2/3}$ vary with the first power of 'a'. By averaging the cube root of c_m/r_i and using the average values of c_m/c_e and 'a', average values of C_m and C_e were obtained:

$$C_m = 18.9 \mu\text{F}/\text{cm}^2 \quad C_e = 40.2 \mu\text{F}/\text{cm}^2 \quad (\text{seven fibres})$$

Average values of R_b , R_m , and R_e were computed by a similar procedure:

$$R_m = 176 \text{ ohm-cm}^2 \quad R_e = 16.9 \text{ ohm-cm}^2 \quad R_b = 6.9 \text{ ohm-cm}^2$$

The weighting procedure resulted in an increase in the average value of the resistances and a decrease in the average value of the capacitances.

Transient Response of the Muscle Fibre.

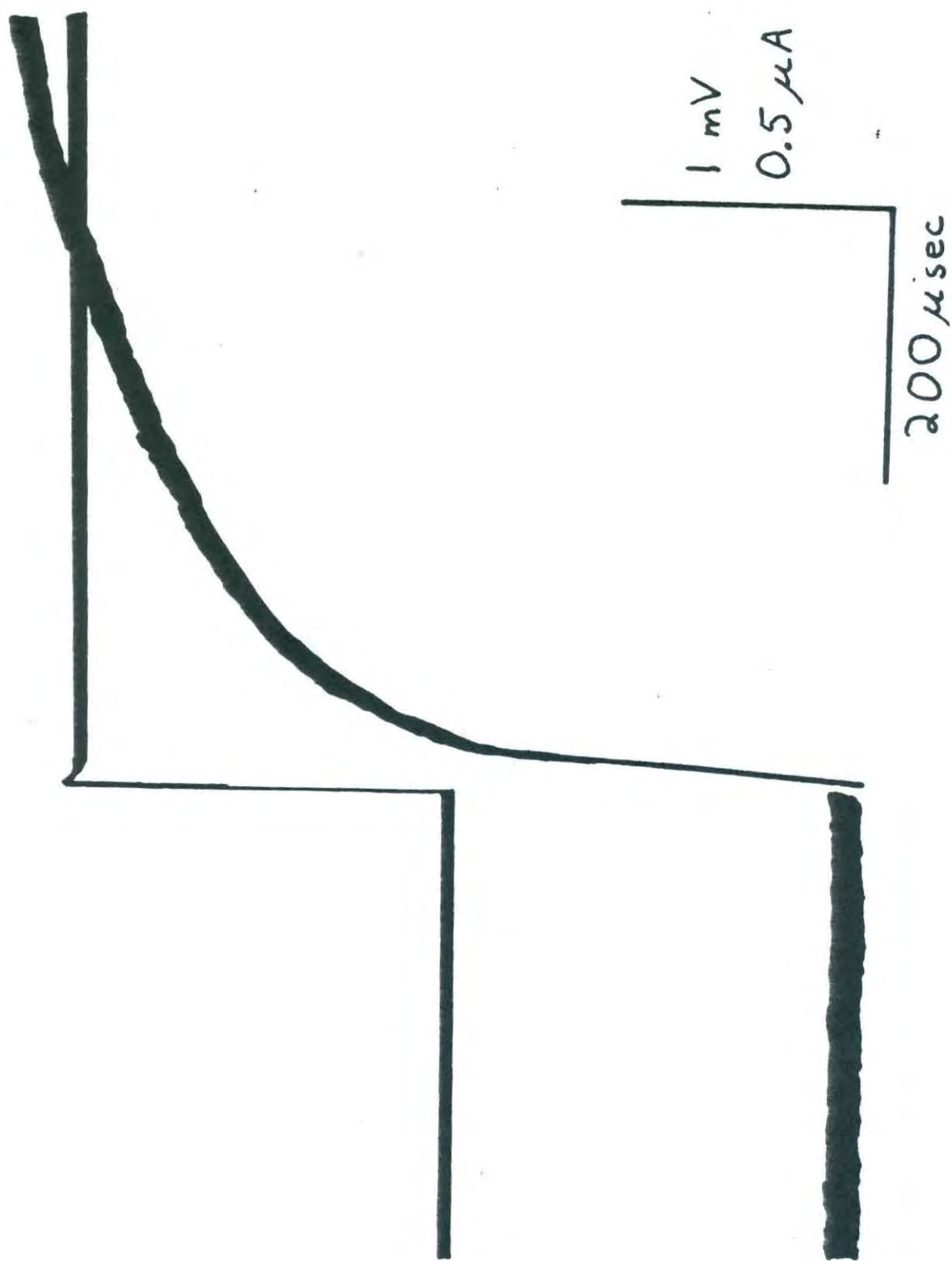
The transient response of the muscle fibre to a step current was determined in a few cases. The off response to a small hyperpolarizing pulse is shown in Figure. 4.5. Impedance measurements were not successfully completed from this fibre. Current was displayed on one trace and potential on the other. The records shown are the superposition of several sweeps. The record shows an initial steep rise of potential followed by a slow rise. Although the time constant of the steep rise is short enough so that the capacitative artifact caused significant distortion, the initial rise was probably produced in large measure by the distributed resistance. The two time constants of most of the fibres examined were close enough so that no obvious deviation from the rise given by one time constant would be expected after the initial phase. Because of the inherent inability of transient response analysis to distinguish between approximately equal time constants

Fig 4.5

Transient Response of Single Crab Muscle Fibre

Tracing of the off response to a small hyperpolarizing pulse of current.

Current is displayed on the upper trace, potential on the lower. The tracing was taken from a record consisting of several superimposed sweeps.



(Lanczos, 1957; p. 272-279) and because of the considerable mathematical difficulties, no theoretical curves for transient response have been worked out.

Appendix 1 of Chapter 4

The Three Dimensional Flow of Current.

The problem of the three dimensional flow of current around a cylinder with a thin high impedance coating involves the solution of Laplace's equation with the boundary condition that there be no discontinuity in the normal component of current at the surface. The solution discussed here has been presented by Falk & Fatt (1964) and is derived from the solution to the problem of an instantaneous point source of heat with analogous geometry and boundary conditions (Carslaw & Jaeger, 1959, equation 7, p.378). The external medium is taken to be isopotential. The methods for converting the solution of the instantaneous heat problem to that of the corresponding steady state problem are also given in Carslaw and Jaeger (p. 422). An analogous and perhaps simpler method of deriving the steady state response is to use the superposition theorem and find the integral

$$\lim_{t' \rightarrow \infty} \int_0^{t'} f(t) dt$$

where $f(t)$ is the solution to the instantaneous problem found in Carslaw & Jaeger. The integration can be performed after a

simple change of variables. If the electrical parameters corresponding to the analogous heat parameters are substituted, the solution is

$$Z_{cyl} = R_{cyl} + j X_{cyl} \quad (1)$$

$$= \frac{1}{2} r_i a \sum_{n=-\infty}^{\infty} \cos n\theta \sum_{\beta} \frac{\beta e^{-\beta x/a}}{\beta^2 - n^2 + \frac{1}{4} (\gamma a)^2}$$

where the source is taken to be just under the surface of the cylinder, at angle 0° and $x = 0$; 'n' assumes only integral values, and

θ is the circumferential angular co-ordinate of the point at which potential is measured.

x is the distance along the fibre axis (the axial co-ordinate) of the point at which potential is measured.

a is the fibre radius.

r_i is the internal resistivity of the fibre in ohms/unit length.

γ is the parameter governing the spatial decrement of potential along the fibre and is given by $(r_i y)^{1/2}$ where y is the distributed admittance of the fibre. For γ real the space constant as conventionally defined is given by $\lambda = 1/\gamma$.

For γ complex the frequency dependent effective space constant

λ_f is given by

$$\lambda_f = \frac{1}{R_e(\gamma)}$$

since only the real part of γ produces spatial decrement
(the imaginary part produces only phase shift).

The β 's are the roots with positive real parts of the expression

$$\beta \frac{J_{n-1}(\beta)}{J_n(\beta)} = n - \frac{1}{2} (\gamma a)^2 \quad (2)$$

For $(\gamma a)^2$ real and positive all the roots are positive real numbers (Watson, 1962 p. 482; Dixon, 1903). Since the β 's (i.e. the real part of the β 's) govern the spatial decrement of potential, they are analogous to reciprocal space constants.

The main difficulty in using this solution is that of finding the roots since the infinite series (1) converges reasonably rapidly provided x is not too small. If y is taken to be purely real (the low frequency case), the roots for $n = 0$ can be found directly from the table of

$$J_n(\beta) \equiv \beta \frac{J_{n-1}(\beta)}{J_n(\beta)} ; \quad \begin{aligned} \beta &= 0(0.01) 20 \\ n &= 1(1) 16 \end{aligned} \quad (3)$$

given in Once (1958). The roots for $n = 0$ (the smallest of which we call the first root) can be found by using the relation

$$\beta \frac{J_{-1}(\beta)}{J_0(\beta)} = -\beta \frac{J_1(\beta)}{J_0(\beta)} = -\frac{\beta^2}{J_1(\beta)} \quad (4)$$

As long as $\frac{1}{2} (\gamma a)^2 = \frac{1}{2} \left(\frac{a}{\lambda}\right)^2$ is quite small all the roots except the first will be very close to the poles (infinities) of $J_1(\beta)$. Since $J_1(\beta)$ is relatively independent of β in a range near zero, the first root will be given by a value of β close to zero. More quantitatively, if $\beta < 0.2$, then

$$1.99 < J_1(\beta) < 2.00$$

and it follows that

$$\frac{1}{2} (\gamma a)^2 = \frac{\beta^2}{J_1(\beta)} \doteq \frac{\beta^2}{2}; \text{ thus,} \quad (5)$$

$$\beta \doteq \gamma a = a/\lambda$$

(This trial value of β can be checked and improved if necessary by substituting directly in (4)). In other words, the first root is the reciprocal space constant in 'natural' units.

Substitution of this root into the sum (1) shows that for small enough (γa) the leading term of the infinite series is the same as the linear cable approximation

$$R = \frac{1}{2} r_i \lambda e^{-x/\lambda}$$

The roots for y and therefore γ complex (applicable for non-zero frequencies) can be found with the help of a table of complex Bessel functions (Lowan, 1947). A good approximation to the first root is again $\beta = \gamma a$. The other roots are very close to the real axis and can be found by finding the real root for the right hand side of (2) equal to

$$\operatorname{Re}\left\{n - \frac{1}{a}(\gamma a)^2\right\}$$

and then moving β a few degrees off the real axis. (The reason that this procedure works is that for $n \gg \frac{1}{a}(\gamma a)^2$ (2) reduces to

$$J'_n(\beta) \equiv \frac{d J_n(\beta)}{d\beta} = 0$$

the roots of which are real (Watson, 1962, p. 507).

The fibre analyzed here is assumed to have the characteristics $r_i = 2.5 \times 10^5$ ohms/cm; $R_i = 50.2$ ohm-cm; $R_m = 725$ ohm-cm²; $a = 80\mu$; high frequency capacitance $5 \mu F/cm^2$. These give the 'observed' characteristics R_o , the input resistance, = 30 kohms; λ , the d.c. space constant = 2.4 mm; and, at high frequency (10 kc/s), $-X_o = R_o = 1$ kohm; $\gamma_f = 225\mu$. All the current at high frequencies is assumed to be carried by the membrane capacitance. In other words the model used for the fibre admittance has no distributed resistance.

The results then show whether three dimensional effects are large enough to make the impedance locus of a fibre without distributed resistance look like the impedance locus of a fibre with distributed resistance.

The roots for this case are shown in Table 1. Table 2 shows the impedance of the cylinder computed for the estimated electrode separation of $x = 0.5a = 40\mu$. R_0 and $-X_0$ and R and $-X$ are the resistance and reactance which would be observed in a linear cable if the electrode separation were nil or 40μ , respectively. Since the observed impedance was $Z = R + jX$, $Z_{cyl} - Z$ is a measure of the error caused by ignoring the effects of three dimensional spread of current. The error in the resistance is seen to be quite independent of frequency. The error in the reactance is in the wrong direction to explain the downwards bend in the impedance locus at high frequencies.

TABLE 1

ROOTS OF EQUATION (2) FOR FIBRE DESCRIBED IN TEXT.

Low frequency

n	β_1	β_2
0	0.034	3.84
1	1.84	4.92
2	3.05	6.70
3	4.20	
4	5.31	
5	6.41	
6	7.50	

High frequency

0	0.35 (1+j)	3.84
1	1.84 + 0.096j	4.92

(other roots same as for low frequency case)

 β_r is the rth root in order of increasing magnitude at a given n.

Only roots of significant size are shown.

Other symbols defined in text of Appendix.

TABLE 2

THREE DIMENSIONAL EFFECTS

Parameter	Low frequency	High frequency
δa	0.034	$0.356 (1 + j)$
R	29.49	0.84
$-X$	---	0.84
R_o	30.00	1.00
$-X_o$	---	1.00
R_{cyl}	30.63	1.96
$-X_{cyl}$	---	1.48
$R_{cyl} - R$	1.14	1.12
$-X_{cyl} - (-X)$	---	0.64

Symbols as defined in the text of the Appendix; units of all impedances are kohms; computed from (1) and (2) in text for

$$r_1 = 2.5 \times 10^5 \text{ ohm/cm}; \quad a = 80\mu; \quad x = 40\mu.$$

Chapter 5

DISCUSSION

Relation of Present Observations to Previous Findings.

Previous studies of the linear electrical properties of crab muscle (Fatt & Katz, 1953a; Atwood, 1963) have used square pulse (transient) analysis. Because of the difficulties of separating time constants of comparable magnitude with this technique, it is not surprising that previous investigations did not find evidence for the existence of two capacitances. The presence of a distributed series resistance would be very difficult to observe with transient response methods, since the initial jump produced by the resistance would be obscured by capacitative artifact (see Fig. 4.5).

The presence of two capacitances in crab muscle can explain some findings of Fatt & Katz (1953b) on the time course of junctional potentials along the lines suggested by Falk & Fatt (p. 105).

Relation of Electrical Parameters to Muscle Structure.

It is necessary to consider the structure of crab muscle fibres in order to choose the most likely equivalent circuit and

Plates 1 & 2

Electron Micrographs of Muscle Fibre of Carcinus

Plate 1 shows in a transverse oriented section one of the infolded surfaces which form clefts (cl). The amorphous material surrounding the fibre (am) can also be seen.

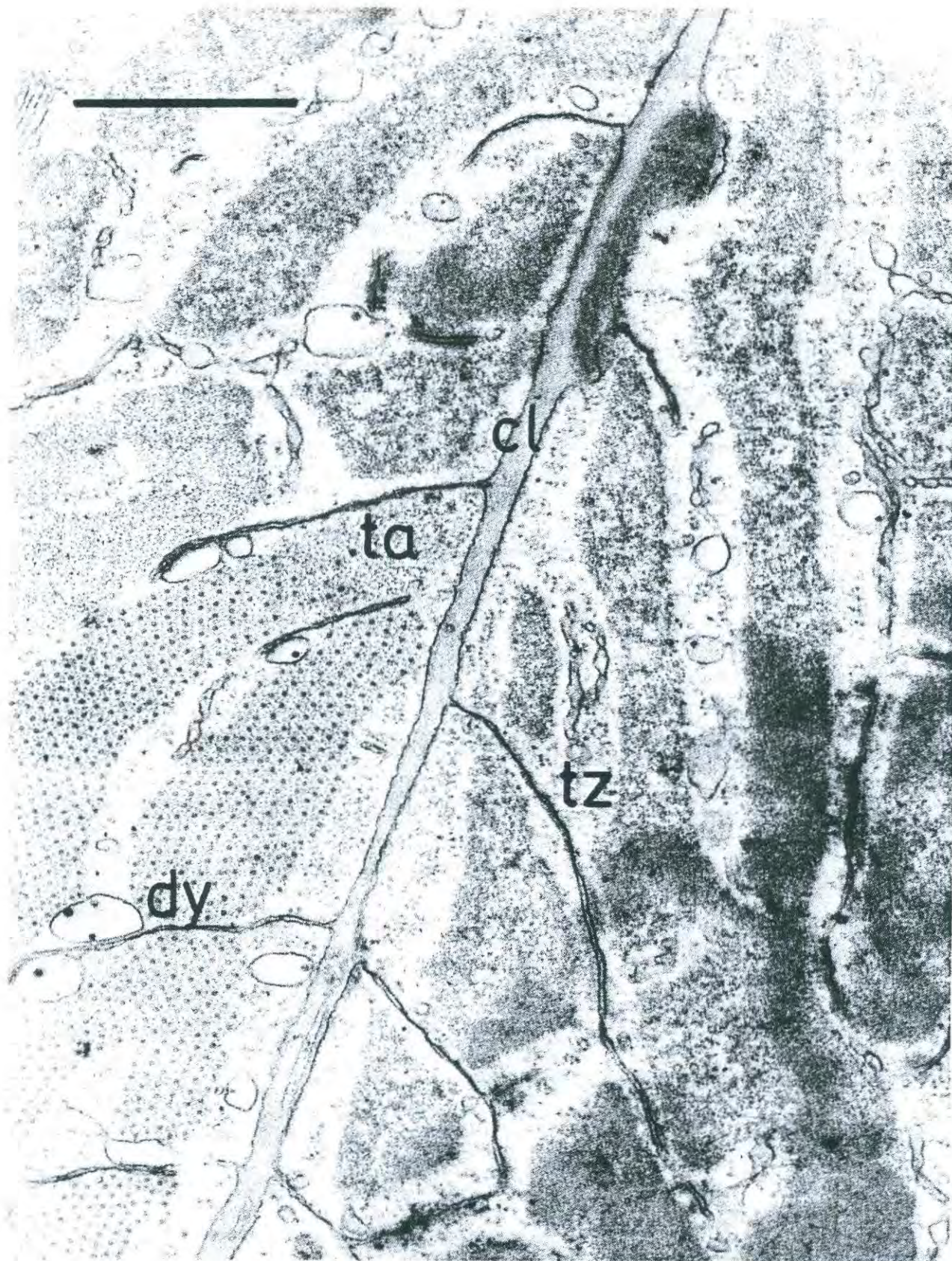
Plate 2, also a transversely oriented section, shows a cleft (cl) filled with amorphous material and sarcotubes branching off the cleft at the Z line (tz) and at the AI boundary (ta). The sarcotubes at the AI boundary form dyads (dy) with elements of the longitudinal reticulum.

The bar in each plate represents 1μ. Both electron micrographs were kindly supplied by L. Peachey and A.F. Huxley.

PLATE 1



PLATE 2



to identify the structures responsible for the different circuit parameters.

The basic features of crab muscle structure as shown in Plates 1 and 2 are described in Peachey & Huxley (1964). The muscle fibres of Carcinus maenas have deep clefts formed by gross infolding of the fibre surface. Two types of tubular infoldings of the plasma membrane extend from both these clefts and the outer surface. One set of the tubules is associated with the Z lines and seems to have no direct connection with excitation-contraction coupling. The other set of tubules is associated with the A-I junctions, forms 'dyadic' elements with part of the longitudinal reticulum, and is implicated in excitation-contraction coupling (see also Huxley and Taylor, 1958). An amorphous material surrounds the fibre and fills the clefts.

The equivalent circuit which one might expect from such a structure is shown in Fig. 5.1. This circuit is simplified in that the impedance of the two sets of tubules have been lumped together into one resistance and capacitance. Furthermore, all the structures associated with the infolded surfaces are assumed to be in series with the same resistance; in other words as a first approximation the distributed nature of these impedances has been ignored. This approximation is necessary because of the considerable complication introduced into the circuit analysis if these impedances are treated as distributed.

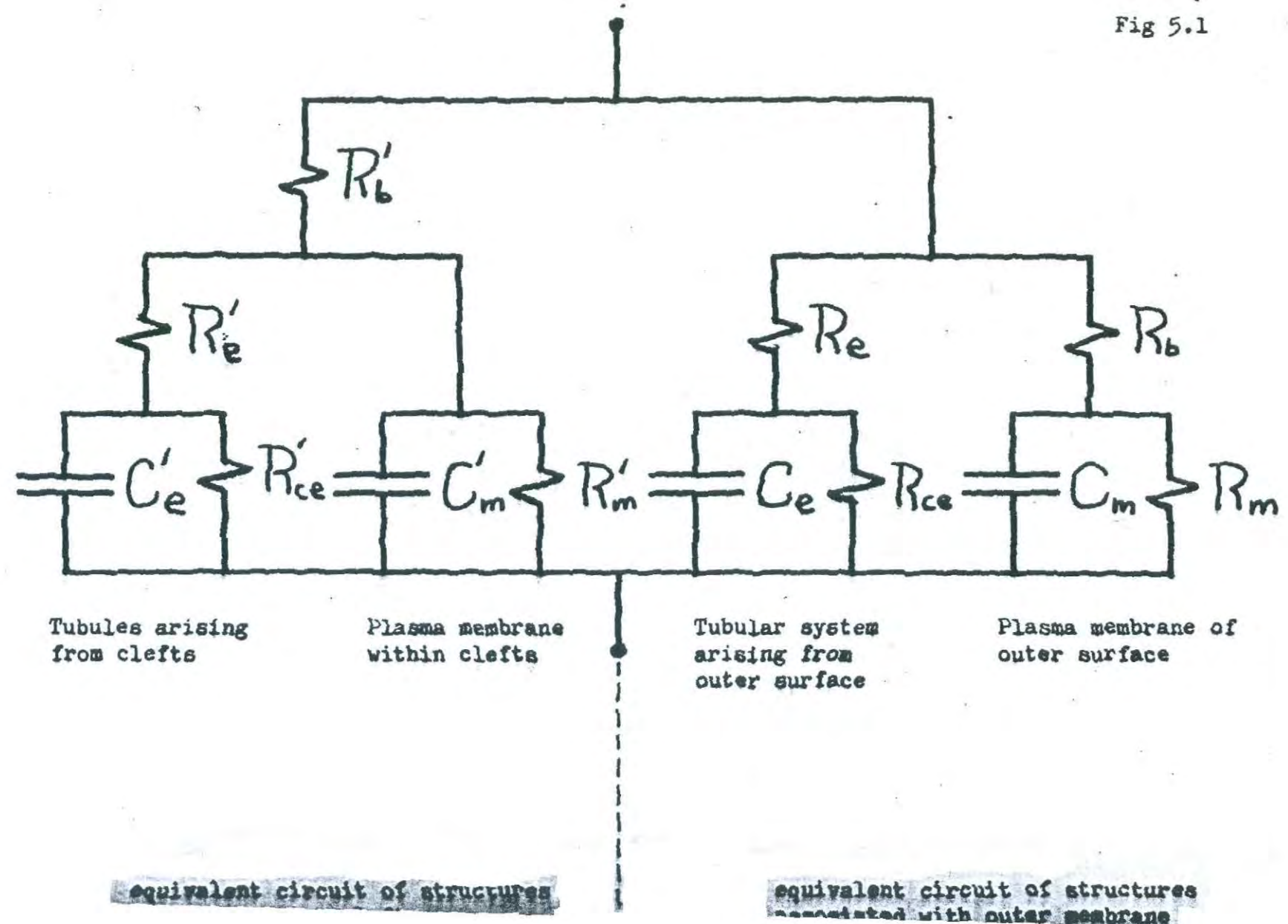
The equivalent circuit shown in Fig. 5.1 is divided into two parts; the impedance of the structures associated with the

Figure 5.1

'Complete' Equivalent Circuit Based on Anatomy of Crab Muscle Fibres

Symbols defined in figure and text. Impedance of Z line and A band
sarcotubular systems lumped together.

Fig 5.1



outer surface of the fibre and the impedance of the structures associated with the infolded surfaces of the clefts. The impedance arising from the outer surface in turn has two components: the impedance of the plasma membrane (R_m , C_m) in series with the resistance of the surrounding amorphous material (R_b); and the impedance of the tubular walls (R_{ce} , C_e) in series with the resistance R_e arising from the resistivity of the material in the tubules. Similarly, the impedance associated with the infolded surfaces of the clefts is divided into a plasma membrane part (R_m' , C_m') and a tubular part (R_{ce}' , R_e' , and C_e'). Here, however, both membrane and tubular part are in series with the resistance of the amorphous material filling the clefts (R_b').

The equivalent circuit just described has four time constants (natural frequencies). Our results do not have the accuracy necessary to resolve this many time constants if they are all of the same order of magnitude. If they are not of the same magnitude it is quite likely that some would lie outside the frequency range examined. It is possible that the observed low frequency dispersion could be produced by one of the capacitances shown in Fig. 5.1. It is more likely, however, that this dispersion arises from some diffusion process since the specific capacitance necessary to explain the low natural frequency of this dispersion would be very large (see the discussion of C_x in Fatt, 1964).

Simplif
ve

It is thus necessary to try to work out which of the capacitances shown in Fig. 5.1 is likely to produce the observed impedance locus. There are two possibilities. First, it could be argued that the area of the infolded surface is so large that the impedance observed is caused almost entirely by the primed elements R'_e , C'_e , etc. (In other words because of the relative surface areas C_e and C_m would be very much smaller than their primed counterparts and their contribution to the observed impedance would be too small to have been observed.) In that case the equivalent circuit is as shown in Fig. 5.2A (with primes omitted).

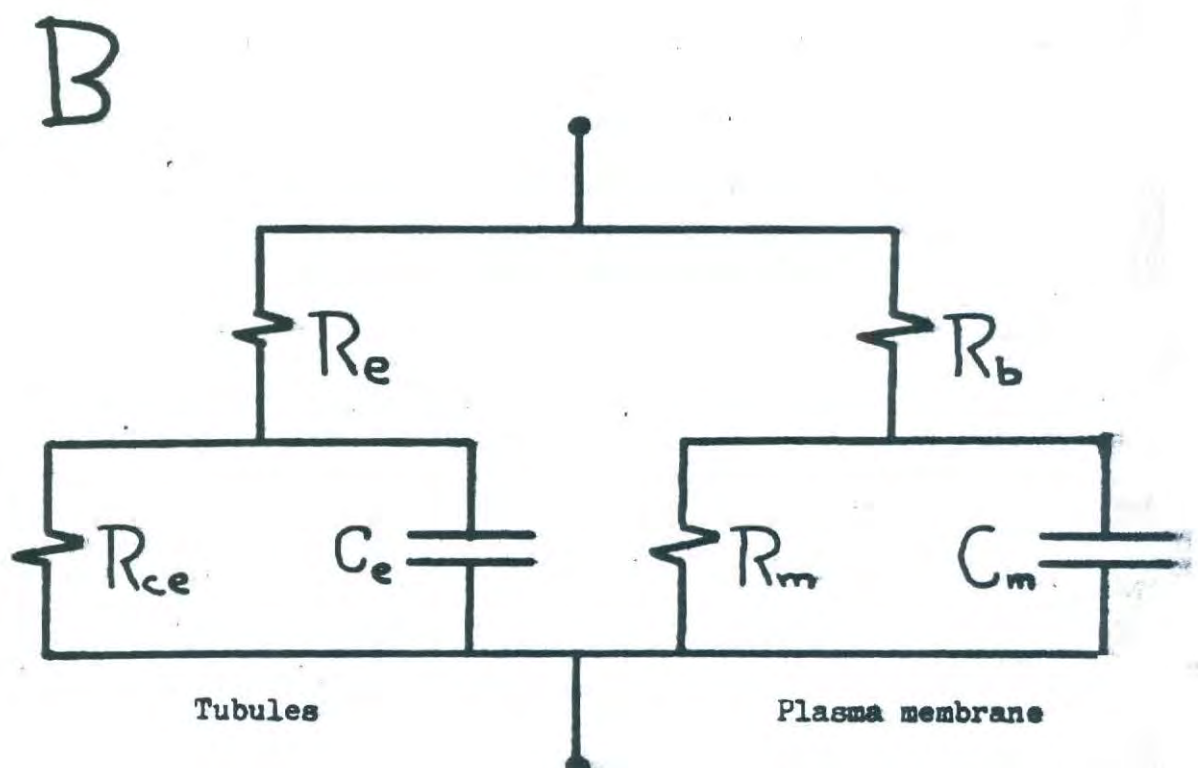
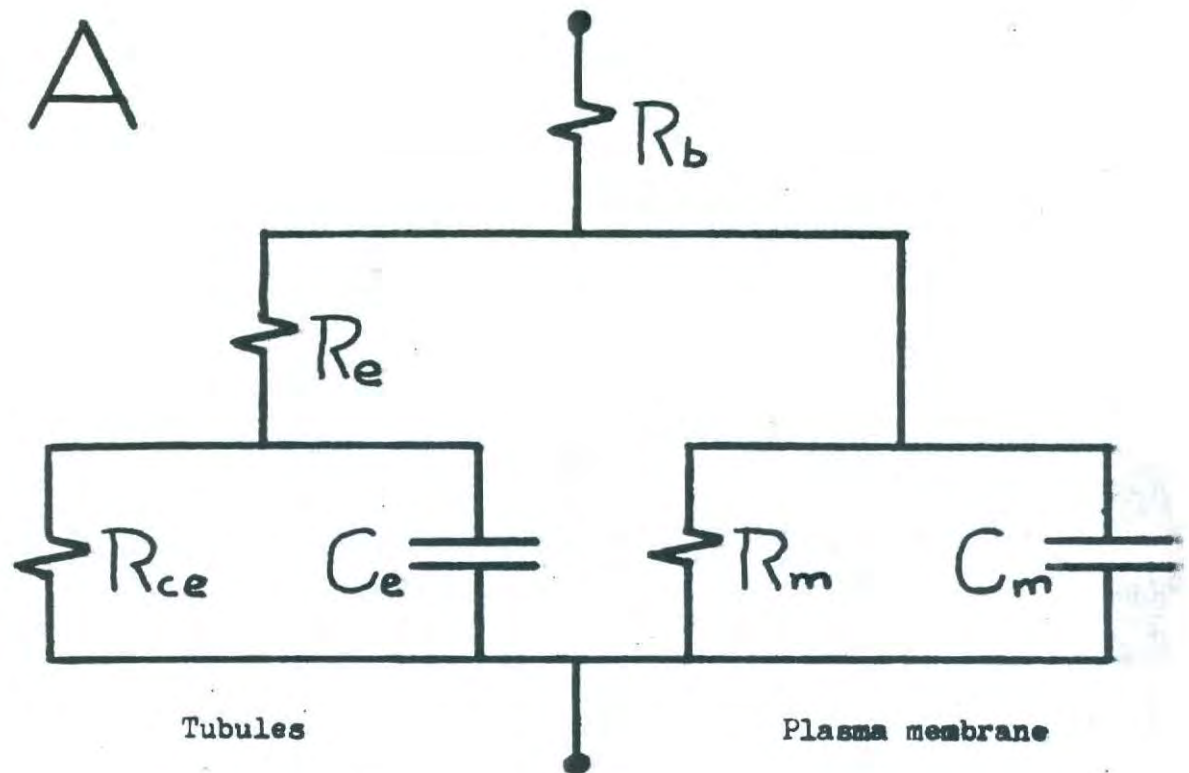
It is more likely, however, that the capacitances associated with the outer surface are not negligible with respect to the capacitances associated with the clefts. In that case the best procedure is probably to lump all the plasma membrane impedance into one set of parameters and all the tubular impedance into another. The resulting equivalent circuit is shown in Fig. 5.2B.

Both circuits shown in Fig. 5.2 contain more than the minimum number of circuit elements necessary to determine their impedance function. They are called non-minimum resistance circuits. In each case one of the resistive paths across the entire circuit is redundant. No information concerning redundant parameters can be derived from impedance measurements made from only one set of terminals (one port) of a circuit. If impedance

Figure 5.2

Simplified Non-minimum Resistance Equivalent Circuits
Symbols and discussion in text.

Fig. 5.2



measurements from another port of the circuit were made (for instance, transverse impedance measurements), a value of the redundant parameter might be derived. In the absence of such information our procedure will be to ignore the shunt R_{ce} on the tubular capacitance. (A similar problem arises in the evaluation of the equivalent circuit of single frog muscle fibres; see Falk & Fatt, 1964). The equation giving the parameters of the full circuits shown in Fig. 5.2 in terms of observed circuit parameters and a known value of R_{ce} are given in Chapter 2: Theory.

If the redundant parameter is eliminated, the equivalent circuits become those shown in Fig. 5.3. The circuit parameters in Fig. 5.3A are the average values computed in Chapter 4: Results. The other circuit values have been derived from these using the equivalence relations derived in Chapter 2: Theory.

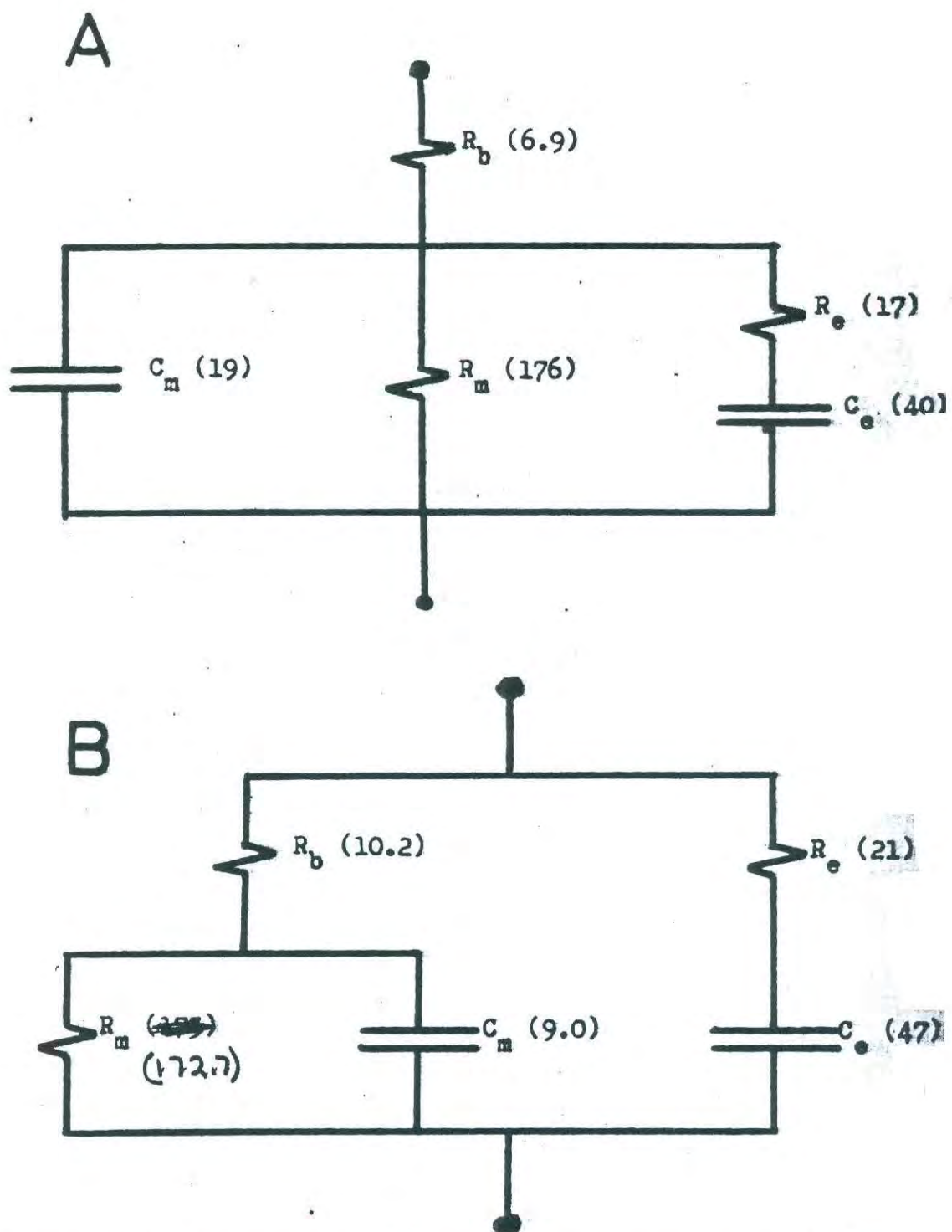
(As discussed in Chapter 2 there is an essential ambiguity in the synthesis of a circuit like that shown in Fig. 3B since the shunt may be placed on either the large or the small capacitance. We have chosen to ignore the shunt on the tubular capacitance and, assuming the tubular capacitance to be larger than the plasma membrane capacitance, have placed the shunt on the smaller capacitance. If the membrane shunt resistance were ignored and the shunt placed entirely across the tubular capacitance, the circuit values would work out to be $R_b = 10.8 \text{ ohm}\cdot\text{cm}^2$, $C_m = 8.0 \mu\text{F}/\text{cm}^2$; $R_e = 18.8 \text{ ohm}\cdot\text{cm}^2$, $R_{ce} = 164 \text{ ohm}\cdot\text{cm}^2$, $C_e = 58.3 \mu\text{F}/\text{cm}^2$).

Figure 5.3

"Final" Equivalent Circuits

**Discussion in text. Numbers in parentheses are the
average circuit values for each model.**

Fig. 5.3



Units of resistances are ohm-cm²; units of capacitances, $\mu\text{F}/\text{cm}^2$.

The size of the two capacitances in either of the two equivalent circuits is consistent with the hypothesis that the capacitances arise from the dielectric properties of the cell membranes. The high specific values when referred to the surface area of a cylinder reduce to the right order of magnitude (around $2 \mu\text{F/cm}^2$) if estimates are made of the surface area of the clefts and tubules (Peachey, personal communication). Peachey's estimates of the relative surface areas of outer and infolded surfaces support our choice of the circuit shown in Fig. 5.3B as being the more realistic.

Either of these models can explain the wide variation of the size of the parameters observed since the size of the parameters would primarily reflect the amount of infolding, a property which is likely to vary considerably from fibre to fibre.

REFERENCES

Abramowitz, A.M. & Stegun, I. (Editors). Handbook of Mathematical Functions. (Applied Mathematica Series - 55, National Bureau of Standards, Washington, 1964).

Amatniek, E. Measurement of Bioelectric potentials with micro-electrodes and neutralized input capacity amplifiers.
IRE Trans. Med. Electron. PGME - 10, 3 (1958).

Atwood, H.L. Differences in muscle fibre properties as a factor in "fast" and "slow" contraction in Carcinus. Comp. Biochem. Physiol. 10, 17. (1963).

Bak, A.F. A unity gain cathode follower. Electroenceph. & Clin. Neurophysiol. J. 10, 745 (1958).

Benson, F.A. Phase angle measurements. Wireless World. 53, 157 (1953).

Benson, F.A. & Carter, O. A critical survey of some phase angle measurements using a cathode-ray tube. Electron. Eng. 22, 238 (1950).

Bode, H.W. Network Analysis and Feedback Amplifier Design.
(van Nostrand, New York, 1945).

* Carslaw, H.S. and Jaeger, J.C. Conduction of Heat in Solids.
2nd Edition. (Oxford University Press, London, 1959).

Churchill, R.V. Complex Variables and Applications. Second Edition. (McGraw-Hill, N.Y., 1960).

Clapp, F.D. Some aspects of cathode follower design at radio frequencies. Proc. IRE. 37, 932 (1949).

** Brooker, T.R.A., Richards, B., Berg, E., & Kerr, R.H.
Mercury Autocode Manual: 2nd Edition (Ferranti, London, 1961)

Cole, K.S. & Cole, R.H. Dispersion and Absorption in Dielectrics

I. Alternating current characteristics. *J. chem. Phys.*

2, 341 (1941).

Copeland, K. Transistor controlled constant temperature device

in Fourth International Conference on Medical Electronics.

(N.Y., 1961).

Copeland, K. Constant temperature devices regulated by semi-

conductors. *J. Physiol.* 161, 33P (1962).

de Levie, R. Influence of surface roughness of solid electrodes

on electrochemical measurements. *Electrochimica Acta.*

10, 113 (1965).

Dixon, A.C. On a property of Bessel's functions. *Messenger of*

Mathematics 32, 7 (1903).

Donaldson, P.E.K. Electronic Apparatus for Biological Research.

(Buttersworth, London, 1961).

Falk, G. & Fatt, P. Linear electrical properties of striated

muscle fibres observed with intracellular electrodes.

Proc. Roy. Soc. B. 160, 69 (1964).

Fatt, P. An analysis of the transverse electrical impedance of

striated muscle. *Proc. Roy. Soc. B.* 159, 606 (1964).

Fatt, P. & Katz, B. An Analysis of the End-Plate Potential Recorded

with an Intra-cellular Electrode. *J. Physiol.* 115, 320 (1951).

Fatt, P. & Katz, B. Electrical properties of crustacean muscle

fibres. *J. Physiol.* 120, 171 (1953a).

- Fatt, P. & Katz, B. Distributed 'end-plate potentials' of crustacean muscle fibres. *J. Exp. Biol.* 30, 433 (1953b).
- Fein, H. Solid-state electrometers with input capacitance neutralization. *IEEE. Trans. Biomed. Eng.* BME-11, 13 (1964).
- Franzini-Armstrong, C. Fine structure of sarcoplasmic reticulum and transverse tubular system in muscle fibres. *Fed. Proc.* 23, 887 (1964).
- Grahame, D.C. Mathematical Theory of the Faradic Admittance. *J. Electrochem. Soc.* 99, 370C (1952).
- Guillemin, E.A. Introductory Circuit Theory. (Wiley, N.Y. 1953).
- Guld, C. Cathode follower & negative capacitance as high input impedance circuits. *Proc. IRE.* 50, 1912 (1962).
- Harris, F.K. Electrical Measurements. (Wiley, N.Y. 1952).
- Huxley, A.F. and Taylor, R.E. Local Activation of Striated Muscle Fibres. *J. Physiol.* 144, 426 (1958).
- Krnjevic, K., Mitchell, J.F. and Szerb, J.C. Determination of ionophoretic release of acetylcholine from micropipettes. *J. Physiol.* 165, 421 (1963).
- Kuo, F. Network Analysis and Synthesis. (Wiley, N.Y. 1962).
- Lanczos, C. Applied Analysis. (Pitman, London, 1957).
- LePage, W.R. & Seely, S. General Network Analysis. (McGraw-Hill, N.Y. 1952).
- Lowan, A.N. Table of the Bessel Functions $J_0(z)$ and $J_1(z)$ for Complex Arguments. (Columbia University Press, New York, 1947).

Macdonald, J. Ross. Some augmented cathode follower circuits.

IRE. Trans. on Audio AU-2 63 (1957).

Macdonald, J. Ross and Brachman, M.K. Linear System Integral Transform Relations. Rev. Med. Phys. 28, 393-422 (1956).

MacNichol, E.F. Jr. & Wagner, H.G. A high impedance input circuit suitable for electrophysiological recording from micropipette electrodes. Nav. Med. Res. Inst. 12, 97 (report 7) (1954).

MacNichol, E.F. Jr. Negative impedance electrometer amplifiers. Proc. IRE, 50, 1909 (1962).

& Strickland, R.E.
McConalogue, D.J. ^ Solution of Analytically Intractable Optimization Problems in Engineering. Proceedings of the Symposium on the Use of Computers in Mechanical Engineering. pp. 31-35 (Institution of Mechanical Engineers, London, 1963).

Murray, C.T. A general purpose wide-range electrometer. in Australian Atomic Energy Symposium (1958). p. 701.

Nastuk, W.L. & Hodgkin, A.L. The electrical activity of single muscle fibres. J. Cell. & Comp. Physiol. 35, 39 (1950).

Onoe, M. Tables of Modified Quotients of Bessel Functions of the First Kind for Real and Imaginary Arguments. (Columbia University Press, New York, 1958).

Pantin, C.F.A. On the excitation of crustacean muscle. J. Exp. Biol. 11, 11-27 (1934).

Peachey, L.D. & Huxley, A.F. Transverse tubules in crab muscle. J. Cell. Biol. 23, 70a (1964).

- Porter, K. The sarcoplasmic reticulum: its recent history and present status. *J. Biophys. & Biochem. Cytol.* 10, 219 (1961).
- Pugsley, I.D. Microelectrode measurements of membrane resistance and capacitance in the sartorius muscle of the toad. *Australian J. Exp. Biol. & Med. Sci.* 41, 615 (1963).
- Rosenbrock, H.H. An Automatic Method for finding the greatest or least value of a function. *Computer, J.* 2, 175 (1960-1).
- Schoenfeld, R.L. Bandwidth limits for neutralized input capacity amplifiers. *Proc. IRE.* 50, 1942 (1962).
- Starr, A.T. Electric Circuits and Wave Filters. Second Edition. (Pitman, London, 1938).
- Tuttle, D.F. Jr. Network Synthesis: Vol. 1. (Wiley, N.Y. 1958).
- Valley, G. and Wallman, H. Vacuum Tube Amplifiers. (McGraw-Hill N.Y. 1948).
- Veratti, E. Investigations on the fine structure of striated muscle fibre. *Memorie of Reale Istituto Lombardo*. 19:87, No. 10 of Series III, 1902; reprinted in English translation in *J. Biophys. & Biochem. Cytol.* 10, 1 (1961).
- Watson, G.N. A Treatise on the Theory of Bessel Functions, Second Edition. (Cambridge University Press, London. 1962).
- Widder, D.V. Advanced Calculus, 2nd Edn. Prentice-Hall, London, 1961.

- Woodbury, J.W. Direct membrane resting and action potentials from single myelinated nerve fibers. *J. Cell. and Comp. Physiol.* 39, 323 (1952).
- Yang, C.C., Hervey, J.B. & Smith, P.E. On amplifiers used for microelectrode work. *IRE. Trans. Med. Electron.* 10, 25 (1958).